QUANTIFYING WATER EXCHANGE BETWEEN THE BRAZOS RIVER AND THE BRAZOS RIVER ALLUVIAL AQUIFER USING HIGH TEMPORAL RESOLUTION MEASUREMENTS

A Thesis

by

KIMBERLY ANNE RHODES

Submitted to the Office of Graduate and Professional Studies of
Texas A&M University
in partial fulfillment of the requirements for the degree of

MASTER OF SCIENCE

Chair of Committee,	Peter Knappett
Committee Members,	Gretchen Miller
	John R. Giardino
Head of Department,	Ronald Kaiser

August 2016

Major Subject: Water Management and Hydrological Science

ABSTRACT

Texas had unmet water supply needs in 2010. These unmet needs are expected to increase through 2040, making accurate water budgeting increasingly more important. Current water budgets use simple assumptions to estimate groundwater discharges (Q_{gw}) to rivers based on established, but limited, hydrograph separation techniques. In this study we compare Q_{gw} estimates obtained with more direct high-frequency techniques, including specific conductance mass balances, differential gaging, endmember-mixing analyses (EMMA), and the Dupuit equation using the observed slope of the unconfined water table, to Q_{gw} estimates obtained using hydrograph separation. Together, these methods provide updated, seasonal estimates of the groundwater discharge component of the water budget for the second longest river in Texas.

Two contiguous stretches of the river were investigated. The first, upstream river stretch primarily gained groundwater and saw strong agreement in Q_{gw} estimated with specific conductance mass balance, differential gaging, EMMA, and hydrograph separation. Q_{gw} ranged from -18 to 50 m^3/s, and correlated positively with river discharge. Negative and positive Q_{gw} indicates net losing and gaining conditions, respectively. The second, downstream river stretch both gained groundwater and lost river water to the aquifer, again with strong agreement in estimated Q_{gw} using the same four methods as above. Calculated Q_{gw} ranged from -155 to 112 m^3/s, and, in contrast to the upstream stretch, correlated negatively to river discharge. The Dupuit equation-based estimates differed significantly from the other methods' estimates in both studied

stretches of the river. It predicted a consistent, negative correlation between Q_{gw} and river stage since the contrast in hydraulic heads between the aquifer and the river drives flow. Interestingly, just the opposite was observed in the upstream river stretch.

Where and when the Brazos River is losing and gaining, and how much water is exchanged has implications for managers of the river and the Brazos River Alluvial Aquifer (BRAA) that surrounds it. The results of this study will help managers of these two water bodies better understand the dynamics of their connection, and make better decisions about how much water can be allotted to prospective users and when.

ACKNOWLEDGEMENTS

I must thank all those who helped me in the field: Taylor Rowley, Daniel Tebo, Jonathan Whitmore, Shishir Basant, Pin Shuai, Katrina Jewell, Jason Paul, Rodrigo Rodriguez, Victoria Lopez, James Hootsmans, Nick Durhman, Azzah Hassan, Hayden Crockett, Jake Zerr, Sam Amin, Amy Price, and Patrick Glass. This was a field work-intensive project, and I would not have any data without you! I particularly want to commend those who got heat-stroke while helping me in the middle of the Texas summer when it was 110˚.

I would also like to thank the Texas Water Resources Institute (TWRI) for generously awarding me the TWRI Mills Scholarship to fund my studies as I completed this project. Gratitude also goes to my advisor, Dr. Peter Knappett, for providing ample guidance along the way.

NOMENCLATURE

A	Drainage basin area
ADCP	Acoustic Doppler current profiler
BFI	Baseflow index
BRA	Brazos River Authority
BRAA	Brazos River Alluvial Aquifer
C_d	Downstream river concentration
C_g	Groundwater concentration
Cl^-	Chloride
C_r	Concentration in river
C_u	Upstream river concentration
D	Time in days until end of overland flow
E	Evaporation
EMMA	Endmember mixing analysis
GWCD	Groundwater conservation district
h	Hydraulic head
I	Groundwater inflows
IC	Ion chromatograph
K	Hydraulic conductivity
masl	Meters above sea level
NOAA	National Oceanic and Atmospheric Administration

O	Outflows
PC	Principal component
PCA	Principal components analysis
Q	River discharge
Q_d	Downstream river discharge
Q_{gw}	Groundwater discharge
Q_{trib}	Tributary discharge
Q_u	Upstream river discharge
R	Rainfall directly onto the river
RTK	Real-time kinematic
SC	Specific conductance
SH21	State Highway 21
SH60	State Highway 60
TDS	Total dissolved solids
TNRIS	Texas Natural Resources Information System
TPWD	Texas Parks and Wildlife Department
TWDB	Texas Water Development Board
USGS	United States Geological Survey
VRS	Virtual reference station
w	River surface width

TABLE OF CONTENTS

Page

Page

Page

LIST OF FIGURES

Page

Page

Page

Page

Page

Page

Page

LIST OF TABLES

Page

1. INTRODUCTION

According to the Texas Water Development Board (2012b), the state of Texas currently does not have enough water to meet demands. This deficiency is expected to increase through the 21st century as demand grows and supply decreases. The shrinking water supply makes it vital to accurately estimate all components of Texas water budgets. Many water plans use numerical and analytical models to estimate groundwater inflows to rivers, but applying these methods requires that many simple assumptions about the system be made (Langhoff et al., 2006). This is particularly true in Texas where few detailed studies about groundwater discharge to streams have been conducted. Groundwater, however, constitutes a significant portion of flow in lowland gaining rivers like many of those in Texas (Larkin and Sharp, 1992). It is a considerable part of many rivers' water budgets, and should therefore be calculated using the best techniques available and few simple assumptions.

The Brazos River is second in Texas, both in terms of length and drainage basin area, only to the Rio Grande (Kammerer, 1990). Surface water managers on the Brazos River who need to accurately predict the amount of water available for downstream users must start incorporating sophisticated groundwater input estimates in their water budget calculations. If they do not, they will likely under- or over-estimate the water available from the Brazos River, resulting in misallocations of increasingly vital water

resources. This study aims to provide a first long-term, high-temporal resolution characterization of groundwater discharges to a stretch of the Brazos River.

1.1 Objectives

1.) Provide a first long-term, high temporal resolution characterization of groundwater discharges to the Brazos River.

2.) Analyze the relationship between river and aquifer levels and groundwater discharge using the Dupuit equation. Aquifer hydraulic gradients are highly dependent on river stage in the BRAA (Chakka and Munster, 1997). Therefore fluctuations in the lateral hydraulic gradient at 200 m distance from the river should correlate to observed groundwater discharge.

3.) Compare Brazos River groundwater discharge estimates derived from multiple, traditional and new, physical and chemical methods.

2. LITERATURE REVIEW

Groundwater discharge to rivers has long been estimated using hydrograph separation. This method has many assumptions associated with it, however, and only measures net gains to the river. The weaknesses of this method have led many studies to start using chemical tracer methods that provide more detail about the waters discharging to rivers from the ground. Many of these studies have been performed in Australia where they have already started coping with scarce water supplies (McCallum et al., 2012; Unland et al., 2013; Yu et al., 2013). The 2011 drought in Texas, the worst single year drought in recorded history for the state (TWDB, 2012b), and the current severe drought in California, have now alerted Americans to the importance of understanding where their water originates.

One way water managers can allay fears of Americans who may be affected by water shortages is by using new methods to update and ensure the accuracy of their water budget calculations. This study will review many established and new methods to estimate the groundwater portion of river water budgets, then use some of them to calculate this variable in a stretch of one of the largest rivers in Texas: the Brazos River.

2.1. Estimating Groundwater Discharge

2.1.1 Hydrograph Separation

Hydrograph separation analysis estimates baseflow, the amount of flow contributed by groundwater, of a river or stream using only daily discharge data from a single gage (Halford and Mayer, 2000). Large peaks in the hydrograph are assumed to

be made up of runoff, and can be separated from the groundwater-derived baseflow portion of flow by connecting low points on the hydrograph (figure 2-1). Hydrograph separation is a simple method that can be performed easily and quickly through automated computer programs. It can be applied at the entire watershed scale to estimate how much baseflow contributes to a stream overall, which is valuable to water managers regulating entire rivers. It is difficult, however, to apply to highly regulated rivers (Yu et al., 2013) because automated programs often mistake dam-release flood pulses for precipitation events. Hydrograph separation also cannot differentiate between different sources of water released slowly to rivers. It combines all sources that flow slowly into the river after a storm event, such as interflow and bank return flow, with groundwater inflow from local aquifers (Halford and Mayer, 2000). Chemical tracers can be used to differentiate between these sources and better understand these components of a river's water budget (Yu et al., 2013).

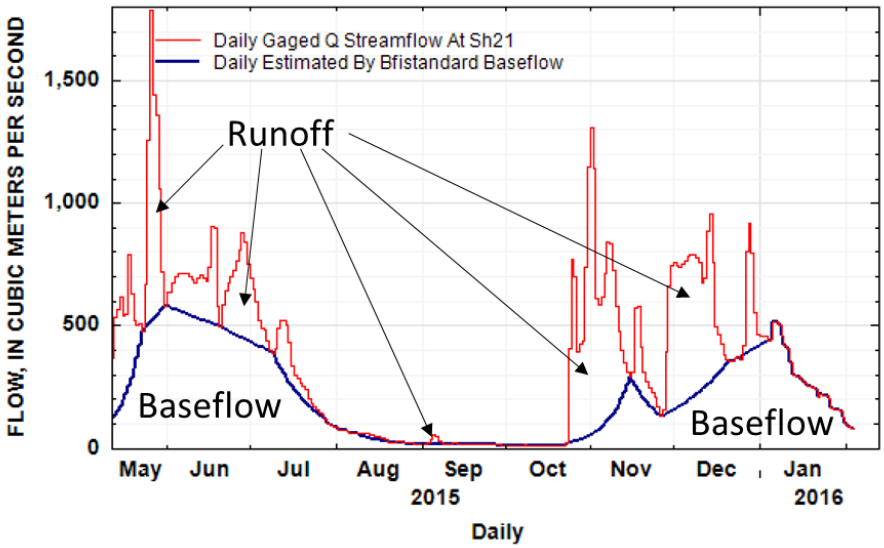

Figure 2-1: Example of the hydrograph separation method used to estimate the baseflow component of river flow. Low points on the stream hydrograph are connected, and the area above the connecting lines is considered runoff, while the area below them is considered baseflow.

Many studies still perform hydrograph separation, however, because it provides a quick check of discharge estimates from other methods. Yu et al. (2013) performed hydrograph separation to compare to groundwater discharge estimates derived using geochemical tracer methods on three different sections of the Ovens River in southeastern Australia. The three reaches Yu et al. (2013) investigated roughly correspond to three different regions from upstream to downstream along the river into which they divided their study area for investigation. The first upstream region is in the mountains and has many narrow v-shaped valleys. The furthest downstream region consists of a flat river flood plain where the river meanders and anastomoses, and the middle region is a transition zone between these two settings. In terms of physiology of the river and landscape, our study site on the Brazos River differs greatly from the

Ovens River stretches studied by Yu et al. (2013) because our site is completely low-land, low-slope, and far removed from any mountains.

For their hydrograph separation, Yu et al. (2013) compared results from the Nathan and McMahon (1990) and Eckhardt (2008) hydrograph separation methods at three different gaging stations. Each selected gage was roughly in the middle of one of the physiographic regions of their study area and presumed to give a valid estimate of baseflow for its respective region. Yu et al. (2013) used daily discharge data from October 2000 to October 2011, and found average baseflow values at each gage for the wet season (May to October) and dry season (November to April) over this period. They then converted these baseflow values to baseflow percentages, or the percentage of river flow made up by groundwater. The Nathan and McMahon (1990) method produced baseflow percentages for the wet and dry seasons, respectively, of 47 and 83% at the most upstream gage, 51 and 78% at the middle gage, and 49 and 79% at the furthest downstream gage. The Eckhardt (2008) method produced baseflow percentages that were generally lower. Baseflow percentages from this method were, for the wet and dry seasons respectively, 36 and 52% at the most upstream gage, 43 and 58% at the center gage, and 54 and 66% at the most downstream gage.

The groundwater discharge values from this method were much higher than values obtained using radon, a method that will be described below. Baseflow percentages obtained from radon measurements for the wet and dry seasons respectively were 3 and 2% at the upstream gage, 10 and 9% at the middle gage, and 16 and 12% at the downstream gage.

2.1.2 Differential Gaging

Various studies have used differential gaging to estimate groundwater discharge to rivers (Turco et al., 2007; McCallum et al., 2012; Unland et al., 2013; Yu et al., 2013). To perform differential gaging, discharge is measured at two different locations in a river, then the difference between those values is found. If there are no tributary or runoff inflows to the river between the two measurement points, then the difference in discharge can be attributed to groundwater inputs (McCallum et al., 2012; Unland et al., 2013). A study by Yu et al. (2013) used the following equation to perform differential gaging over three reaches of the Ovens River in southeastern Australia:

$$Q_{gw} = Q_d - Q_u + E - Q_{trib} - R \qquad (2\text{-}1)$$

where Q_{gw} is the groundwater discharge, Q_d is the river discharge at the downstream location, Q_u is the river discharge at the upstream location, E is evaporation, Q_{trib} is the discharge of all tributaries flowing into the river between the upstream and downstream measurement points, and R is rainfall onto the river during the differential gaging period. They performed these calculations over four separate dry periods when river discharge was low, R was zero, and surface runoff could be considered negligible. The Q_{trib} from three gaged tributaries were included in these calculations.

Using differential gaging the estimated groundwater discharge was 3.41×10^4 to 1.72×10^5 m^3/d in the upstream region, 5.58×10^4 to 2.00×10^5 m^3/d in the middle region, and 2.28×10^5 to 6.44×10^5 m^3/d in the downstream region. These were the ranges of average estimates obtained for March 2010, June 2010, June 2011, and October 2011. The river discharges at the downstream gages over these periods ranged

from 1.08×10^5 to 3.40×10^5 m^3/d in the upstream region, 2.81×10^5 to 8.12×10^5 m^3/d in the middle region, and from 9.96×10^5 to 2.61×10^6 m^3/d in the downstream region. They did not incorporate water travel times into their calculations likely because they were making average monthly estimates. This trend of increasing groundwater discharge to rivers as they flow downstream has been widely observed and is due to the relatively low elevation of the river relative to higher elevation areas where regional aquifer recharge occurs (Larkin and Sharp, 1992).

Unland et al. (2013) estimated groundwater discharges to the Tambo River in southeastern Australia, also using differential gaging. Their study, however, did not focus on dry periods when runoff could be considered negligible. Unland et al. (2013) instead included values for R of measured direct rainfall on the river that were greater than zero. Whereas Yu et al. (2013) did not incorporate water travel times into their calculations, Unland et al. (2013) did incorporate them. When no peak flows occurred during the study period, they used the water velocity and distance from upstream gage to downstream gage to estimate travel time. They found water velocity from gage-measured discharge, and river width and depth that were measured in the field with a tape-measure. When storm peaks did occur, they time-shifted the data at one of their gages until the peak events appeared to occur at the same time. Differential gaging was performed by subtracting the upstream discharge from the downstream time-shifted discharge.

2.1.3 Tracer Methods

Tracers used to calculate groundwater discharge to a river can be naturally occurring in the watershed, or injected during a study. In order for natural chemicals to make good tracers, they must have contrasting concentrations in groundwater and surface water (Huggenberger et al., 1998; Kendall et al., 2001; McCallum et al., 2012; Yu et al., 2013). This contrast in the water bodies' chemistries makes differentiation of the two sources possible. Heterogeneity in the sources is ideally minimal, but if it exists, should be understood as well as possible (McCallum et al., 2012; Yu et al., 2013). Natural tracer methods are unlike differential gaging in that they can measure only groundwater discharge to a river, not water losses from the river. Some injected tracers, like sulfur hexafluoride (SF_6), are particularly useful for estimating groundwater discharge because their background concentration in groundwater is extremely low or zero (Gamlin et al., 2001). This eliminates the problem of heterogeneous groundwater concentrations that often occurs when using natural tracers, though it must be noted that injection of foreign substances can alter the natural river habitat and thereby have adverse effects on the ecosystem.

2.1.3.1 Specific conductance. A useful natural tracer for estimating groundwater discharge to a river is total dissolved solids (TDS), which can be approximated from specific conductance. Specific conductance values may be converted to total dissolved solids (TDS) by multiplying them by 0.65 (Pai et al., 2015). Specific conductance is the conductivity of the water normalized to a specific temperature, usually 25˚C (Maupin et al., 2013). Conductivity is a measure of how well electricity can flow through the water,

and is related to the concentration of ions in the water, as well as the temperature of the water (Maupin et al., 2013). It is commonly measured in milliSiemens per cm (mS/cm) or microSiemens per cm (µS/cm). The specific conductance of precipitation is usually ~10 µS/cm, and surface waters from quick runoff that have had limited interaction with soils tend to have specific conductances less than 100 µS/cm. The specific conductance of groundwater is usually relatively high with values greater than 500 µS/cm (Kronholm and Capel, 2014). The contrast in typical specific conductance values of ground and surface waters makes specific conductance a highly useful indicator of groundwater discharge to a river in many settings.

One way specific conductance can be used to estimate groundwater discharge is by travelling downstream the run of the river and taking specific conductance measurements every few meters along the way. This technique is referred to as a longitudinal survey throughout this thesis. A longitudinal survey can provide high spatial resolution information about where exactly groundwater discharge is occurring. Pai et al. (2015) conducted this kind of survey 13 times on a reach of the Lower Merced River in Central California over a range of flow conditions at different times of the year. The Lower Merced River is a low-land meandering river like the Brazos, but it receives water from snow-melt, as well as reservoirs. The researchers used the following equation and specific conductance measurements taken only a few river-m apart to calculate average groundwater discharges along every river-km:

$$Q_{gw}C_g = Q_dC_d - Q_uC_u \qquad (2\text{-}2)$$

where Q_{gw} is groundwater discharge to the river (m^3/s), C_g is the total dissolved solids of the groundwater (mg TDS/L), Q_d and Q_u are, respectively, the downstream and upstream discharges of the river (m^3/s) as derived from an upstream river gage, and C_d and C_u are the downstream and upstream total dissolved solids of the river water, respectively (mg TDS/L). To obtain groundwater discharge estimates, Pai et al. (2015) used specific conductance values observed in the river at the beginning and end of each 1-km estimation reach.

Natural tracer methods only work if the endmember concentrations of the tracer are well characterized in the aquifer. To find appropriate specific conductance values Pai et al. (2015) obtained historical groundwater specific conductance values in their study area and used GIS to interpolate the values closest to each of their 1-km estimation reaches. They assumed a constant river discharge during each of the 13 surveys, though this could be improved upon in future studies by taking actual river discharge measurements at the beginning and end points of each estimation reach.

Pai et al. (2015) found that the central area of their studied river reach was consistently gaining the most groundwater. This area corresponded to locally high groundwater levels according to historical water table elevation data. They acknowledged that their study could have been improved by obtaining groundwater level and quality data at more locations within 1 km from the river. Much of their data came from a larger region around the river and was only available seasonally. They found that the specific conductance of the groundwater did not vary substantially over time, but values taken closer to the river would have been useful. Having continuous rather than

seasonal water level data during their study period would also have helped improve understanding of local gradients affecting groundwater discharge to the river at different times of year. Overall they found that cumulative groundwater discharge over their entire study area made up less than 15% of river flow and that most of that was entering the river in the middle of their study segment.

2.1.3.2 Chloride. Chloride (Cl^-) is a naturally occurring element present in nearly all watersheds around the world. It is generally considered conservative and therefore can be used as a natural tracer of groundwater flows when its concentrations in ground and surface water are highly contrasting. Yu et al. (2013) calculated groundwater discharge to the Ovens River in southeastern Australia using chloride mass balances. They used measured Cl^- concentrations and the following equation to estimate groundwater discharge:

$$I = \left(\frac{Q \frac{dC_r}{dx} - wEC_r}{C_g - C_r} \right) \qquad (2\text{-}3)$$

where I is groundwater inflows, Q is river discharge, C_r is the concentration of chloride in the river, x is the length of the stretch of river, w is river surface width, E is evaporation, and C_g is the concentration of chloride in the groundwater. They accounted for variation in groundwater chloride concentrations by using thee different C_i values depending on where in the watershed they were calculating groundwater discharge.

Using this method, Yu et al. (2013) calculated groundwater discharge in the three different regions of their study area (described above) at both high and low river flows. At high river flows they calculated groundwater inflow of 0.5 to 34.8 $m^3m^{-1}d^{-1}$ (with an

average of 3.3) in the upper region, 0.1 to 1400 $m^3m^{-1}d^{-1}$ (with an average of 1.1) in the middle region, and 0.1 to 13.2 $m^3m^{-1}d^{-1}$ (with an average of 0.3) in the lower region. During low river flows the estimates were generally lower, with inflows of 0.3 to 3.4 $m^3m^{-1}d^{-1}$ (with an average of 0.8) in the upper region, 0.1 to 6.0 $m^3m^{-1}d^{-1}$ (with an average of 0.5) in the middle region, and 0.1 to 0.8 $m^3m^{-1}d^{-1}$ (with an average of 0.2) in the lower region. This method calculated decreasing groundwater inflow in the downstream direction, which contradicted the increasing trend observed using the hydrograph separation and differential gaging methods described above.

To investigate the effects of differing background groundwater Cl^- concentrations, Yu et al. (2013) performed their calculations again using higher and lower Cl^- concentrations. Whereas increased groundwater Cl^- concentrations led to lower calculated groundwater discharges, decreased Cl^- concentrations led to higher calculated groundwater discharges. They also found that smaller differences between river and groundwater Cl^- concentrations increase the error in the groundwater discharge estimate. That is why the best tracers are those with highly contrasting values in ground and surface waters.

Unland et al. (2013) also used river discharge and Cl^- concentrations to estimate groundwater discharge to two southeastern Australian rivers. To estimate the groundwater concentration to input into equation 2-3 Unland et al. (2013) averaged Cl^- concentrations from five separate wells in the northern part of the watershed of the Tambo River. The same value was used for calculations in the nearby Nicholson River. This was because no closer wells were available and historical data from Australia's

department of Environment and Primary Industries indicated the watersheds have similar chemistries. On the Tambo River, they found that during low flow their calculations estimated that groundwater made up 2.4% of flow, and 0.61% of flow during intermediate flow conditions. On the Nicholson River Cl^- measurements indicated that groundwater comprised 29.4% of flow during low flow, and <7% of flow during high flow.

2.1.3.3 Radon. Radioactive isotopes of radon, like specific conductance, are groundwater tracers that can be used to measure groundwater discharge to surface water bodies. Unlike specific conductance, they are non-conservative tracers (McCallum et al., 2012). The radioactive isotopes of radon are ^{222}Rn and ^{220}Rn, originating from the parent elements ^{238}U and ^{232}Th, respectively (figure 2-2). Radon isotopes can typically be found in high concentrations in water residing in clastic sediments (Baeza et al., 1995) or granitic, igneous rocks (Shabana, 2013) made up of high concentrations of U and Th (de Oliveira Lucas and Ribeiro, 2006).

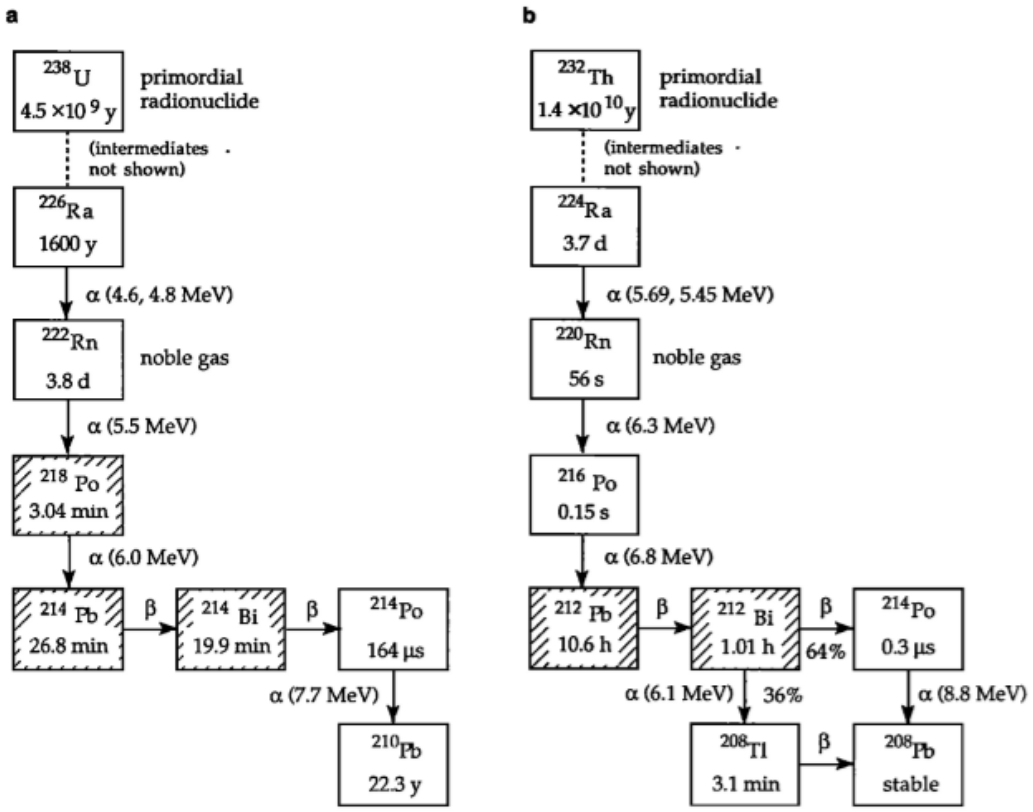

Figure 2-2: Decay chains of ^{222}Rn and ^{220}Rn. ^{222}Rn originates from ^{238}U, and ^{220}Rn originates from ^{232}Th. Diagram from Nazaroff (1992).

The radioactive isotope ^{222}Rn is a useful indicator of areas where groundwater is seeping into surface water. This isotope has a half-life of 3.8 days (Swarzenski, 2007), which means it will not stay in the surface water body long after groundwater discharge occurs, but it will remain long enough for measurements of its concentration to be made. In contrast to ^{222}Rn, ^{220}Rn has a half-life of only 55.6 seconds, making it more difficult to use as a tracer of groundwater inflow (Swarzenski, 2007) because it does not remain in the water long enough for measurements of its concentration to be made. ^{222}Rn also generally occurs in the highest concentrations out of all the elements in its decay series

because it is an inert noble gas that does not easily react to form different chemical compounds. The fact that it is a gas also means that it degasses out of surface waters quickly. Its detection in a surface water body very likely means that a groundwater source is close to the detection point (McCallum et al., 2012). These characteristics make ^{222}Rn the more powerful of the two radon isotopes as a tracer of groundwater inflow to rivers in many watersheds.

A study by Yu et al. (2013) used radon isotopes to estimate groundwater discharge to the Ovens River in Victoria, Australia, between September 2009 and October 2011. They conducted eight individual sampling rounds during which they found radon activities of the Ovens River at 19 different locations along a 200-km long stretch. They input these values into the following equation to find groundwater discharge in each stretch:

$$Q\frac{dC_r}{dx} = I(C_i - C_r) + wEC_r + F_h - kdwC_r - \lambda dwC_r \quad (2\text{-}4)$$

In this equation, Q is stream discharge, C_r is the ^{222}Rn activity in the stream, x is the distance downstream, I is the inflow rate of groundwater per unit stream length, C_i is the ^{222}Rn concentration of the groundwater, F_h is the ^{222}Rn flux from the hyporheic zone, w is the river surface width, d is average stream depth, E is the evaporation rate, k is the gas transfer coefficient, and λ is the radioactive decay constant.

For their groundwater discharge calculations, Yu et al. (2013) found Q at each of their 19 locations by linearly interpolating stream discharge measurements from five gaging stations. They found d and w by estimating while at each sampling site, and used E values obtained from Australia's Bureau of Meteorology. They assumed the F_h would

be small, so they left it out, but they estimated k using the O'Connor and Dobbins (1958) and Negulescu and Rojanski (1969) modified gas transfer models. For λ they used the value of 0.181 day^{-1} for ^{222}Rn. They used three different groundwater ^{222}Rn activities (C_i) depending on where in the basin they were calculating groundwater discharge. These values were chosen based on multiple groundwater ^{222}Rn activity measurements taken throughout the watershed.

Using these measurements they found most reaches of the river to be gaining during all 8 of their sampling rounds. They split their study area into three regions as described above. Using radon measurements they found the first region to be gaining 0.4 to 9.0 $m^3m^{-1}d^{-1}$ (with an average of 1.0 $m^3m^{-1}d^{-1}$), the middle region to be gaining 0.3 to 24.4 $m^3m^{-1}d^{-1}$ (with an average of 2.3 $m^3m^{-1}d^{-1}$), and the lower region to be gaining 0.2 to 24.1 $m^3m^{-1}d^{-1}$ (with an average of 1.1 $m^3m^{-1}d^{-1}$). They found one location in the upper region that had consistently high ^{222}Rn activities, suggesting a major seepage point of groundwater into the river. In general they found that groundwater discharge increased with increasing river discharge, though the percentage of flow made up by groundwater tended to be higher during low flows.

To investigate the effects of variability in groundwater ^{222}Rn activities, they re-calculated groundwater discharge using the higher and lower observed groundwater ^{222}Rn activities. They found that with the higher groundwater activities, calculated groundwater discharge decreased, and with lower activities, calculated groundwater discharge increased.

These ^{222}Rn activity-based measurements gave lower groundwater discharge estimates than differential gaging and hydrograph separation. The calculations based on ^{222}Rn for the upper and middle regions gave lower groundwater discharge values than Cl mass balance calculations, and higher values of groundwater discharge than obtained from Cl mass balance calculations in the lower region.

Another study by Unland et al. (2013) also used ^{222}Rn as a tracer to estimate groundwater discharge to the Tambo and Nicholson Rivers in southeastern Australia. For their mass balance calculations, Unland et al. (2013) used river discharge measurements interpolated from nearby gages, and an average of five groundwater radon activities to represent the groundwater endmember. River depths and widths were measured in upstream reaches using a tape measure, and widths were estimated for wide downstream reaches using Google Earth. For their calculations Unland et al. (2013) found average river depths, widths, and gas transfer velocities for each river stretch over which they estimated groundwater discharge. On the Tambo River they found groundwater discharge calculated from ^{222}Rn activities made up 10.5 to 21.4% of river flow at low flows, and 6.83 to 7.44% of river flow during intermediate river flows. During high flows they calculated that groundwater made up 8.2 to 12.7% of river flow. On the Nicholson River they found groundwater made up 18.9% of river flow under low flow conditions, <1% of flow under intermediate flow conditions, and 10.9 to 14.9% of river flow at high flow.

2.1.3.4 Endmember mixing analysis (EMMA). Another effective method to estimate groundwater discharge to rivers, established by Hooper et al. (1990), is

endmember mixing analysis. Endmember mixing analysis has been employed in many studies on quantifying the mixing of soil, surface runoff and alluvial aquifer water in rivers and streams. It has been used to estimate groundwater discharge to rivers, and characterize river water losses to aquifers (Filippini et al., 2015; Gracz et al., 2015; Rahman et al., 2015; Li et al., 2016). This method assumes that the studied body of water receives water from at least three other water bodies, called endmembers. It uses the concentrations of natural tracers found in these endmembers and the water body of interest, and an "unmixing model" to determine the contribution of water from each endmember to the water body being studied. It is different from the other tracer methods described above in that it does not only estimate the input of a single groundwater endmember to a surface water body. It can be used to find out how much of at least three different water bodies make up the water in a river at a given time. These water bodies can include precipitation, runoff, and tributary inflows, as well as different kinds of groundwater, such as those from different soil horizons, or older or younger groundwater.

When performing an endmember mixing analysis, the best ions to use for the studied area must first be determined. The only ions that can be used must occur with very different concentrations in each endmember (Hooper et al., 1990). When this is not the case, the mixing ratios cannot be determined using that ion. Ions that are highly reactive or strongly affected by biological activity cannot be used (Hooper et al., 1990). The study by Hooper et al. (1990) found that potassium, ammonium, and nitrate were either highly reactive or strongly affected by biological activity at their study site,

making them inappropriate to use in their analysis. Such ions are non-conservative and do not make good tracers. In the study by Hooper et al. (1990), alkalinity, sulfate, sodium, magnesium, calcium and dissolved silica were found to be conservative, and therefore appropriate solutes to use in their endmember analysis.

After identifying the correct ions to use in the analysis, the average concentrations of the three endmembers can then be identified. As with all natural tracer methods, the EMMA method works best if there is a homogeneous distribution of ions throughout each endmember body (e.g. aquifer). When the concentration of one of the selected conservative ions is plotted against the concentration of another, the endmembers should plot as three corners of a triangle that encloses the stream water sample concentrations (Christophersen et al., 1990; Hooper et al., 1990). Such a bivariate plot can be made for every possible pair of all the selected ions used in the analysis ($B = \frac{p!}{2(p-2)!}$ where B is the number of bivariate plots and p is the number of parameters). If the selected endmembers' concentrations form triangles surrounding the stream water concentrations on every plot, they can be called the correct endmembers with high confidence. If they do not form encapsulating triangles on a majority of the plots, then they are not representative endmembers and further work must be done to find ones that are appropriate. This is valuable because it informs researchers that they have missed an important contributing source to the stream or river they are studying (Hooper et al., 1990).

The EMMA method is useful because it can tell researchers whether they have found all the contributing sources to a stream. If the stream water contains conservative

elements or ions that were not found in any of the identified endmembers, that is an indication that there is another unidentified endmember for the stream (Hooper et al., 1990). This informs researchers that they must do further sampling to find the appropriate endmembers if they want to have a detailed, accurate characterization of the watershed of interest. This knowledge could be highly useful when endmember mixing analyses are used in conjunction with ^{222}Rn or specific conductance surveys to estimate groundwater inflow. If the major ions in the stream water do not match those of the waters used to determine the ^{222}Rn and specific conductance endmember values, it is an indication that a better characterization of the groundwater must be made before radon and specific conductance measurements can be used to estimate groundwater inflow.

Once the proper endmembers are identified, the proportion of stream flow contributed by each can be determined using an unmixing model. The unmixing model used by Hooper et al. (1990), from Christophersen et al. (1990), was

$$x = (C^T C)^{-1} C^T s \qquad (2\text{-}5)$$

where x is a matrix of the proportion of each endmember in a given water sample, C is a matrix of the concentrations of conservative chemical tracers in the endmembers, and s is a matrix of the concentration of conservative chemical tracers in the water samples. In the Hooper et al. (1990) study they identified three endmembers: groundwater, organic or soil water, and hillslope water. Using stream water samples they determined the proportion of flow that each endmember contributed to the stream at the time of sampling. Any study that identifies the proportions of different endmembers and takes stream flow discharge measurements at the time of sampling can calculate the amount of

groundwater in a stream. This is called chemograph separation (Genereux, 1998). If this is done concurrently upstream and downstream along the same river or stream, the groundwater discharge between the sites can be calculated.

2.1.3.5 Injected tracers. Many studies have used injected tracers to investigate water exchange between rivers and adjacent aquifers. Use of injected tracers to determine net water gains or losses over a stream reach is often referred to as dilution gaging. Payn et al. (2009) performed dilution gaging on a mountain stream in Montana during a baseflow recession. To estimate discharge at the beginning of their study reach they injected a known mass of sodium chloride (NaCl) a mixing length upstream from the beginning of their study reach. They monitored NaCl concentrations at the beginning of their study reach using an electrical conductivity meter. Assuming constant discharge and complete tracer mass recovery they estimated discharge at the starting point of their study reach using the known mass of NaCl released and the integral of the breakthrough curve of the tracer concentration observed at the point of interest until concentration returned to background levels. The equation they used was:

$$Q = \frac{M}{\int_0^t C(\tau)d\tau} \qquad (2\text{-}6)$$

where Q is stream discharge at the point of interest downstream of tracer injection, M is the known mass of tracer injected simultaneously, t is the time from injection until the concentration of tracer at the point of interest returns to background level, C is concentration at the point of interest, and τ is the time variable of integration. They repeated this process to find the discharge at the end point of their study reach, as well,

and found net groundwater inflows by subtracting upstream discharge from downstream discharge.

Injected tracers would be useful to quantify groundwater discharge to rivers from heterogeneous aquifer systems. A tracer with a concentration of zero in the aquifer, such as SF_6 (Gamlin et al., 2001), can be selected, eliminating the need to control for heterogeneity of the chemical in the groundwater. The concentration upstream can be calculated based on a known volume of tracer released and the river discharge at the time of release. The downstream segment can then be monitored for arrival of the tracer, and samples can be taken and tested to determine the concentration. Discharge measurements would need to be made at the time of sample collection to use this method, which is essentially a mass balance. An added benefit of tracking tracer arrival at the downstream location is that the travel time between upstream and downstream sites is indicated directly by the arrival time of the tracer. It does not have to be calculated indirectly using water speed and reach length. One drawback of this method, however, is that injection of foreign substances can be harmful to ecosystems. Ideally, tracers that are not harmful to biota would be selected.

2.2 Multi-Method Comparisons

Most studies estimating groundwater discharge to rivers use multiple different methods to obtain many comparable estimates. Yu et al. (2013) compared groundwater discharge estimates obtained using hydrograph separation, differential gaging, chloride mass balance, and ^{222}Rn mass balance. They found hydrograph separation and differential gaging gave larger estimates than Rn mass balances. Chloride mass balances

sometimes gave larger and sometimes gave smaller estimates than ^{222}Rn mass balances. Possible reasons Yu et al. (2013) gave for Cl^--based groundwater discharges being greater than Rn-based discharges include under-estimation of evaporation, and ground and surface water Cl^- concentrations being too similar.

Overall, Yu et al. (2013) observed that differential gaging and hydrograph separation distinguish between runoff and slow-release (delayed) components of flow. They do not, however, distinguish between the different components of delayed flows to the river, including bank storage, interflow, and regional groundwater, the way geochemical tracers can. Runoff is precipitation that lands on the land surface, then flows quickly to the river without infiltrating into the subsurface. Interflow is precipitation that infiltrates into the top layer of the subsurface, then flows fairly quickly to the river. Bank storage is dilute river water that flows into the banks adjacent to a river when direct precipitation and runoff inputs cause high river levels during a storm event. This water is dilute, with chemistry very similar to rain water, because it is made up primarily of direct precipitation and precipitation-derived runoff. Regional groundwater is water deeper in the ground than interflow water, and water that was in the ground before the water recharged to the banks of the river during the most recent storm event. It is further from the river than bank storage and is often characterized on a regional scale. Regional groundwater has been in the ground longer than interflow or bank storage, and therefore is referred to as old groundwater, while interflow and bank storage are referred to as young groundwater in this thesis (figure 2-3).

Recently recharged groundwater and bank storage that have been in the ground less than one to two weeks will have lower ^{222}Rn activities than older regional groundwater. This is because it takes one to two weeks for groundwater to reach equilibrium with aquifer sediments in terms of ^{222}Rn activities (Unland et al., 2013). Chloride concentrations in bank storage are also likely to be lower than that in regional groundwater because of the relatively short amount of time bank storage water has been in contact with aquifer sediments. It takes longer than one to two weeks for groundwater to come into equilibrium with aquifer sediments in regards to Cl^-, making Cl^- even less likely than ^{222}Rn to show young groundwater discharges to a river (Unland et al., 2013). Frequent exchange between the river and aquifer waters can lead to constant dilution of Cl^- concentrations in bank storage water, further decreasing Cl^-'s ability to trace young groundwater discharges (Unland et al., 2013). Using the regional groundwater values for ^{222}Rn and Cl^- concentrations, which are usually higher than bank storage and interflow concentration values, in groundwater discharge calculations would therefore estimate inputs to the river from regional groundwater and leave out the bank storage and interflow components of groundwater discharge to the river. This is why, Yu et al. (2013) explains, their geochemical methods produced lower total groundwater discharge values than differential gaging and hydrograph separation.

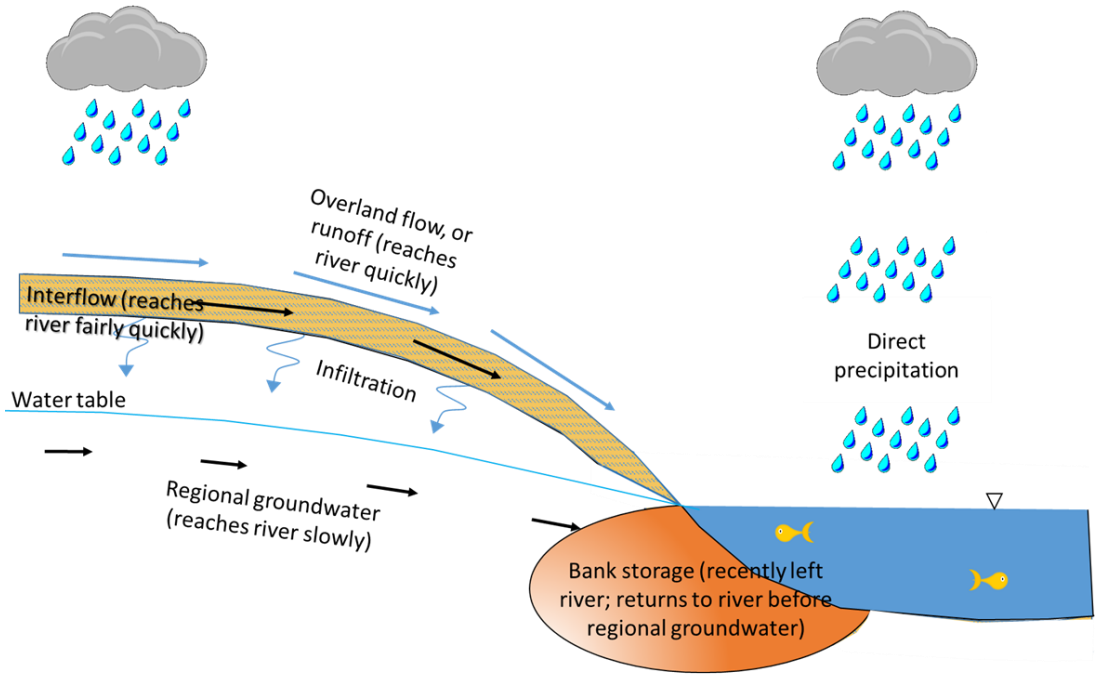

Figure 2-3: This figure shows a conceptual model of the waters that contribute flow to a river: Overland flow, or runoff, does not infiltrate into the ground. It flows over the land surface and reaches the river fastest during and immediately after a storm event. Interflow infiltrates into the top layers of soil before flowing toward the river slower than overland flow. Some precipitation infiltrates deeper into the ground than for interflow and becomes part of regional groundwater. This water flows slowest toward the river and arrives after runoff, interflow, and direct precipitation. Bank storage is river water that flowed into the ground immediately adjacent to the river when the river was at high flow during and immediately following a rain event. This water has a mix of river and rain water chemistry (i.e. dilute river water). Theoretically, before any regional groundwater can be detected in the river by geochemical tracers, bank storage must empty out and allow regional groundwater to take its place immediately adjacent to the river.

Unland et al. (2013) also compared groundwater discharge estimated with Cl^- and ^{222}Rn mass balance methods and differential gaging. They found groundwater discharge estimates from Cl^- mass balances were 1 to 2 orders of magnitude less than estimates derived from ^{222}Rn mass balances and differential gaging, while their radon-based estimates matched their differential gaging estimates well on the Tambo River.

One reason they thought their estimates differed was that there was inherent error in characterizing the groundwater endmember Cl^- and ^{222}Rn values. They took six samples from three different locations all within 20 m of the river, which may have resulted in sampling bank storage water with dilute chemistry not characteristic of the regional groundwater. They argue that their method of sampling so few samples from so close to the river may not have been adequate to accurately characterize regional groundwater in order to estimate its discharge to the river (Unland et al., 2013).

Unland et al.'s (2013) conclusions as to why their methods did not provide matching estimates of groundwater discharge mostly agree with those of Yu et al. (2013). Groundwater discharge estimates using the Cl^- mass balance approach were likely lower than those obtained with differential gaging because they measured only inflows from water similar to their six groundwater samples, and not total inflows from regional groundwater, bank storage, return flows, and interflow. The similar estimates of groundwater discharge obtained with the ^{222}Rn mass balance and differential gaging differ from the findings of Yu et al. (2013). Unland et al. (2013) argue that ^{222}Rn mass balance measurements may capture young groundwater inflows because ^{222}Rn goes into water quickly, even within a few weeks. Chloride does not dissolve into water as quickly from the majority of host minerals and therefore cannot be used to detect or quantify inflows of young groundwater.

2.3 Temporal Trends in Groundwater Discharge

Studies by Yu et al. (2013) and Unland et al. (2013) both found that groundwater made up the highest percentage of river flow during low flow periods, and the lowest

percentage during intermediate to high flows. They also found that groundwater discharge increased with river discharge. Both studies attributed this positive relationship to recharge of the surrounding aquifers by rainfall leading to higher water table levels immediately following a rain event, and high hydraulic gradients towards the river. Each of these studies only had a few spot groundwater level measurements to verify these conclusions, however, with nine measurements from Yu et al. (2013) and four from Unland et al. (2013). We attempt to verify these studies' conclusions by taking more frequent groundwater elevation measurements adjacent to the Brazos River.

2.4 Past Studies of the Brazos River and BRAA

Previous studies have specifically investigated the connection between the Brazos River and the BRAA. Chakka and Munster (1997) installed nine well nests in the alluvial aquifer, within 300 m of the river, just downstream of the intersection of the Brazos River with SH60, near College Station, TX. From these monitoring wells, they determined that groundwater flowed toward the river. These findings agreed with studies by Cronin and Wilson (1967), Chowdhury et al. (2010), and Turco et al. (2007), all of whom assert that the Brazos is gaining near College Station, TX. A more recent study by Proffitt (2015) provided geologic cross-sections of the alluvial aquifer. These cross-sections showed that the Brazos River is downcutting into sand and gravel layers of alluvium, providing more evidence of the hydrologic connectivity between the river and the aquifer. Both the Turco et al. (2007) as well as Chowdhury et al. (2010) studies, based on hydrograph separation, determined baseflow of the Brazos River. These efforts provided low temporal-frequency baseflow measures based solely on stream gage data.

Our study will provide much higher frequency groundwater discharge values obtained through more robust, modern methods, giving us more detailed knowledge about groundwater discharges to the Brazos River.

One previous study has undertaken an in-depth characterization of groundwater discharge to the Brazos River from the alluvial aquifer. This study by Turco et al. (2007) found a history of Brazos River baseflow using hydrograph separation. Using this method they compiled annual average baseflow values for the years 1966-2005 at three locations on the Brazos River between McLennan County, TX, and Fort Bend County, TX. They used these baseflow numbers and annual average streamflows to find annual baseflow indices for each of the three sites.

The baseflow index for a given time period is the average baseflow for that period divided by the average streamflow for the same period. Turco et al. (2007) found that annual baseflow as a percentage of streamflow was always higher at Hempstead, TX, (downstream) than at Highbank, TX, (upstream), indicating that the Brazos River has been consistently gaining in that stretch over time. This study provided useful insights into where the Brazos River is generally gaining groundwater. More detailed investigations, however, into exactly how much water the Brazos River is gaining and when have not yet been performed. Such studies would be useful to water managers who have to account for differing seasonal water table levels in the aquifer and demands from the river, and make sub-daily decisions on reservoir water releases. A study on the Brazos River of this nature would aid the Brazos River Authority (BRA), the governing body that controls dam releases from Lake Whitney near Waco, TX.

To verify the results of their hydrograph separation, Turco et al. (2007) also used direct paired, near-synoptic discharge measurements to perform differential gaging to find gaining and losing stretches of the river during the wet season (March, 2006) and dry season (August, 2006). The region of Texas encompassing their study area is typically wet in the spring and fall, and dry in the summer and winter (TWDB, 2012b). Turco et al. (2007) found that their differential gaging measurements qualitatively agreed with their hydrograph separation results in indicating the gaining stretches of the river. Their physical study covered a large spatial area of the Brazos River and the BRAA, but provided estimates of groundwater discharge to the river at only two times of the year. Our study covers a smaller spatial area, but provides groundwater discharge estimates at high temporal frequency over eight months. This high frequency of measurements allows for close investigation of temporal changes in groundwater discharge volumes, and an improved understanding of the timing of groundwater discharge to a meandering, lowland river. Seasonal characterization of changes in groundwater discharge to a river has not been performed before using continuous records of both river and groundwater levels.

3. STUDY AREA

The main stem of the Brazos River begins in Stonewall County, Texas, at the confluence of the Salt and Double Mountain Forks. It meanders southeast through Texas for 1,352 river-km (TPWD, 1974) to where it empties into the Gulf of Mexico. The upper stretches of the Brazos River course through hilly terrain that transitions into flat coastal plains south of Waco (Cronin and Wilson, 1967). The river is dammed at Lake Whitney, which releases water periodically, causing hydropeaking detectable in our study area 266 river-km downstream.

The Brazos River Alluvial Aquifer (BRAA) starts below the Lake Whitney reservoir in Bosque County and follows the run of the river 563 km to Fort Bend County (Ashworth and Hopkins, 1995). The BRAA is composed of sand, gravel, and silt in a fining-upward sequence and is a semi-confined water table aquifer that receives recharge from rainfall, the Brazos River, and possibly other larger aquifers that underlie the BRAA (Chakka and Munster, 1997; O'Rourke, 2001; Wong, 2012). It is underlain by bedrock of interlayered shales and sandstones of marine and non-marine origin from the Tertiary. These formations underlying the aquifer also include impermeable mudstones that confine the bottom of the alluvium (Wrobleski, 1996). The alluvium is of Holocene and Pleistocene age, and is bounded on its sides by elevated Eocene deposits (Phillips, 2006). The river valley is generally made up of a floodplain and up to three alluvial

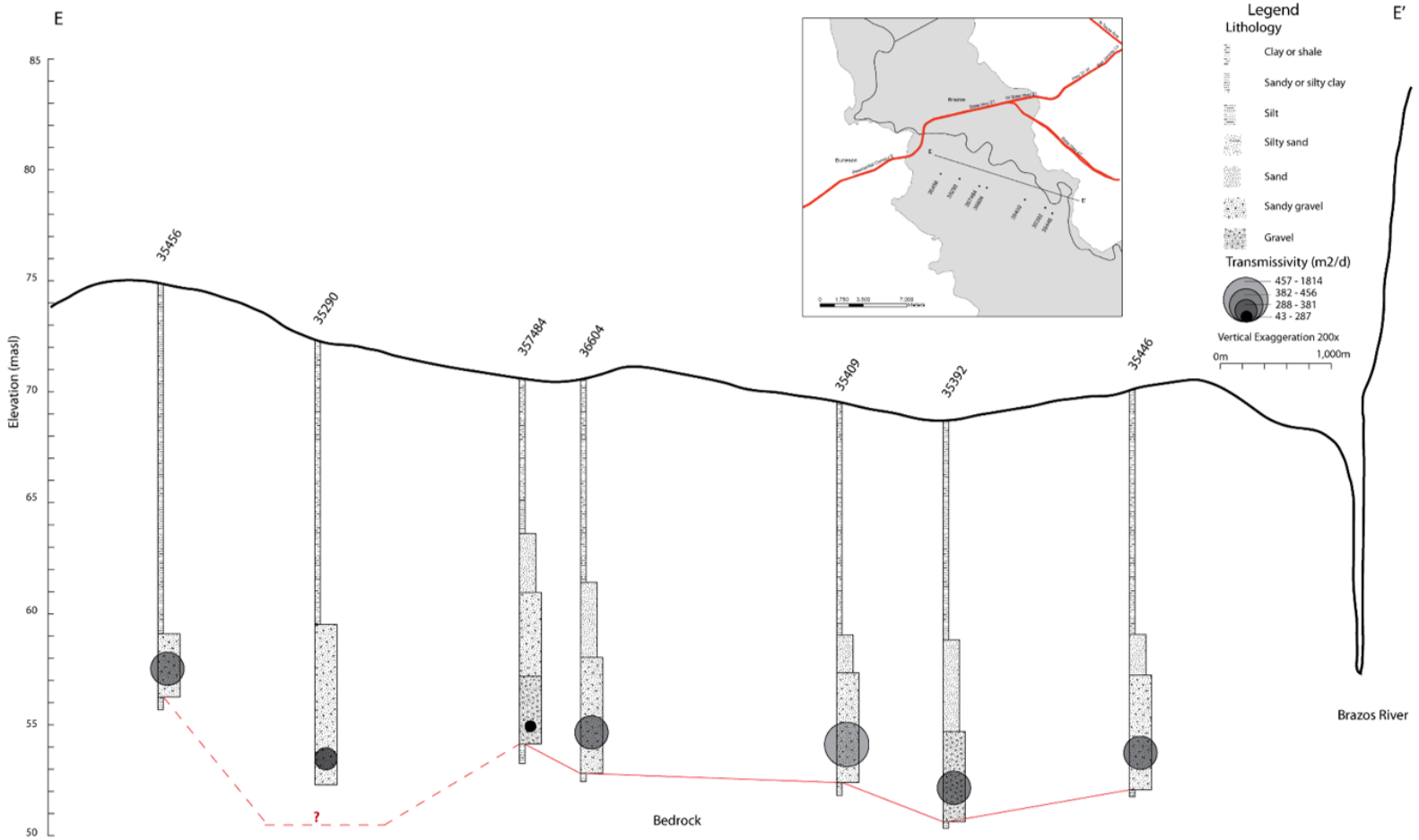

Figure 3-1: Cross-section of the BRAA and Brazos River generally parallel to the river from SH21 to SH60. The river downcuts into the sand and gravel layers of the aquifer. Cross-section from Proffitt (2015).

Pleistocene terraces (Phillips, 2006). Figure 3-1 shows a cross-section of the Brazos River and BRAA approximately from SH21 to SH60, the area corresponding to our upstream study stretch.

The major aquifers underlying the river near our study area include the Queen City, Sparta, Yegua-Jackson, and Gulf Coast aquifers (figure 3-2). The alluvial aquifer is thought to lose water to evapotranspiration in addition to wells that pump water almost exclusively for irrigation (HDR Engineering, 2001). The water table slopes towards the Brazos River in most places, causing aquifer water to discharge to the river, as well (Cronin and Wilson, 1967; Chakka and Munster, 1997; Shah et al., 2007; Turco et al., 2007; Chowdhury et al., 2010). The aquifer ranges from a negligible thickness to 51 m thick, with the majority of the aquifer being 15 to 24 m thick in our study area (Shah et al., 2007).

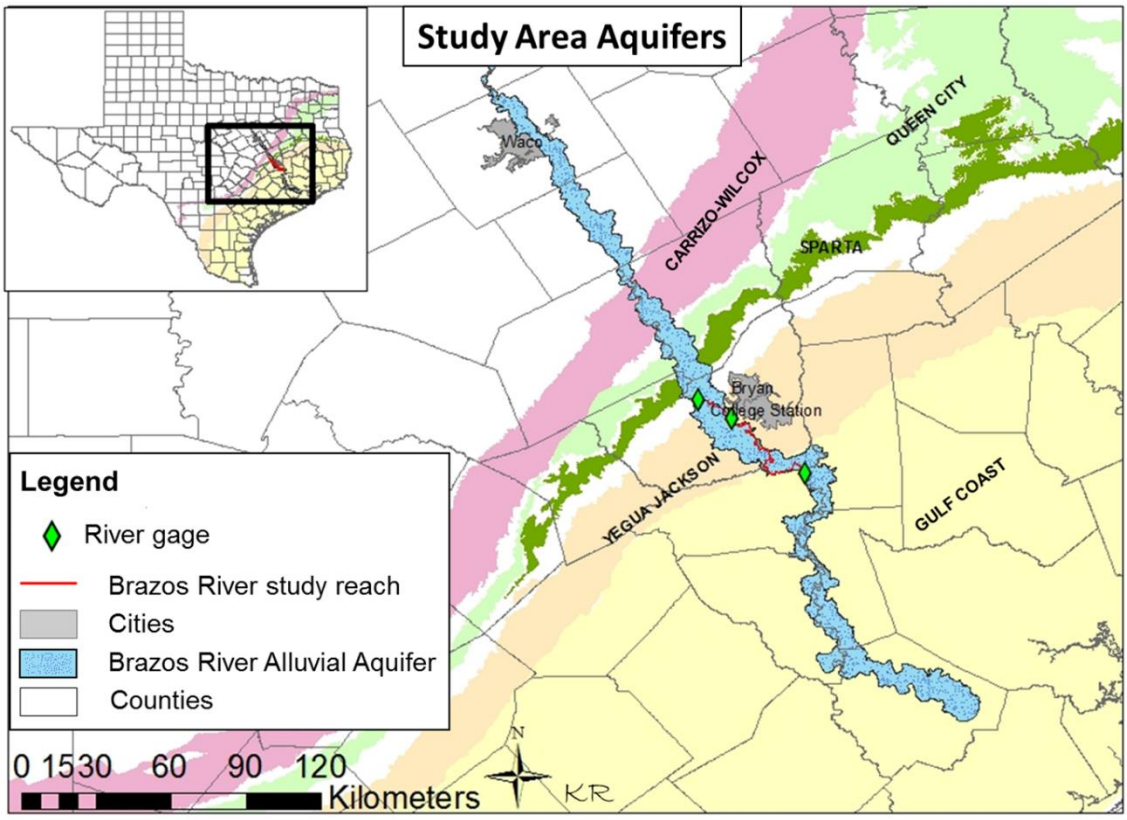

Figure 3-2: Map showing the extent of the Brazos River Alluvial Aquifer, outcrops of other aquifers, and our study area. Our gage sites are demarcated by green diamonds, and the studied stretches of the Brazos River are shown in red. Data provided by TNRIS (2015).

This study focuses on the stretch of the Brazos River and its alluvial aquifer from the intersection of the river with State Highway 21 near Bryan, TX, to its intersection with State Highway 105 by Navasota, TX (figure 3-3). In this stretch, the Brazos River meanders 96.3 river-km through alluvium, abutting the side of the river valley for long parts of the stretch (figure 3-3). In this stretch, the Brazos River borders Brazos, Burleson, and Washington Counties, which are in three climate regions of Texas: North Central, East Texas, and South Central (NOAA, 2016). Normal annual precipitation

ranges from 102 to 112 cm from the northwest to southeast parts of our study area (Nielsen-Gammon, 2011). Minimum temperatures were ~2 to 4˚C, and maximum temperatures were ~33 to 36˚C from 1971 to 2000 (Nielsen-Gammon, 2011).

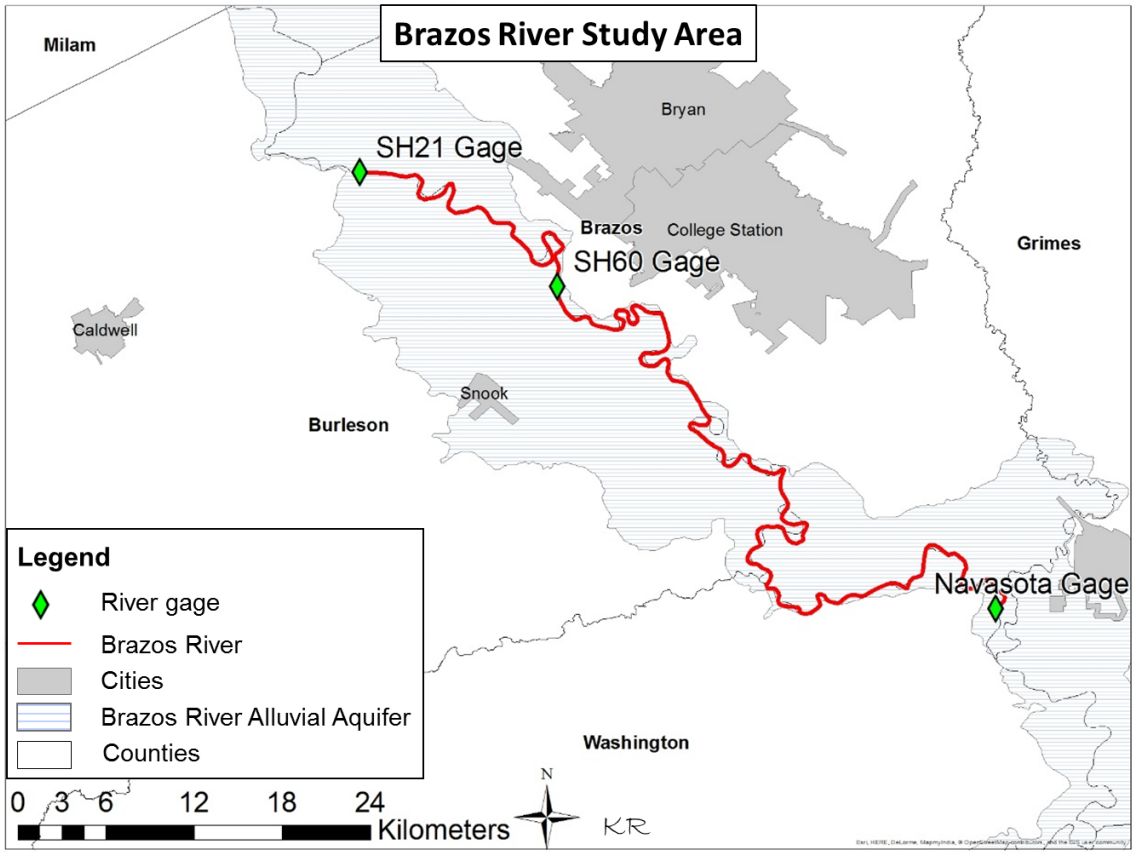

Figure 3-3: Map of the study area with political boundaries. The area starts at the Brazos River's intersection with SH21 by Bryan, TX, and continues to its intersection with SH105 by Navasota. The stretch of Brazos River studied is shown in red. Data provided by TNRIS (2015).

4. METHODS

4.1 Differential Gaging

River stage can be used to determine river discharge through use of a rating curve. A rating curve is a best fit line that correlates river level (the elevation of the surface of the river water, also referred to as river stage) to river discharge (Di Baldassarre and Montanari, 2009). It can be linear, but is usually exponential due to the parabolic shape of river channels. For this study we constructed three rating curves on the Brazos River, one each at SH21, SH60, and Navasota.

4.1.1 Rating Curve Development

Rating curves were constructed at each of the three study sites using static river stage measurements and corresponding discharge measurements taken with an Acoustic Doppler Current Profiler (ADCP) (M-9, SonTek, San Diego, CA). To obtain river discharge measurements, the ADCP was mounted to the front of an aluminum canoe using a custom built aluminum brace. Three to 10 perpendicular transects from shore to shore were made successively until measurements had a standard deviation less than three. Nearly all measurements met this criteria, though some high flow measurements had standard deviations as high as 16. The ADCP transects were performed about 100 m upstream of the bridges at each site when possible, usually at low flows. Sometimes at high flow the measurements had to be made about 100 m downstream of the bridge to avoid running into the pylons. The values for the 3 to 10 discharge measurements were averaged to get each single discharge value that was input into the rating curve. The

rating curves relate 5 to 11 discharge measurements to a corresponding river water surface elevation taken within 15 minutes of the last discharge measurement. This relation of river water elevations to discharges allowed us to obtain discharge measurements at each of our 3 gaging stations for all times that we had river stage measurements. Stage measurements were obtained at gaging stations every 20 minutes for 8 months by pressure transducers installed in stilling wells.

4.1.2 Obtaining High Frequency River Stage

We used two main types of pressure transducers to measure river stage within stilling wells: 1) those capable of measuring pressure and temperature, referred to herein as "LT" transducers (Levelogger Edge, Solinst Canada Ltd., ON, Canada), and 2) those that could also measure specific conductance, referred to herein as "LTC" transducers (LTC Junior Levelogger, Solinst Canada Ltd., ON, Canada). Initially, an LT transducer was installed at State Highway 60 (SH60, figure 3-3), from November 7, 2014 through September 11, 2015. After this time it was replaced with an LTC transducer at the same time as new LTC transducers were installed in new stilling wells at State Highway 21 (SH21) and State Highway 105 (Navasota). These provided 20 minute river stage, temperature and specific conductance through February 5, 2016. On this date two of the LTC transducers were downloaded at SH60 and Navasota. The remaining LTC transducer at SH21 could not be downloaded because the water level was too high to detach the stilling well from the bridge pylon. All stilling wells were attached to bridge pylons using non-destructive large hose clamps or metal bands (Everbilt Worm Gear Clamp, Homer TLC Inc., Wilmington, DE).

While river stage and temperature readings were taken at SH60 starting in 2014, these measurements can only be correlated to discharge with high certainty from May 28, 2015, to February 5, 2016. This period of known discharges at SH60 formed the time period of interest for our study. We had an LT transducer installed at SH21 only from September 10 to October 2, 2015. To supplement the river stage data collected at SH21 by our own gage, we also used river stage data from USGS gage 08108700 at SH21 near Bryan, TX, (http://waterdata.usgs.gov/nwis/uv?site_no=08108700) from May 28, 2015, to September 10, 2015, and from October 2, 2015, to February 5, 2016. This gave us a complete eight month period over which we could compare discharges at SH60 and SH21.

The pressure readings from our gages were corrected for atmospheric pressure fluxes using data from an air pressure logger (Barologger Edge, Solinst Canada Ltd., ON, Canada) that was stored in a lab on the Texas A&M campus from May 28 to December 4, 2015. We noticed in November, however, that the air pressure corrections for the submersed loggers located furthest away from campus were not fully removing air pressure fluctuations from the submerged pressure data. To resolve this, an additional air logger was installed at Batts Ferry Road (figure 4-1), and the existing logger was moved to SH21 for the last two months of the study period (December 4, 2015 to February 4, 2016). For these last two months we corrected Navasota and SH60 gage data using the Batts Ferry air logger. When data from the SH21 gage is downloaded in the future, it will be corrected using the SH21 air logger.

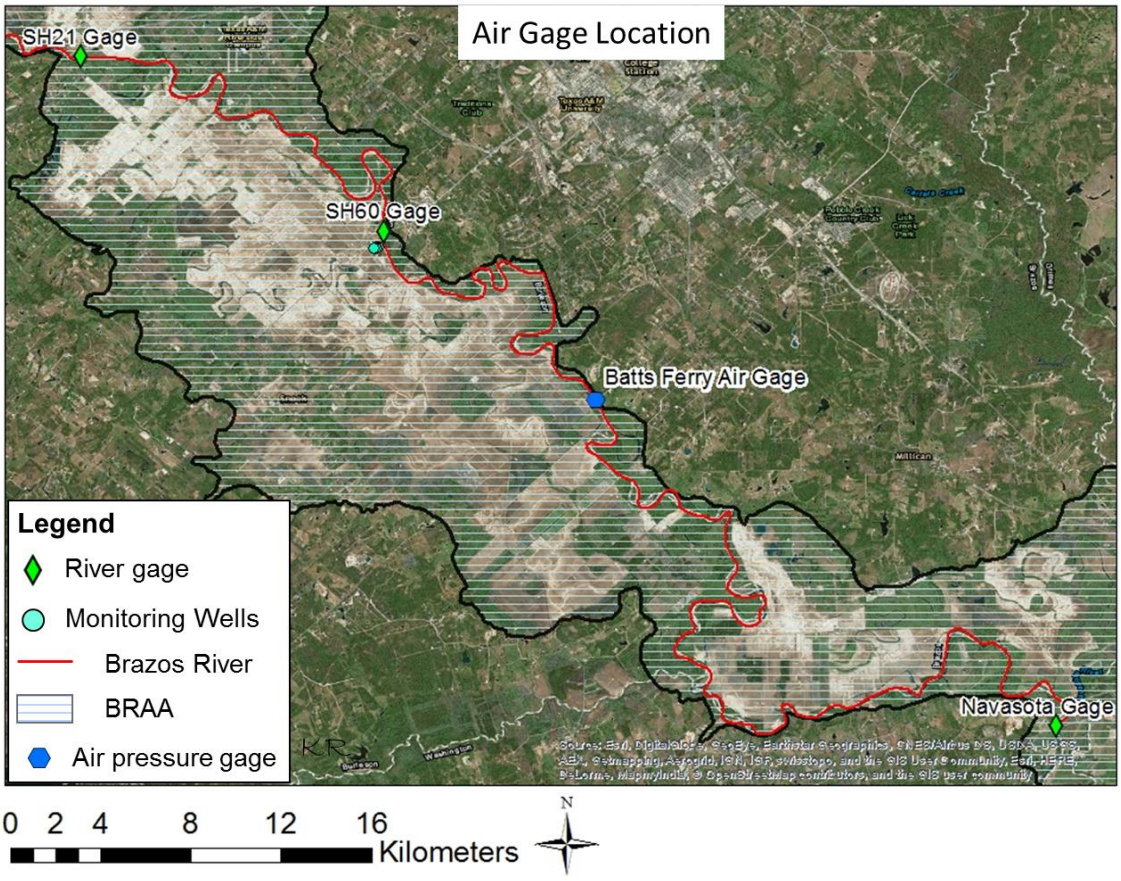

Figure 4-1: Map of the location of the Batts Ferry air pressure gage in relation to the river gages (SH60 and Navasota), and groundwater wells its data was used to correct. Satellite imagery provided by ESRI.

Atmospheric pressure-corrected submerged pressure readings were related to river stage by measuring the stage while the logger was in the river recording pressure data. To find the stage we installed onshore benchmark points and found their precise elevations (<1 cm accuracy) using a GPS receiver that performed real-time kinematic (RTK) measurements using a virtual reference station (VRS) network (Trimble R10, Trimble Navigation Ltd., Sunnydale, CA). We then routinely used a Total Station (GTX-226, TopCon Positioning Systems, Inc., Tokyo, Japan) to find the relative

difference between the water surface and the benchmark at 5 to 10 different river stages (figure 4-2).

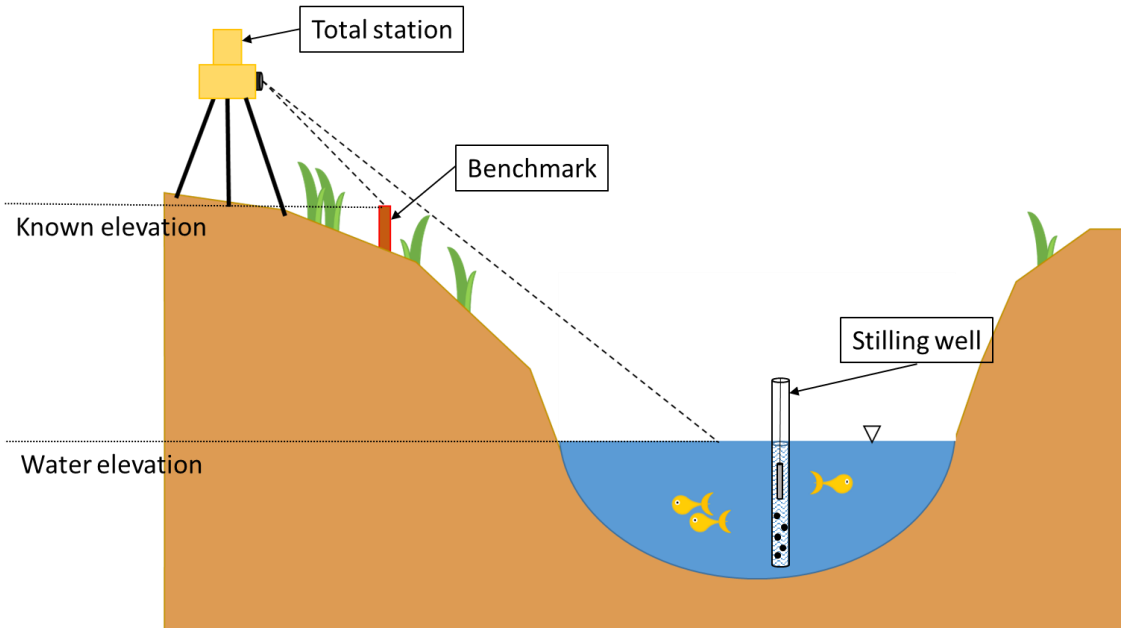

Figure 4-2: Depiction of how river stages were found in meters above sea level (masl). The elevation of the benchmark was known in masl, and the difference in elevation between it and the water level were found using a total station. This allowed us to find precise, comparable river elevations with which to construct rating curves.

4.1.2.1 Incorporating USGS stage data. The water surface elevation data obtained from the USGS gage 08108700 at SH21 was available every 15 minutes, while our data at SH60 was available every 20 minutes. To make these two data-sets comparable, water levels at SH21 were found every 20 minutes by finding weighted averages from the 15 minute data. For example, to find the river level at 20 minutes past the hour, the measure from 15 minutes past the hour was given a weight of 66.7%, and the measure at 30 minutes past the hour was given a weight of 33.3%, and the two

weighted levels were added to obtain the new 20 minutes past the hour measurement. We used the following equation for these calculations:

$$.667F + .333T = X \qquad (4\text{-}1)$$

where F is the USGS gage height at 15 minutes past the hour, T is the USGS gage height at 30 minutes past the hour, and X is the calculated gage height at 20 minutes past the hour. To find the gage height at 40 minutes past the hour, the 30 minute USGS measurement was again given the weight of .333, and the 45 minute USGS measurement was given a weight of .667. Measures taken on the hour were incorporated without weighted averaging.

To additionally ensure the USGS gage height-derived discharge values from SH21 were comparable to discharge data derived from our own gages, we input the USGS gage heights into the same rating curve equations into which we put our own SH21 gage heights. This gave us discharge measurements acquired using the same method throughout our study period (for additional information, see Appendix I). We did not use the USGS's discharge measurements because we do not know how they were obtained. They most likely were made using a method different from the one we used to obtain discharge measurements. Using the discharge equation derived from our method makes it more likely that any observed differences in discharge between SH21 and SH60 are real, not a byproduct of different measurement methods.

4.1.3 Differential Gaging Calculations

Once river stage had been related to river discharge, and high frequency discharge values were calculated from available stage data at all three river gages, we

were able to perform differential gaging. For these calculations we focused on dry periods when ungaged tributaries were inactive or stagnant (figure 4-3). Differential gaging was not performed during wet periods or storm events since we could not control for the amount of water entering the river from runoff. The equation used for differential gaging, from Turco et al. (2007), is

$$Q_{gw} = Q_{ds} - Q_{us} - I + O - R + E \qquad (4\text{-}2)$$

where Q_{gw} is the groundwater discharge to the river, Q_{ds} is the river discharge at the downstream site, Q_{us} is the river discharge at the upstream site, I is tributary inflows, O is outflows, R is return flows, and E is evaporation. Outflows, R, and E were not included in our differential gaging calculations because their values were considered small relative to errors in river discharge measurements (Turco et al., 2007). The need to include I was avoided in the stretch from SH21 to SH60 by focusing on dry periods. It was included between SH60 and Navasota because a gaged tributary, Yegua Creek, with discharge from the dam at Somerville Lake flowed into the river along that stretch.

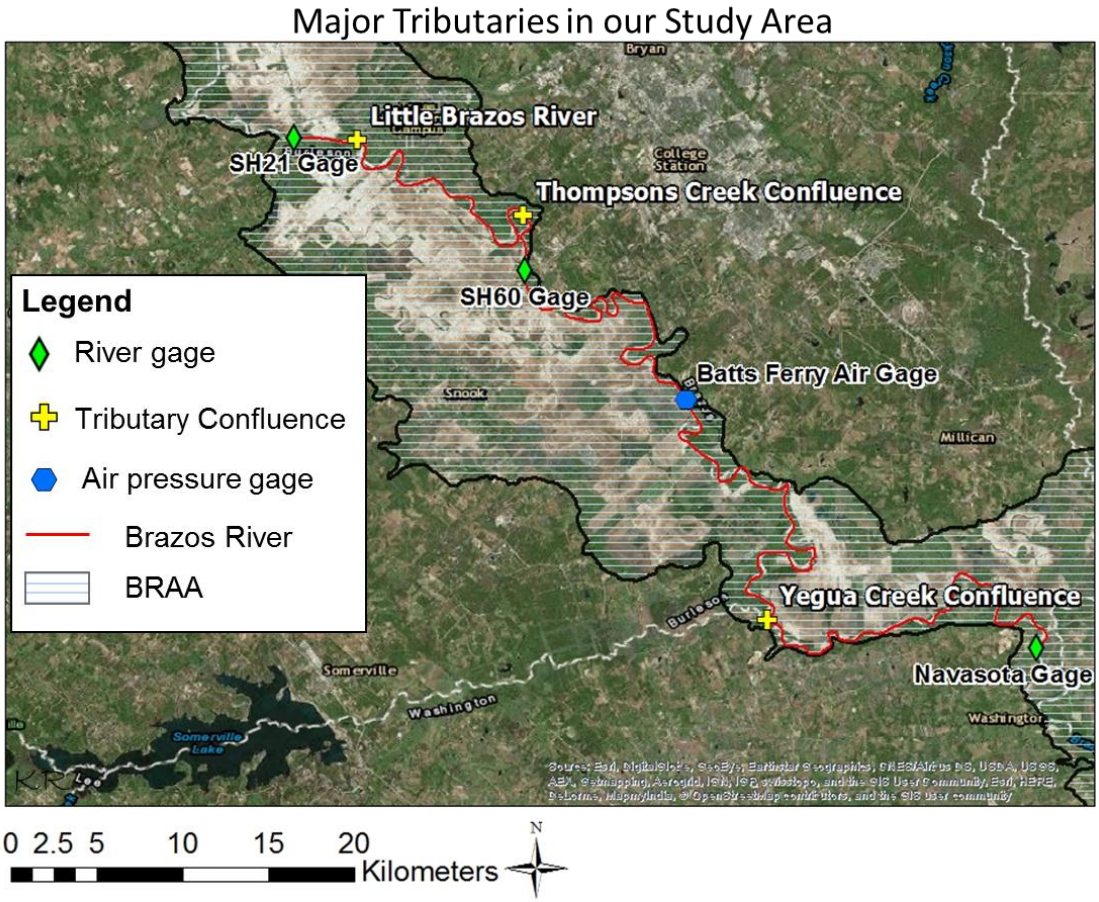

Figure 4-3: Locations of tributary inflows within our study area. Satellite imagery provided by ESRI.

4.1.3.1 Determining differential gaging periods. Differential gaging could not be performed while runoff was occurring or ungaged tributaries to the Brazos River were active. To estimate when runoff to the river ended, the time between a storm peak and the end of overland flow was determined using the relation

$$D = 0.827A^{0.2} \qquad (4\text{-}3)$$

where D is the time in days between a peak in river flow and the end of overland flow, and A is the area of the drainage basin in square kilometers (Linsley et al., 1975). The

drainage areas between SH21 and SH60, and SH60 and Navasota were calculated in ArcGIS using watershed outlines provided by the Texas Natural Resources Information System (TNRIS), and added to the area for SH21 to find the runoff times for those two gages. We further verified that tributaries were inactive during multiple longitudinal sampling campaigns down the river (see Longitudinal Surveys section under Specific Conductance below).

To determine periods for differential gaging, rain storm peaks were found for all three gages largely by both visual inspection of precipitation data and hydrographs, and finding local maxima in hydrographs in Microsoft Excel. Each period of differential gaging started D days after each storm peak. If another storm peak occurred within D days after the previous storm peak, then a differential gaging period would not be started until D days past the later storm peak. Differential gaging periods ended at the start of each new rapid rise in the river caused by storm events. These end points were determined by visual inspection of gage height graphs and precipitation data.

4.1.3.2 Determining lag times. As part of our differential gaging calculations, we had to correct for travel times of flood pulses from one river gage to the next. Subtracting discharges from gages when a flood pulse is passing one and a low point is passing another would distort the observed difference in discharge between the two sites. To correctly find the amount of water entering or losing a river in a stretch between two gage sites, the travel time of water from one site to another, or the lag time, must be accounted for in calculations (figure 4-4).

A different lag time was found for each period of differential gaging. The same lag time could not be used for all comparison periods because the water velocity, and therefore travel time between gages, changed with season and river stage. The lag times were found by close-up visual inspection of river stage data for each dry period. Three to four local maxima and minima were found in the stage data from the upstream and downstream gage sites during each dry period. The lag times between corresponding maxima and minima at the upstream and downstream gages were found and averaged to obtain a single representative lag time for each dry period.

Once the lag times were found, we subtracted them from the upstream site's measurement times during every dry period. This assigned each discharge measurement at the upstream gage new times that corresponded to the times at which distinct flood pulses passed the downstream gage. This time adjustment facilitated the comparison of distinct flood pulses as they appeared upstream and downstream so that we could see whether they had gained or lost water as they travelled from SH21 to SH60, or SH60 to Navasota (figure 4-4). In our differential gaging, discharge measurements with newly-matched times were subtracted upstream from downstream to find the change in discharge between sites.

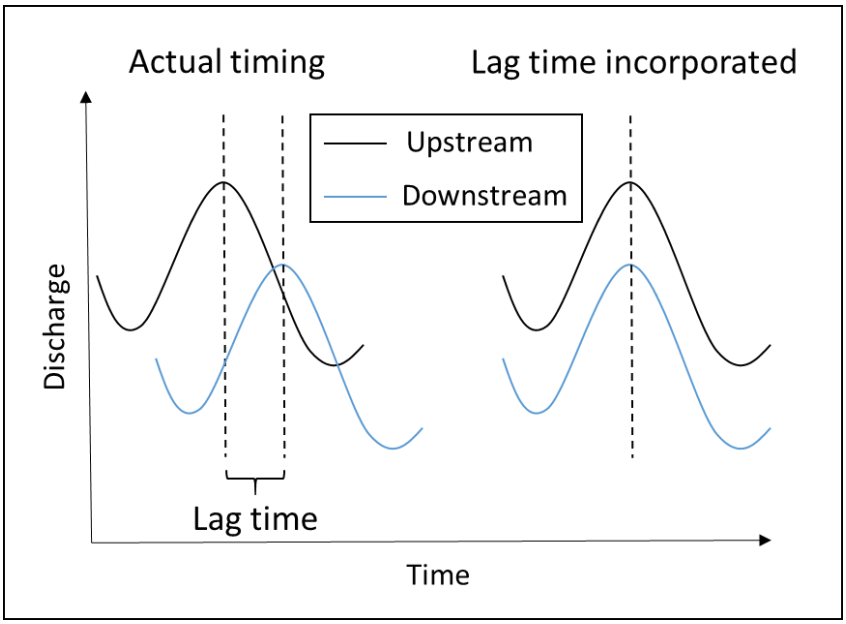

Figure 4-4: Depiction of hydrograph flood pulses at two gages graphed with real measurement times versus with a lag time incorporated.

4.2 Measuring Hydraulic Gradient in the Brazos River Alluvium Aquifer

Three LT transducers were installed in groundwater monitoring wells at the Research Farm site, just downstream of the intersection of the Brazos River with SH60 (figure 4-5). The monitoring wells were installed by a previous study (Chakka and Munster, 1997) in the Brazos River Alluvium Aquifer in a line perpendicular to the Brazos River, approximately 200, 280, and 420 m away from the river bank. All monitoring wells are 18 m deep and have 15 cm long screens at the bottom (Chakka and Munster, 1997). The LT transducers recorded water level data synchronously with the river gages every 20 minutes for approximately two years. Only eight months of data, from May 28, 2015, to January 29, 2016, was used in this study, however, because that

is the time period over which the other groundwater discharge calculation methods were completed.

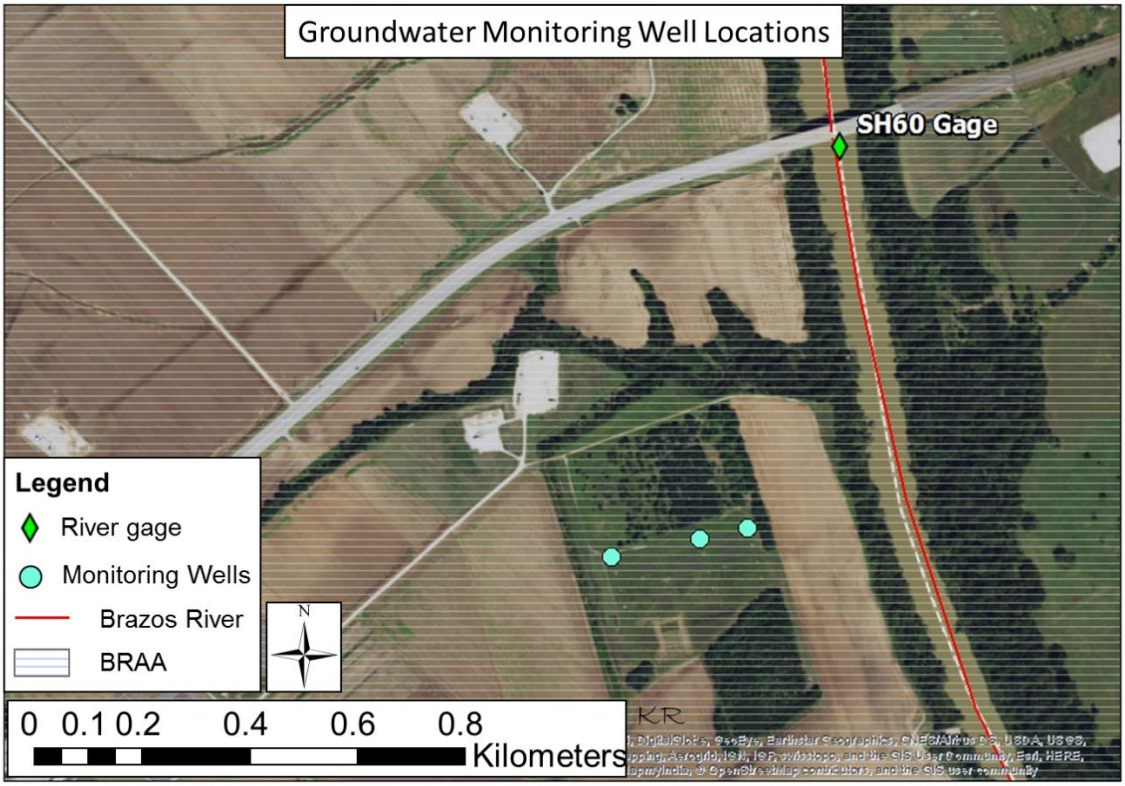

Figure 4-5: Map of the gaged groundwater well transect. All wells recorded aquifer levels, but only levels from the center well were used in Q_{gw} calculations. Satellite imagery provided by ESRI.

A correlation was made between groundwater discharge over the SH21 to SH60 Brazos River stretch and alluvial aquifer levels using the Dupuit equation:

$$q' = \frac{1}{2}K\left(\frac{h_1^2 - h_2^2}{L}\right) \qquad (4\text{-}4)$$

where q' is groundwater flow per unit width, K is hydraulic conductivity, h_1 is the head at the origin where L = 0, h_2 is the head at L, and L is flow length (Dupuit, 1863). We

chose this equation because it is appropriate for unconfined aquifers like the BRAA, and it accounts for a non-linearly sloping water table.

Using the Dupuit equation requires aquifer levels from only a single well. We chose to use water levels from the well in the middle of the transect because we were unable to download data from the pressure transducer in the well closest to the river. We did not use the well furthest from the river because we presumed larger fluctuations in aquifer level would be seen closer to the river. The data from the center well was corrected for air pressure fluctuations by subtracting air pressure readings taken from an air logger stored on the Texas A&M campus and then at Batts Ferry Rd, from May 28 to December 4, 2015, and December 4, 2015, to January 29, 2016, respectively. We found the aquifer water levels in meters above sea level (masl) by surveying the top of the well with a GPS receiver with RTK and VRS capabilities and measuring the water level in meters below the well top at the start and end of pressure measurements. The raw submerged pressure data was converted to water table elevation using the same two-step process described above for correcting the pressure data from submerged transducers in stilling wells (the Obtaining High Frequency River Stage section under Differential Gaging above).

Once we had obtained corrected aquifer levels, we were able to calculate groundwater discharge to the Brazos River from the BRAA using the Dupuit equation. The water table in the aquifer and river stage from SH60 in masl were input into MATLAB. Well water levels were entered into the Dupuit equation (equation 4-4) as h_1, and SH60 river levels were input as h_2. Length (L) was given a value of 280 m, the

perpendicular distance from the center well (Well B3-4) to the Brazos River. A value of $5.13x10^{-4}$ m/s, as previously calculated by slug tests at this Research Farm site by Shuai et al. (2014), was assigned to K. These calculations were run in MATLAB to obtain q' in m^2/s every 20 minutes from May 28, 2015, to January 29, 2016. To find groundwater discharge in the stretch from SH21 to SH60, these values were then multiplied by the straight distance from the SH60 gage to the SH21 gage. This calculation, however, only gives discharge from one side of the river. To obtain total Q_{gw} considering BRAA inflows from both sides of the river, these values were multiplied by two. These steps were repeated to find groundwater discharge from SH60 to Navasota using the straight distance from our SH60 gage to our Navasota gage.

4.3 Specific Conductance

4.3.1 Longitudinal Surveys

Four longitudinal surveys of specific conductance were carried out on the stretch of river between SH21 and SH60. For each survey a multi parameter meter (YSI Professional Plus, YSI Inc., Yellow Springs, OH) was mounted to the side of a canoe with the probe in the water. It was set to log specific conductance readings every 6 minutes as the canoe was paddled downstream from SH21 to SH60. The boat location during the survey was logged by a handheld GPS receiver (Garmin eTrex20, Garmin International Inc., Olathe, KS). Paddlers attempted to remain in the thalweg for the entire survey, but a few stops were made and recorded for on-the-spot chemistry sampling. Specific conductance data that appeared to be affected by sediments kicked up during these stops were filtered out of the final results. At these stops, which

occurred approximately every 4 river-km, water samples were taken and alkalinity measurements were made.

The specific conductance of alluvial aquifer water was measured at nine different wells within an approximately 4x4 km^2 area near the SH60 gaging site (figure 4-6). Prior to sampling the wells were purged until temperature, pH, and specific conductance stabilized. At this point the value of all parameters were recorded. The specific conductance values from all nine wells were averaged to provide a representative specific conductance for the aquifer water.

Once river water and groundwater specific conductance values were measured, they were converted to total dissolved solids (TDS) concentrations by multiplying by 0.65 (Pai et al., 2015). The following equation from Pai et al. (2015) was then used to calculate groundwater discharge to the river based on the results of the longitudinal surveys:

$$Q_{gw}C_g = Q_dC_d - Q_uC_u \quad (4\text{-}5)$$

In this equation, Q_{gw} is groundwater discharge to the river (m^3/s), C_g is the total dissolved solids of the groundwater (mg TDS/L), Q_d and Q_u are, respectively, the downstream and upstream discharges of the river (m^3/s), and C_d and C_u are the downstream and upstream total dissolved solids of the river water, respectively (mg TDS/L).

This method was used to obtain a single direct groundwater discharge estimate for the day the survey was completed. The upstream river discharge, Q_u, used in these calculations was measured using an ADCP at the beginning of the longitudinal survey.

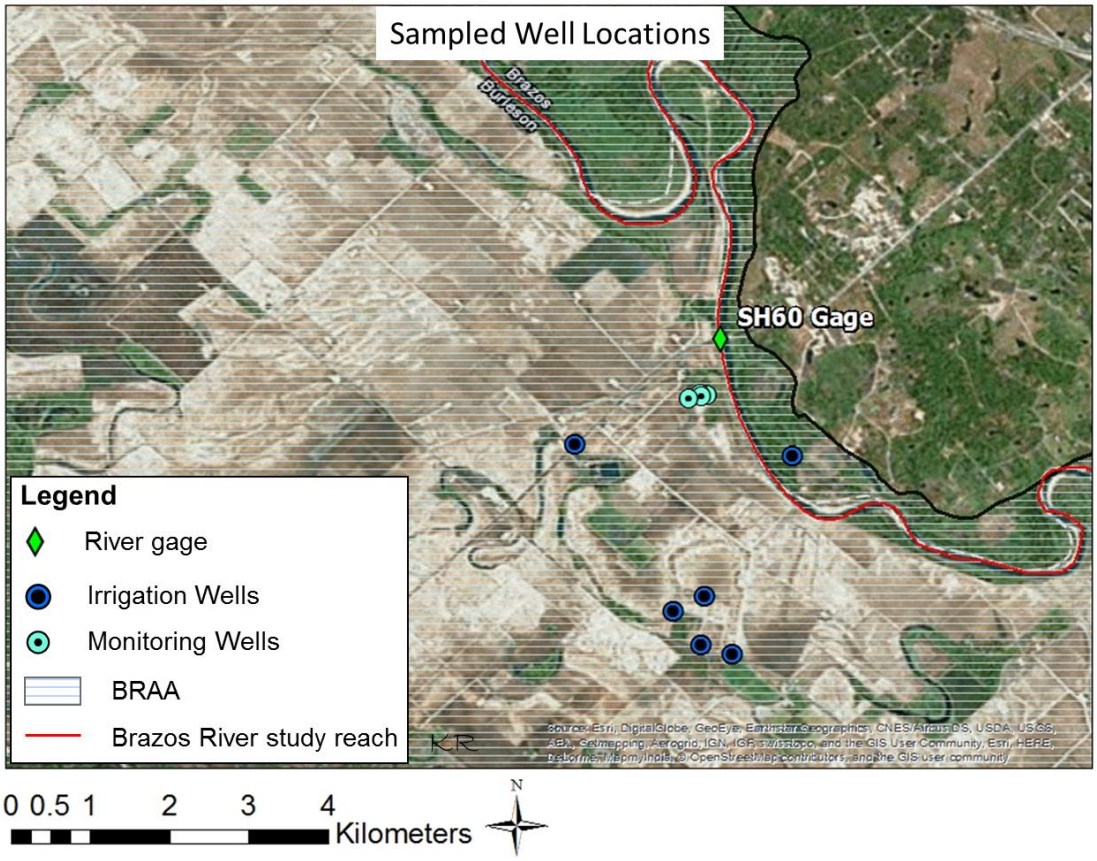

Figure 4-6: Locations of the 10 sampled wells with respect to the SH60 gage. The well on the eastern side of the river, although it appears to be within the BRAA extent provided by the TNRIS (2015) dataset, has different chemistry from the wells in the west side of the river. This suggests to us that it is in a different aquifer, likely the Yegua. Satellite imagery provided by ESRI.

The downstream river discharge, Q_d, was either directly measured with an ADCP at the end of the survey, or the value from the SH60 river gage at the time of the end of the survey was used. The specific conductance measurement taken at the upstream site (SH21) at the beginning of the survey and the specific conductance measurement taken at the downstream site (SH60) at the end of the survey, were used for C_u and C_d,

respectively. The values of specific conductance taken along the longitudinal survey were used to confirm a consistent trend between SH21 and SH60.

4.3.2 Continuous High Frequency Measurements

In addition to measuring specific conductance in longitudinal surveys, it was also recorded at the SH60 and Navasota river stations continuously every 20 minutes by Solinst LTC Junior Levelogger pressure transducers from September 10, 2015 to February 4, 2016. Specific conductance was also recorded at SH21 over this period, but it has not yet been possible to download that data due to high water conditions. To obtain specific conductance, thereby making every measurement comparable even when they were taken at different water temperatures, conductivity was input into the equation:

$$\mathrm{SC} = \frac{AC}{1 + r * (T - 25)} \qquad (4\text{-}6)$$

where SC is specific conductance, AC is conductivity, or actual conductance, r is the temperature correction coefficient, and T is the temperature of the water in degrees Celsius (Maupin et al., 2013). The standard value of 0.0191 was used as the temperature correction coefficient. Once conductivity values were converted to specific conductance, they were converted to TDS concentrations by multiplying by 0.65 (Pai et al., 2015). These values of SC were then used to calculate groundwater discharge between SH60 and Navasota by inputting them into equation 4-5. River discharge measurements from our river gages were also used in these calculations.

All of the specific conductance values taken from September 10, 2015, to February 4, 2016, could not be used to estimate groundwater discharge, however.

Periods in which precipitation occurred or tributaries were active could not be used because we did not have specific conductance measurements for rain or tributary waters. The addition of rain and tributary water with unknown specific conductance values could not be accounted for by equation 4-5. Therefore, groundwater discharge was calculated using specific conductance only during dry periods during which tributaries were inactive. We used the same time periods as were used for differential gaging. The same lag times to account for water travel time from SH60 to Navasota as were used for differential gaging were also incorporated into the calculations. The specific conductance and river discharge at SH60 were input into equation 4-5 with the lag time-corrected specific conductance and discharge measurements from Navasota.

4.4 Major Ions

Thirty-one water samples were collected from the Brazos River at various points in time and various levels of flow, usually on days when we measured river discharge in creation of our rating curves. Samples were also taken from each of nine alluvial aquifer wells (the same wells used to obtain the aquifer's representative specific conductance value), and one well on the other side of the river that we presume not to be in the alluvium because it has different chemistries than the other nine wells (figure 4-6). These samples were analyzed with an Ion Chromatograph (IC) (Dionex 600, Thermo Fischer Scientific Inc., Waltham, MA) to find concentrations of major anions and cations including Cl^-, Fl^-, NO_2^-, SO_4^{2-}, Br^-, NO_3^-, Li^+, Na^+, NH_4^+, K^+, Mg^{2+}, and Ca^{2+}. See Appendix I for a description of how we used the IC to find the ion concentrations in our samples.

Once the concentrations of ions were found, a principal components analysis (PCA) was completed on standardized concentrations (Z-scores for each ion) using the built-in MATLAB function *princomp* to find endmember values. Principal components analysis is a multivariate data reduction method that reduces the overall variability in a data set with m parameters and n samples to several new synthetic parameters oriented orthogonally to each other. The values of samples mapped onto Principal Component 1 (PC1) (the axis accounting for the most variability) will have a zero correlation with the values of the samples mapped onto PC2 (the axis accounting for the second most variability). In practice, PCA has proved useful in identifying groupings of samples based on their similarities in parameter values (Rencher, 2012). We plotted PC1 against PC2 and PC3, and PC2 and PC3 against each other. These plots were used to identify groups of samples that could be considered endmembers. The groups with principal component values that lay outside most river sample values were identified as endmembers.

Once the endmember groups were identified, the ion concentrations of all samples in each group were averaged together to obtain a single endmember concentration per ion for each group. These endmember values were included in plots of every ion versus every other ion to determine which ions could be considered conservative tracers. When the endmembers formed the vertices of a polygon encapsulating all or most of the river samples, they were considered acceptable conservative endmembers to use in an Endmember Mixing Analysis (EMMA). When they did not encapsulate the river samples, they were determined not to be conservative

tracers, and were excluded from the EMMA. Ions that had concentrations below the detection limit in most samples were also excluded because they could not be used to differentiate source waters. Potassium and nitrate were found to be non-conservative, and phosphate was usually below the detection limit. These three ions were excluded from the EMMA. Nitrite concentrations were not available for one of our identified endmembers (Lake Whitney water), so nitrite was excluded, as well. Sodium, magnesium, calcium, chloride, sulfate, and bicarbonate were included in these calculations.

Once the appropriate ions were identified, EMMA was performed to determine the percentage of streamflow each endmember made up in each stream water sample using equation 2-5. Once the percentage of each endmember in each river sample was found, samples from consecutive gages taken on the same day could be compared. Since the percent of each endmember in each sample was known, and river discharge at the time the sample was taken was known, total volume of each endmember in the river at that time and location could be determined. The volumes of river water made up of alluvial aquifer water, Yegua water, and bank storage were added to find the total volume of groundwater in the river. The total volume of groundwater at the upstream gage was subtracted from the total volume of groundwater at the downstream gage to determine groundwater discharge between gages on a certain day.

4.5 Baseflow Indices (BFI)

Daily average stream discharges from SH21, SH60, and Navasota were imported to the USGS GW Toolbox program so that it could be used to automatically find

baseflow indices (BFIs) at each gage. Daily averages were used because the program works best with smoothed data. The program requires that a full year of data be imported at a time, so when a full year of data was not available, dummy discharge values of 0 m^3/s were input into the missing dates. This was done for SH60 and Navasota, but not SH21 because USGS data was available for an entire year.

To find baseflow indices, both the BFI-standard and BFI-modified methods were selected. Calculated drainage basin areas above each gage were entered and the program was run. This program partitions the hydrograph into periods N days long. For our calculations we used the default value of N = 5 days. Within each N days long period the program found the minimum discharge value, then compared it to adjacent minimums to find turning points. Identified turning points were then connected and water volumes below the connected lines were considered baseflow (Barlow et al., 2015). The program output a baseflow index, runoff rate, baseflow rate, and river discharge for each day for which an average river discharge was available. Once daily BFIs and baseflows were found, groundwater discharge between our gage sites was found by subtracting the upstream baseflow from the downstream baseflow for each day.

5. RESULTS

5.1 Differential Gaging

5.1.1 Determining when Surface Runoff Ends

The contributing drainage area to the Brazos River above SH21 is 76,361 km^2 (USGS, 'Site Map for the Nation'), resulting in an estimated time period of 7.8 days for runoff to end according to equation 4-3. The polygon of the drainage basin area between SH21 and SH60 is shown figure 5-1. The area of this polygon was determined to be 417 km^2, which, added to the drainage area up to SH21, results in a total drainage area of 76,778 km^2, and a D value of 7.8 days. The polygon drawn to determine the drainage area to the Brazos River between SH60 and our Navasota gage is shown in figure 5-2. The area of this polygon is 3,872 km^2, resulting in a total drainage basin area up to that point of 80,650 km^2. This area led to a D value of 7.9 days. The results of these calculations are summarized in table 5-1.

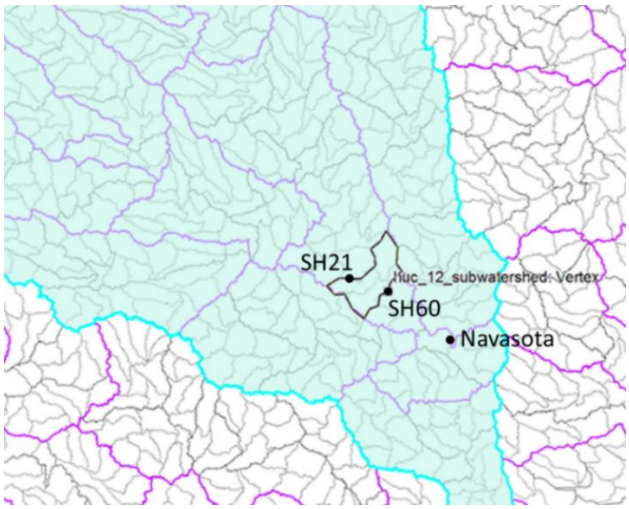

Figure 5-1: The polygon used to find the drainage area between SH21 and SH60 is shown with black outline. The black dots represent the gage locations, which are, in order from northwest to southeast: SH21, SH60, and Navasota. The purple outlines represent large drainage areas, such as the watersheds for the Navasota River and Yegua Creek, and the grey lines outline smaller drainage areas. Drainage basin data provided by Texas Natural Resources Information System (TNRIS) (2015).

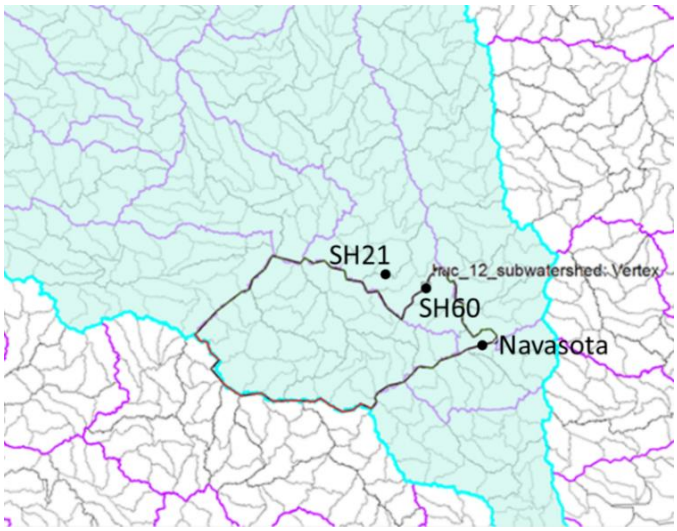

Figure 5-2: The polygon used to find the watershed drainage area between SH60 and Navasota is shown with black outline. The area excludes the drainage area for the Navasota River because it enters the Brazos River downstream of our gage. The polygon includes the drainage area for Yegua Creek because this stream flows into the Brazos upstream of our gage. Drainage basin data provided by TNRIS (2015).

Table 5-1: Table summarizing the drainage basin areas used to calculate the time, D, for overland flow to end upstream of each of our gaging locations following a rainfall event, and D values.

Gaging Station	Total Drainage Area (km^2)	Time from Storm Peak to End of Overland Flow, D (days)
SH21	76,361	7.8
SH60	76,778	7.8
Navasota	80,650	7.9

5.1.2 Developing Rating Curves and Discharge Hydrographs

Rating curves were constructed to relate river stage, measured every 20 minutes by pressure transducers installed in the river at each of our three gage sites, to river discharge. They allowed us to obtain high frequency river discharges at each study site. The constructed rating curves are shown in figures 5-3, 5-4, 5-6, 5-7, 5-9, and 5-10. Exponential rating curves were used to determine discharge below 100 m^3/s at all three gage sites because they provided a far superior fit to the observed discharges over linear. Linear rating curves were used to calculate discharges above 100 m^3/s because they provided reasonable estimates that matched our direct ADCP measurements better than exponential equations. Direct ADCP measurements are plotted on the calculated discharge hydrographs in figures 5-5, 5-8, and 5-11 for each gage site.

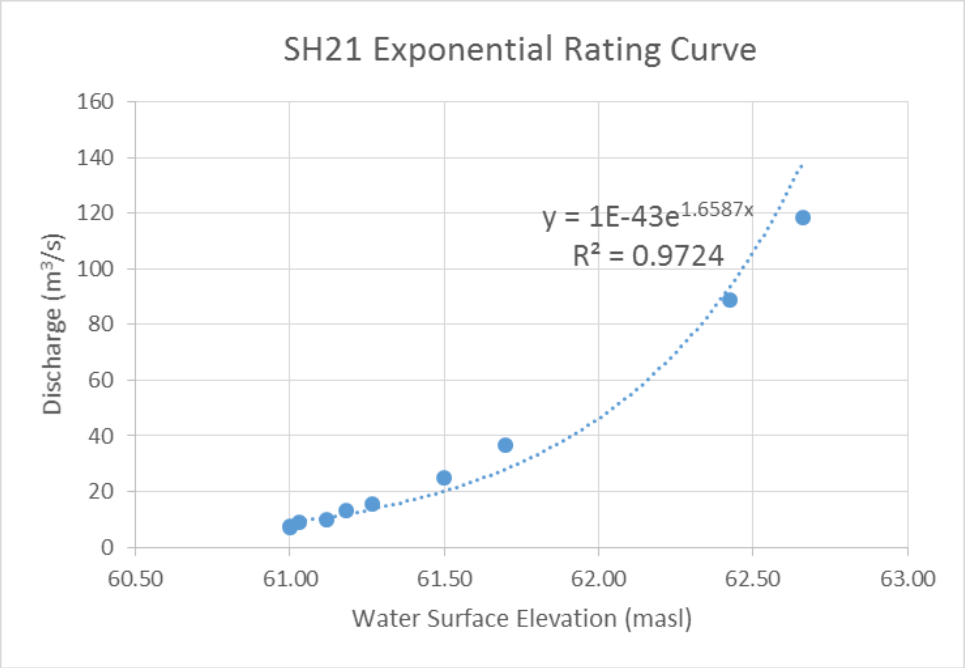

Figure 5-3: Exponential rating curve developed using the lowest measured discharge values, and used to estimate discharges below 100 m^3/s.

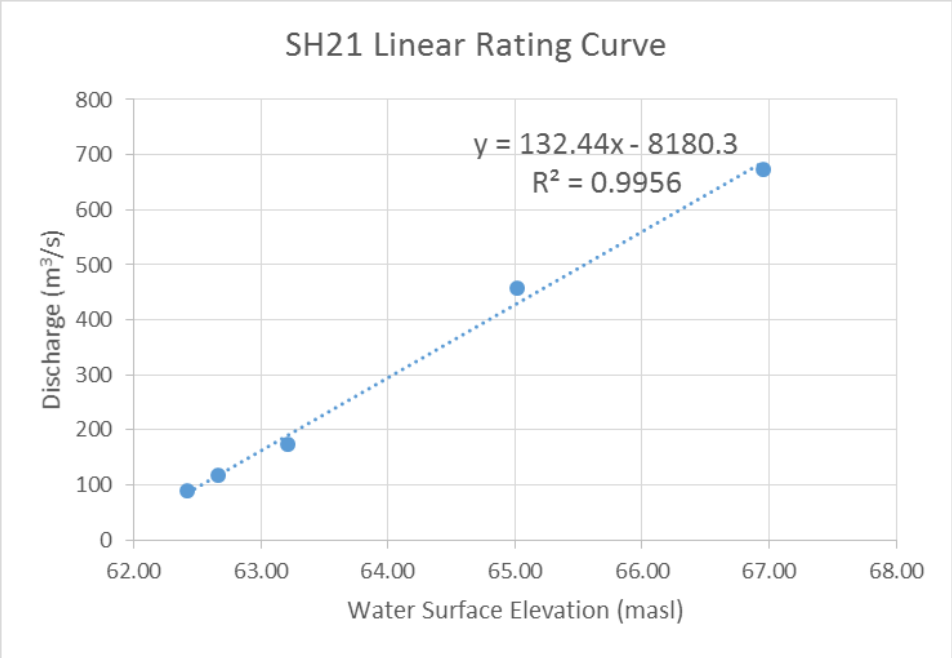

Figure 5-4: Linear rating curve developed using the highest measured discharge values, and used to estimate discharges above 100 m^3/s.

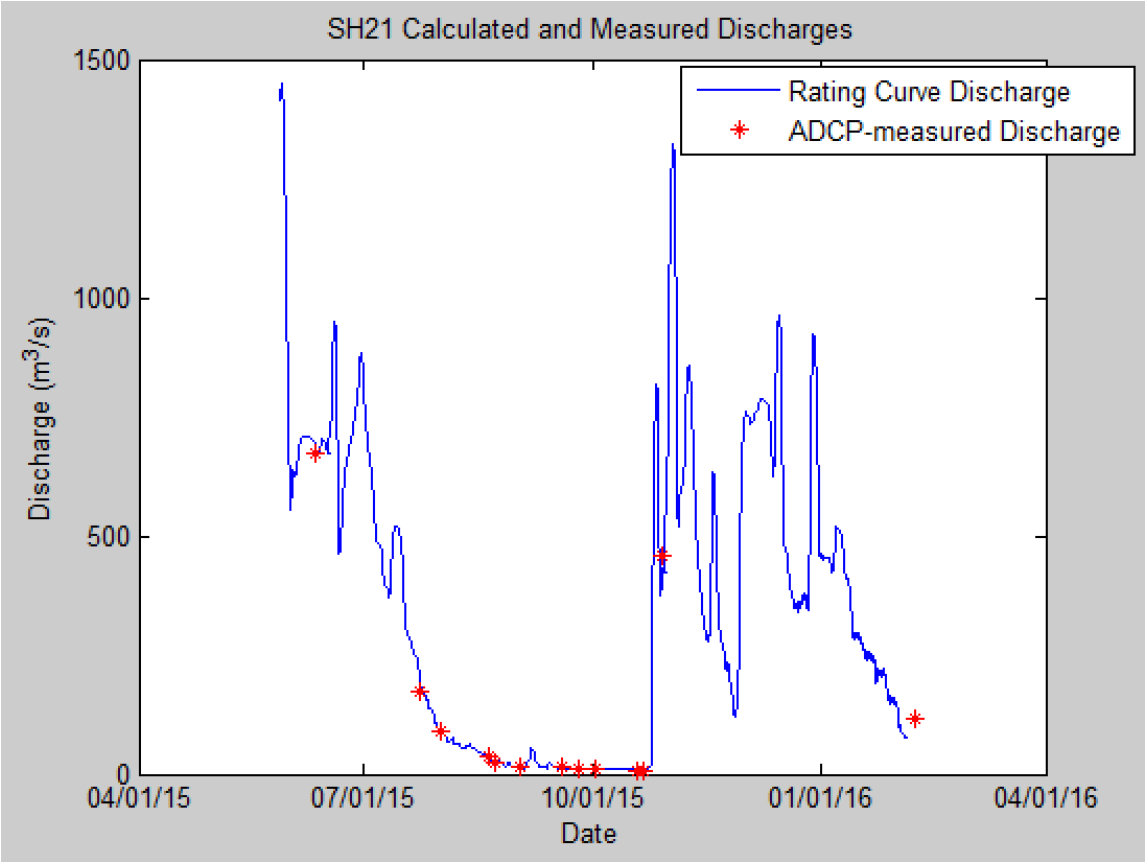

Figure 5-5: ADCP discharge measurements overlaid on top of rating curve-derived discharge measurements at SH21. The red asterisks show the actual measurements that were used to create the rating curves. The last ADCP measurement was taken after data was collected from the SH21 gage.

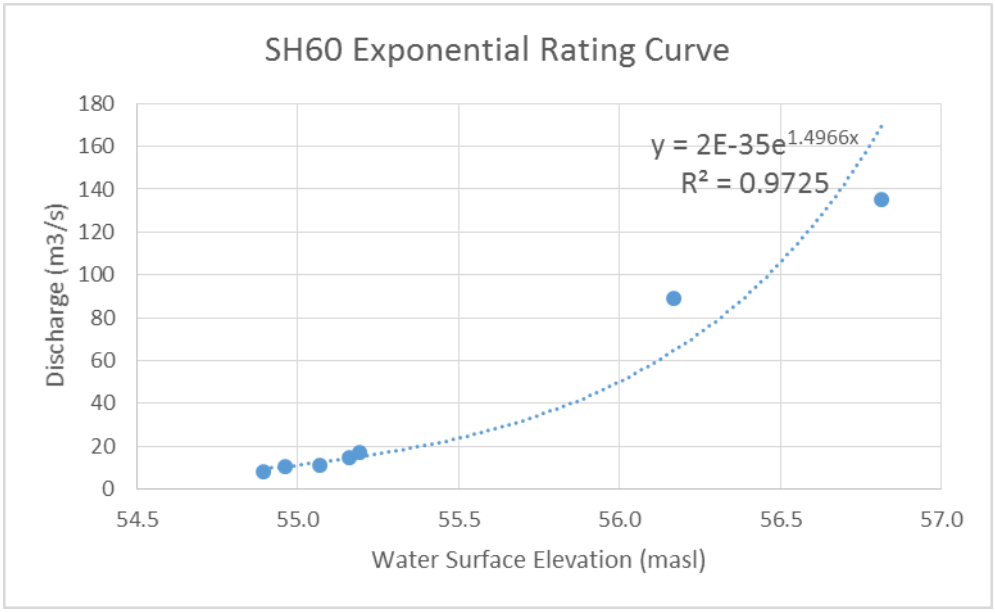

Figure 5-6: Exponential rating curve developed using the lowest measured discharge values, and used to estimate discharges below 100 m^3/s.

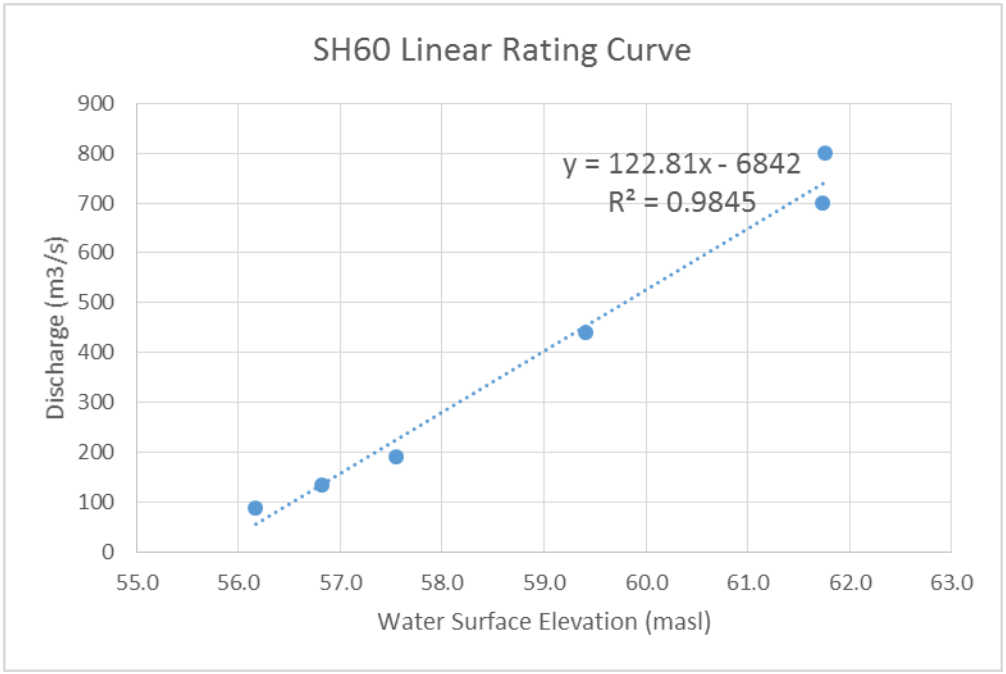

Figure 5-7: Linear rating curve developed using the highest measured discharge values, and used to estimate discharges above 100 m^3/s.

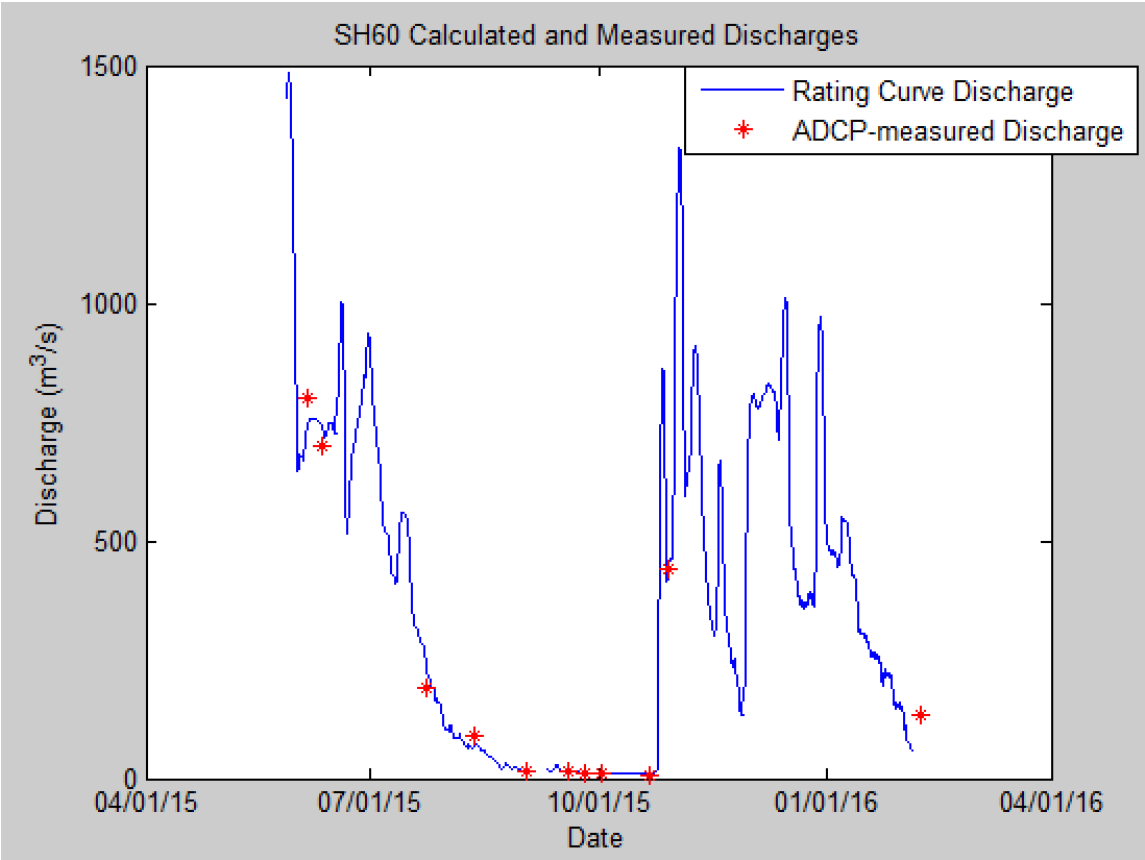

Figure 5-8: ADCP discharge measurements overlaid on top of rating curve-derived discharge measurements at SH60. The red asterisks show the actual measurements that were used to create the rating curves. The last ADCP measurement was taken after data was collected from the SH60 gage.

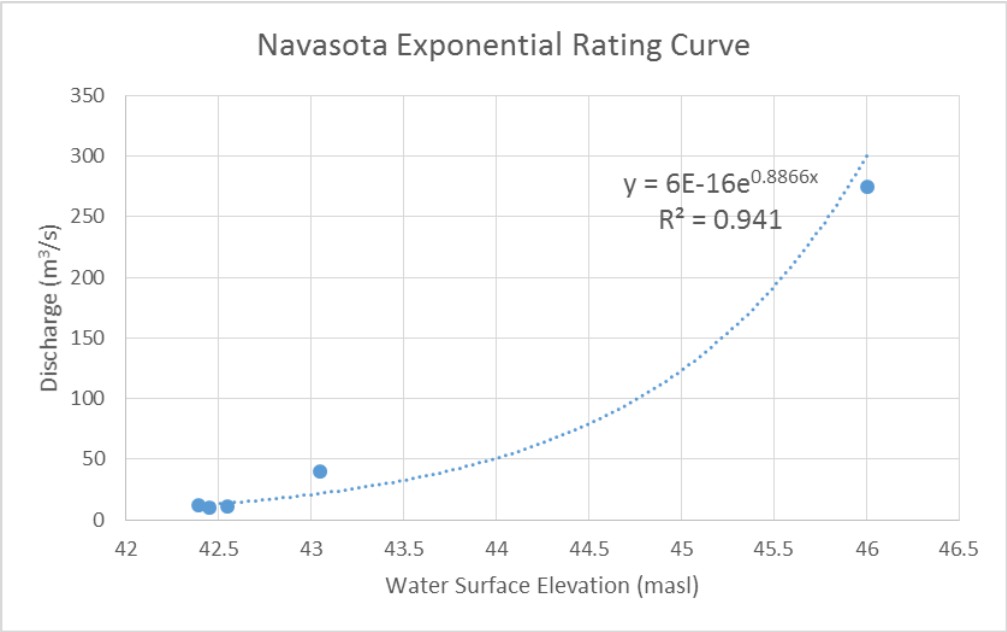

Figure 5-9: Exponential rating curve developed using the lowest measured discharge values, and used to estimate discharges below 100 m^3/s.

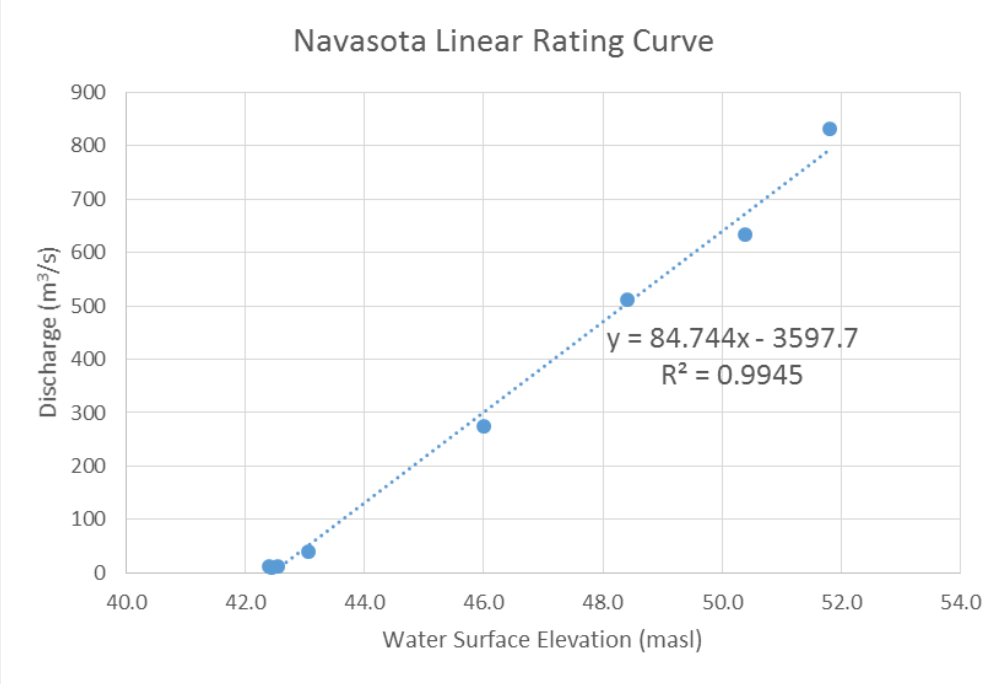

Figure 5-10: Linear rating curve developed using the highest measured discharge values, and used to estimate discharges above 100 m^3/s.

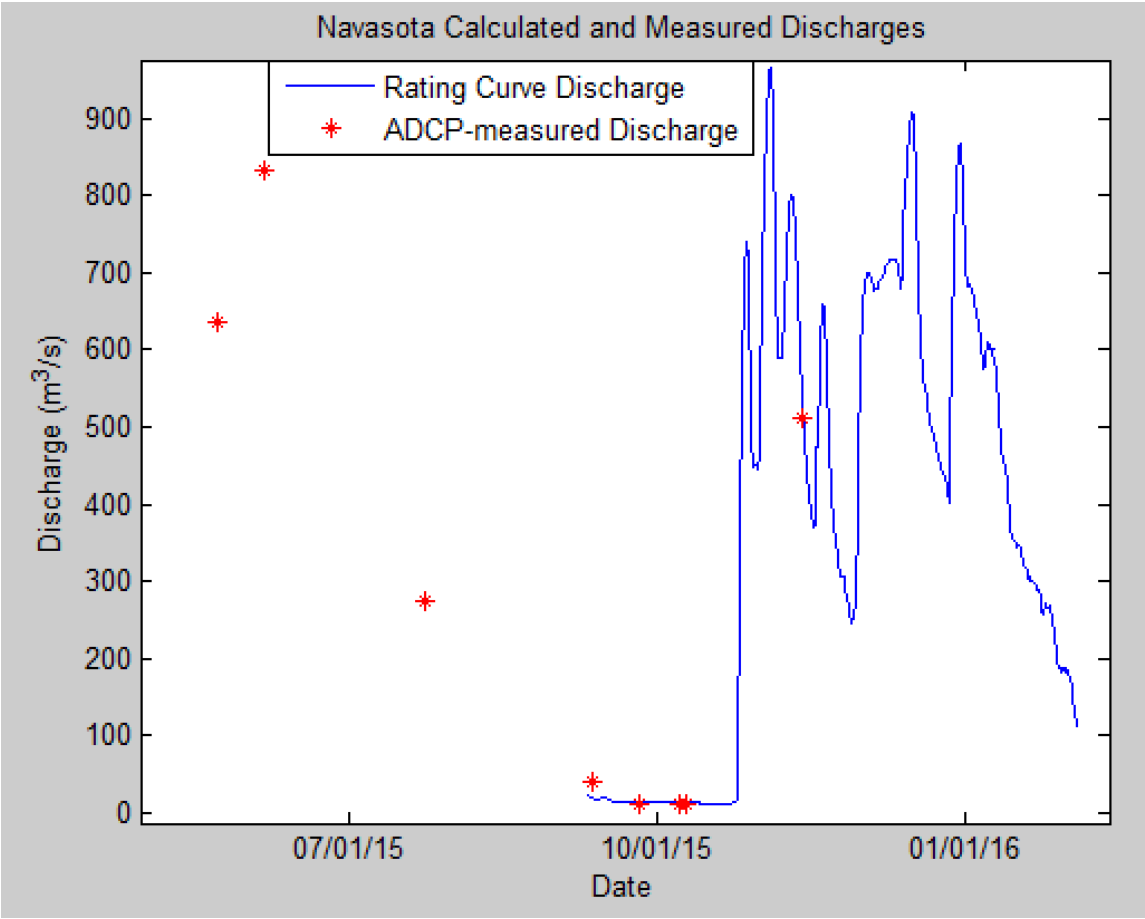

Figure 5-11: ADCP discharge measurements overlaid on top of rating curve-derived discharge measurements at Navasota. The red asterisks show the actual measurements that were used to create the rating curves. Some of the ADCP measurements were taken before the river gage was installed.

5.1.3 Differential Gaging between SH21 and SH60

River stage data is available at both SH21 and SH60 from November 7, 2014, through February 5, 2016. Discharge measurements, however, were not begun until May 22, 2015. Comparisons between SH21 and SH60 started at midnight on May 28, 2015, because this was the beginning of stable readings at SH60. The gage seemed to have moved with flooding conditions prior to May 28, but was stable thereafter. Changes

in stream morphology likely occurred during the record floods of May 2015, which may make our discharge measurements non-applicable to the period before May 22, 2015.

Once the beginning of the study period was determined, dry periods in which differential gaging could be conducted were identified. The beginnings of dry periods were determined according to the D values in table 5-1, and the ends were determined by comparing precipitation data with gage height data to determine when a rise in river discharge was caused by precipitation. Precipitation and SH21 and SH60 gage heights, as well as dry periods selected based on these data are shown in figure 5-12. The lag times determined for these periods are shown in table 5-2. River discharges at SH21 and SH60 over the entire eight month study period are shown with precipitation data and highlighted dry periods in figure 5-13.

Groundwater discharge estimates from differential gaging are shown in figures 5-14 through 5-21 for the eight dry periods. Over the first dry period river discharge at SH21 (upstream), ranged from 671 to 710 m^3/s, while discharge at SH60 (downstream) ranged from 717 to 758 m^3/s. In the second dry period river discharge at SH21 ranged from 19 to 520 m^3/s, while discharge at SH60 ranged from 21 to 561 m^3/s. During the third period, river discharge at SH21 ranged from 9 to 12 m^3/s, while discharge at SH60 ranged from 10 to 13 m^3/s. In the fourth period river discharge at SH21 ranged from 285 to 290 m^3/s, while discharge at SH60 ranged from 308 to 311 m^3/s. In the fifth period river discharge at SH21 ranged from 122 to 161 m^3/s at SH21, while discharge at SH60 ranged from 132 to 169 m^3/s. During the sixth period river discharge at SH21 ranged from 669 to 777 m^3/s, while discharge at SH60 ranged from 713 to 819 m^3/s. In the

seventh period river discharge at SH21 ranged from 341 to 381 m^3/s, while discharge at SH60 ranged from 356 to 394 m^3/s. In the eighth period river discharge at SH21 ranged from 73 to 257 m^3/s, while discharge at SH60 ranged from 58 to 266 m^3/s.

Calculated groundwater discharge during each of the eight periods ranged, in order from period 1 to period 8, from 45 to 50 m^3/s, 3 to 42 m^3/s, 0 to 2 m^3/s, 21 to 23 m^3/s, 6 to 10 m^3/s, 34 to 44 m^3/s, 9 to 18 m^3/s, and -18 to 14 m^3/s. Negative groundwater discharge indicates a net loss in the river discharge across the differentially gaged stretch.

Table 5-2: Periods of differential gaging and corresponding lag times used for differential gaging between SH21 and SH60.

Differential Gaging Period	Date Range Start at SH60	Date Range End at SH60	Lag Time
1	6/5/15 6:40pm	6/12/15 5:20pm	5 hours, 20 minutes
2	7/7/15 8:40pm	8/23/15 7:40am	4 hours, 40 minutes
3	9/22/15 4:00am	10/23/15 4:20am	13 hours
4	11/17/15 12:40am	11/17/15 9:00am	4 hours 40 minutes
5	11/26/15 10:20pm	11/27/15 9:00pm	6 hours, 20 minutes
6	12/10/15, 3:00pm	12/12/15 6:00pm	5 hours, 20 minutes
7	12/23/15, 2:00pm	12/27/15 11:20am	5 hours
8	1/20/16 10:00am	2/5/16 4:00pm	4 hours, 40 minutes

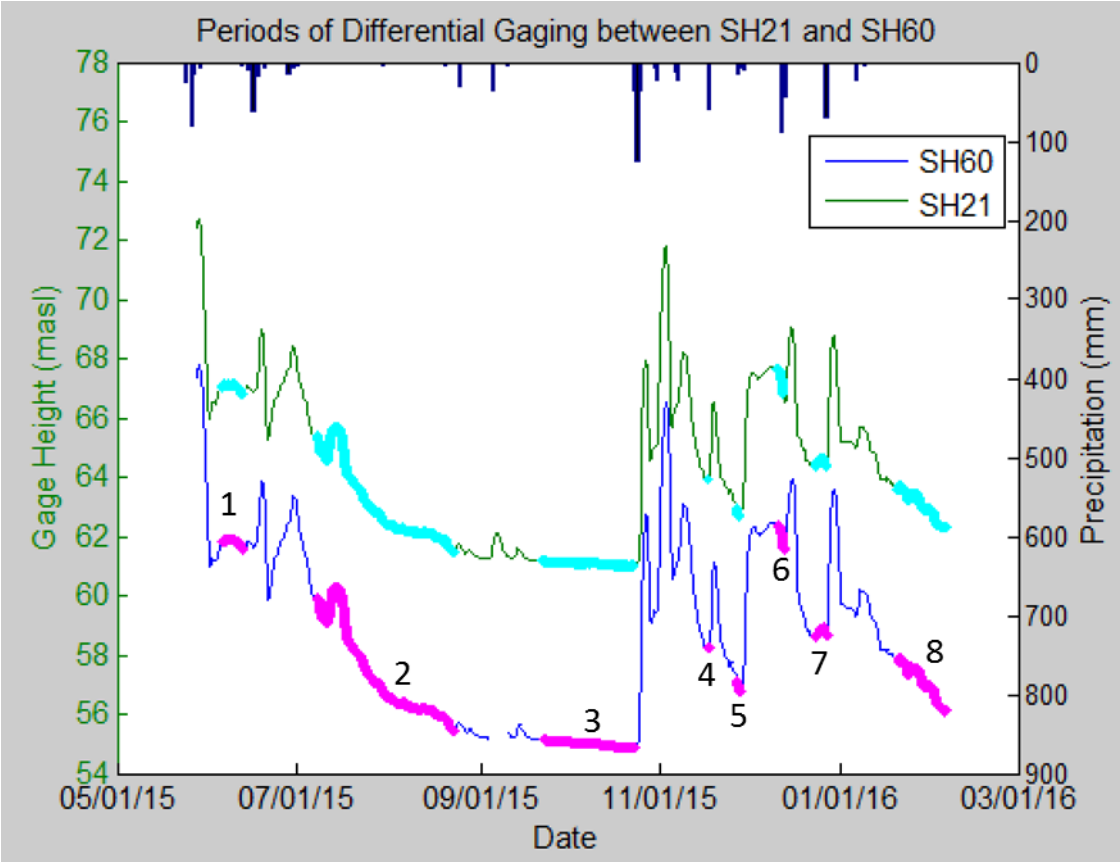

Figure 5-12: The dry periods used for differential gaging between SH21 and SH60 are shown in light blue and pink, respectively, with the gage height data from each site. Each period of differential gaging is labeled in order from 1 to 8. Precipitation data from the National Oceanic and Atmospheric Administration's (NOAA) College Station Easterwood Airport rain gage were used to help define dry periods and are shown on the top axis.

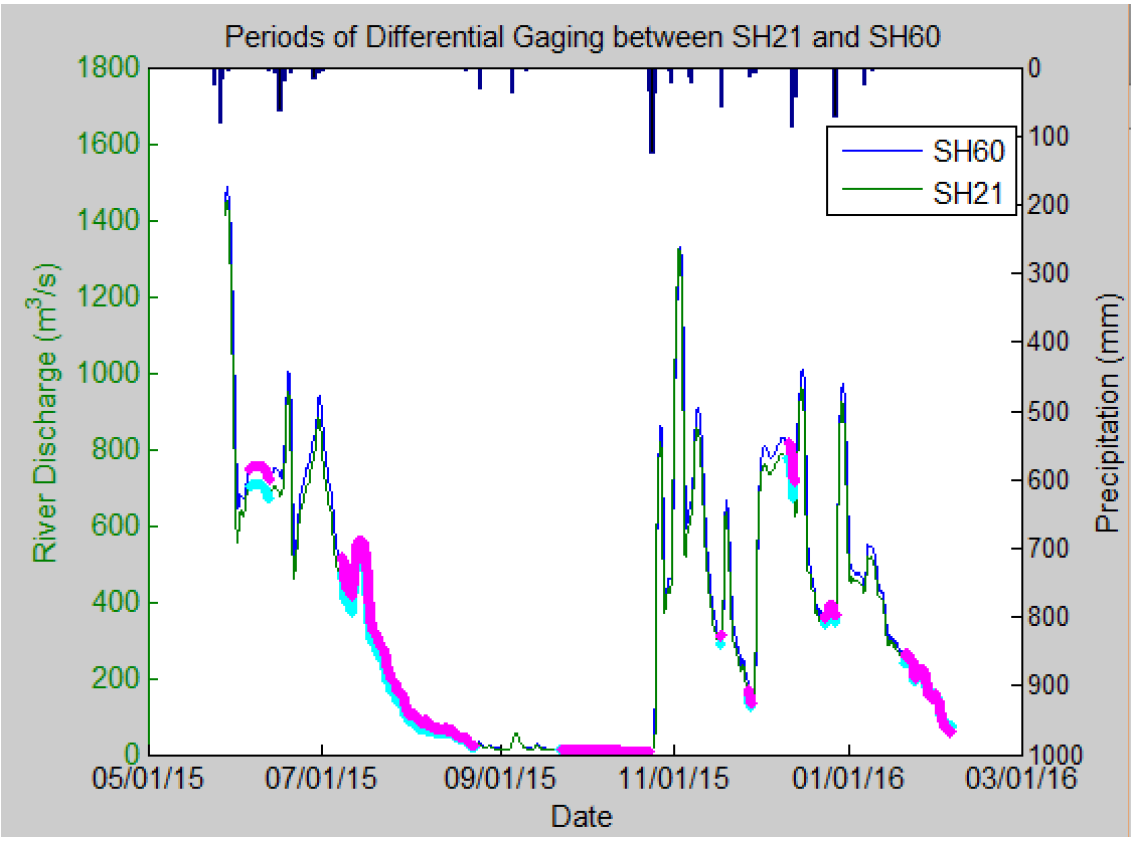

Figure 5-13: The dry periods used for differential gaging between SH21 and SH60 are shown in light blue and pink, respectively, with the calculated discharges at each site. Precipitation data from NOAA's College Station Easterwood Airport rain gage were used to help define dry periods and are shown on the top axis.

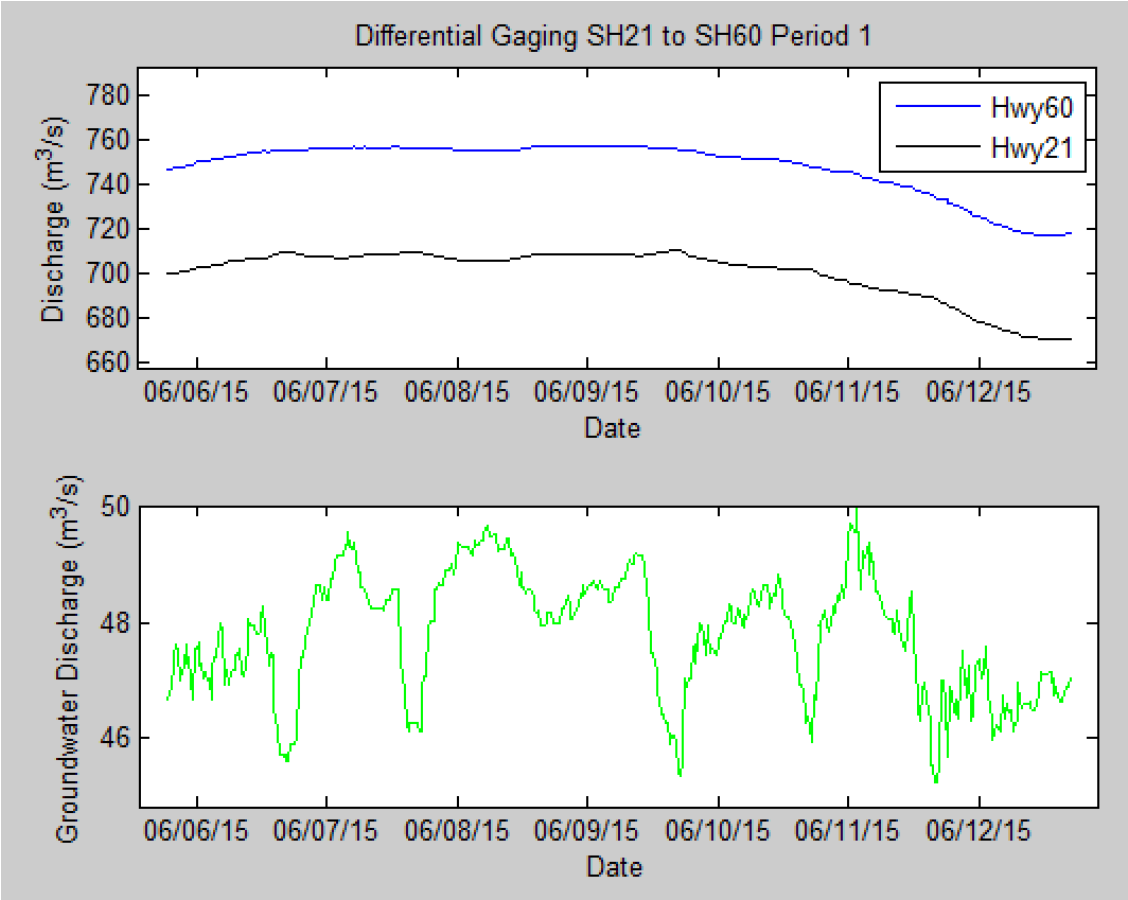

Figure 5-14: Discharges at Highway 21 and Highway 60, as well as groundwater discharge calculation results for the first differential gaging study period. Tick marks are placed at the start of each day at midnight.

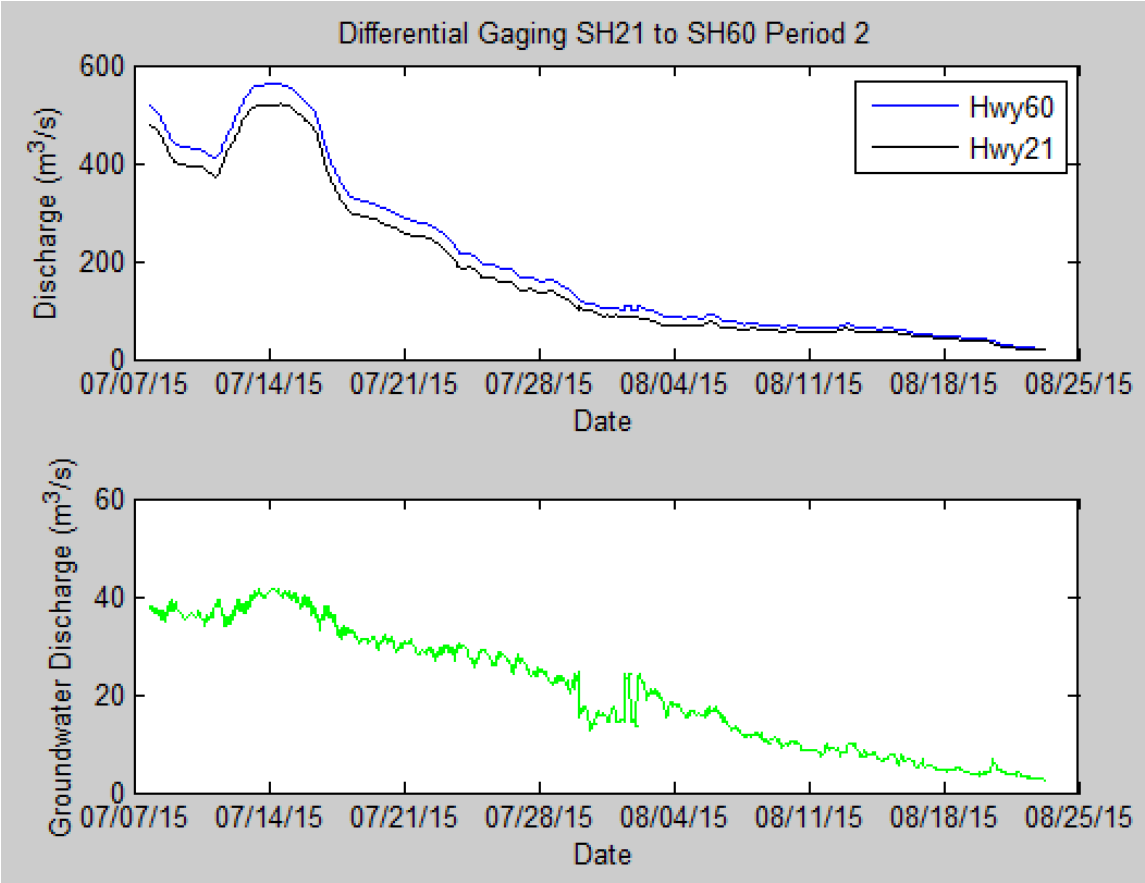

Figure 5-15: Discharges at Highway 21 and Highway 60, as well as groundwater discharge calculation results for the second differential gaging study period. Tick marks are placed at the start of each day at midnight.

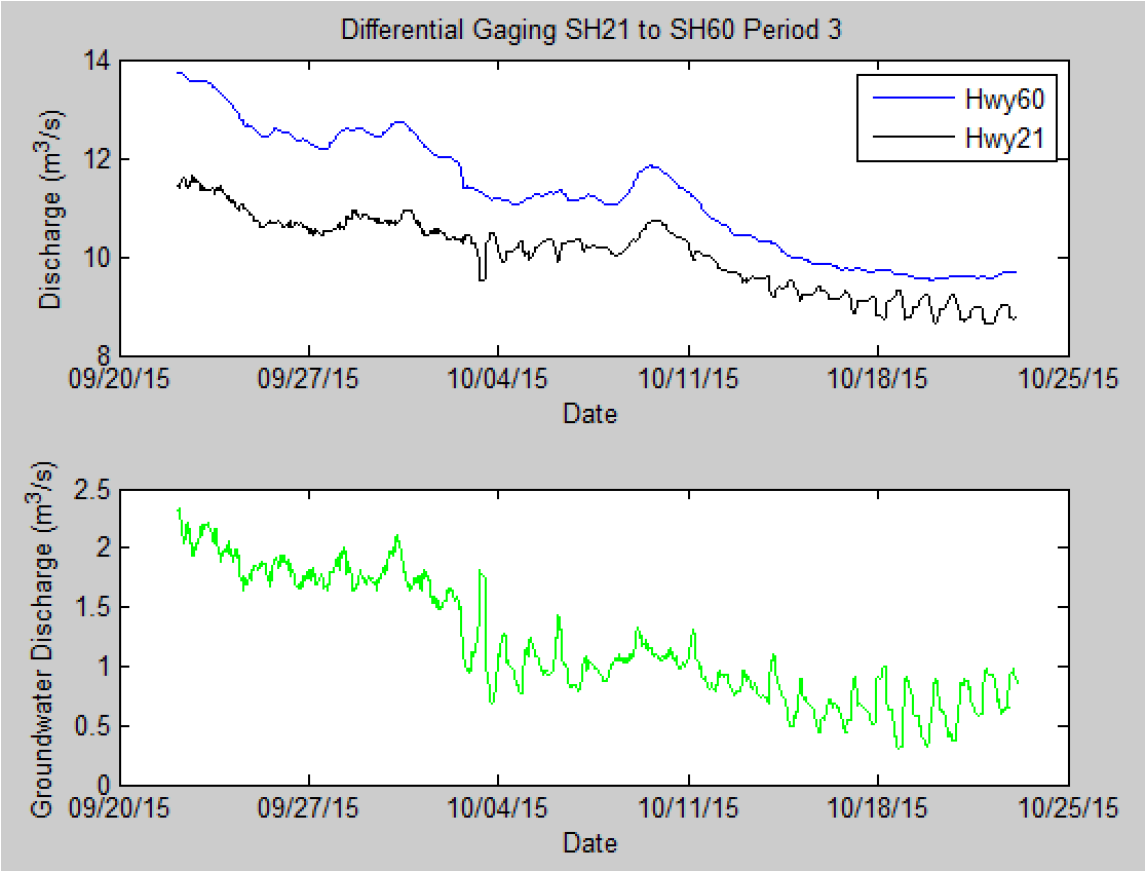

Figure 5-16: Discharges at Highway 21 and Highway 60, as well as groundwater discharge calculation results for the third differential gaging study period. Tick marks are placed at the start of each day at midnight.

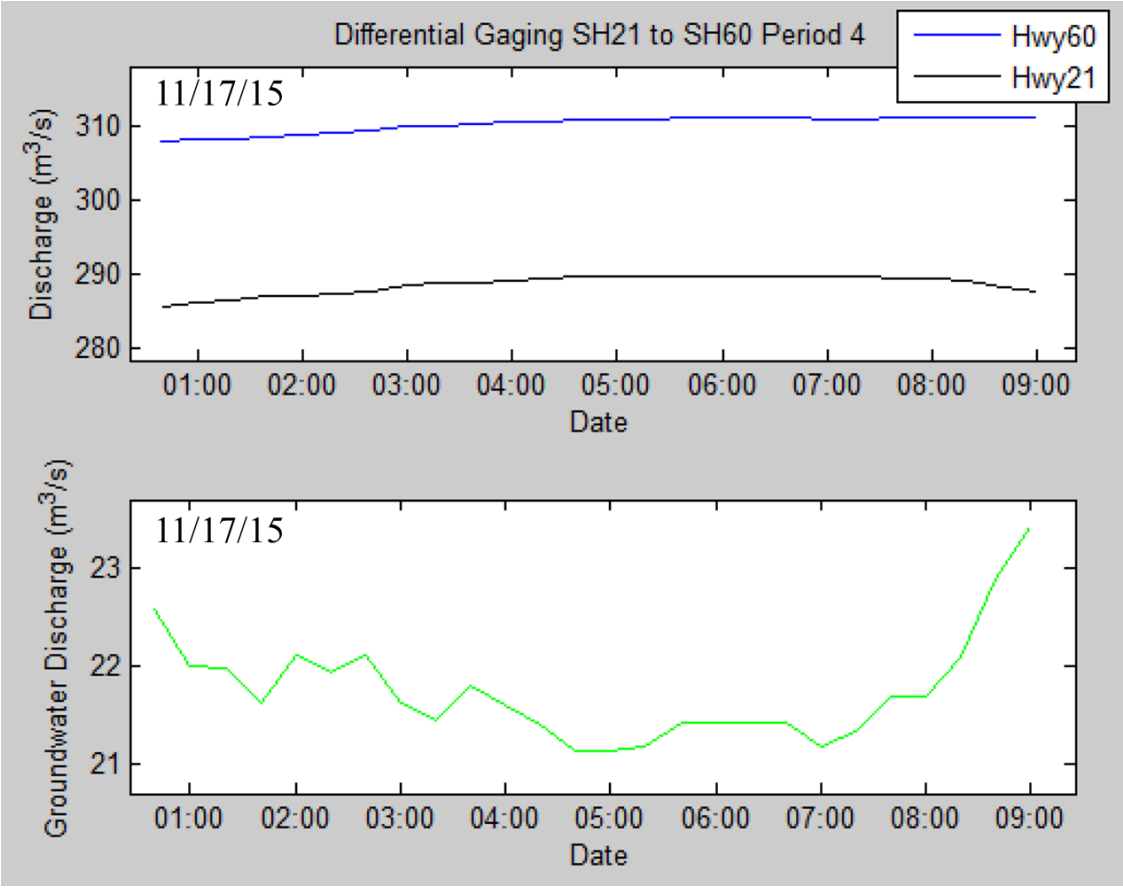

Figure 5-17: Discharges at Highway 21 and Highway 60, as well as groundwater discharge calculation results for the fourth differential gaging study period. Tick marks are placed at the start of each day at midnight.

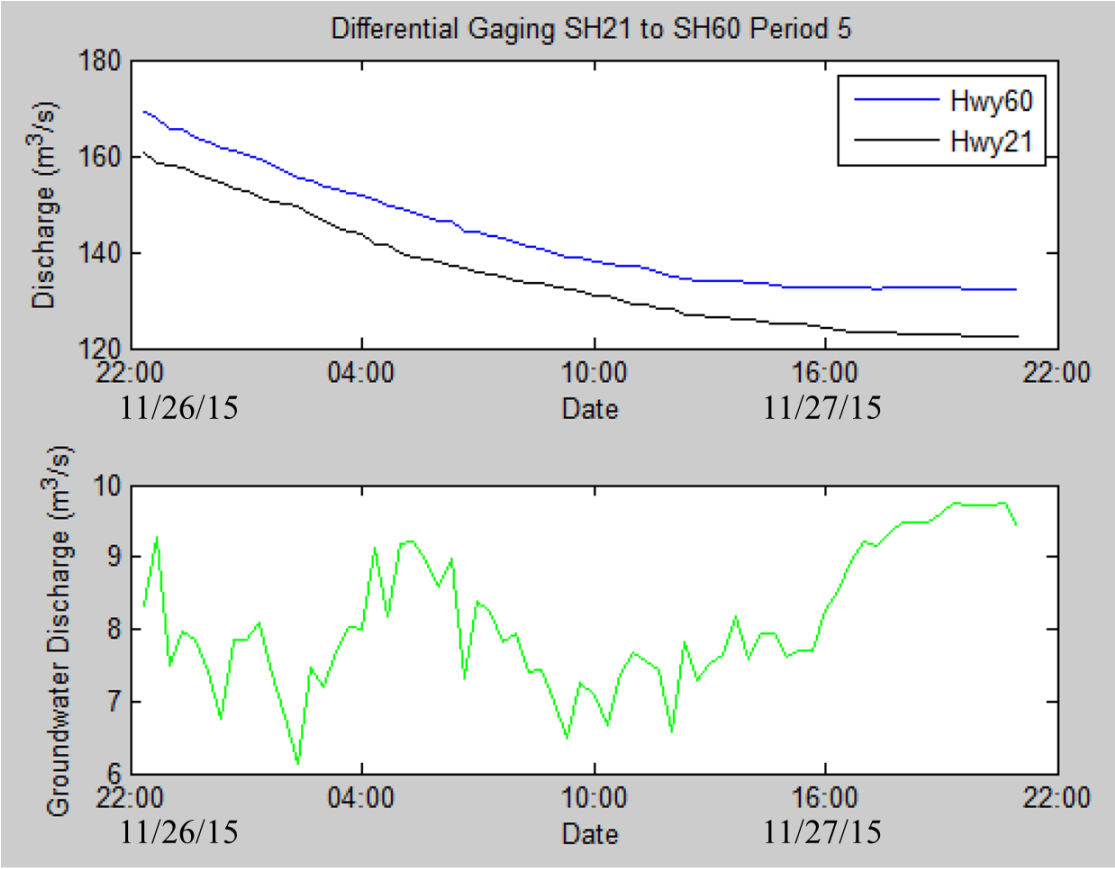

Figure 5-18: Discharges at Highway 21 and Highway 60, as well as groundwater discharge calculation results for the fifth differential gaging study period. Tick marks are placed at the start of each day at midnight.

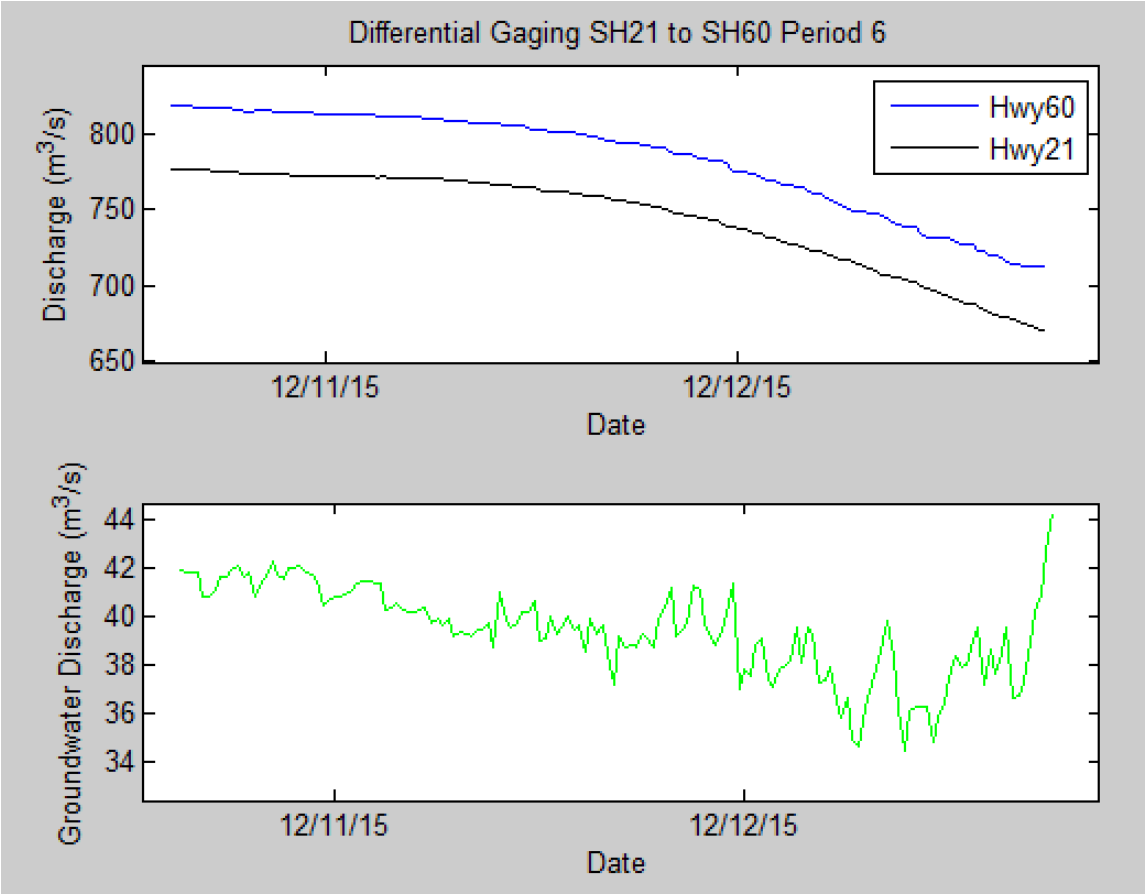

Figure 5-19: Discharges at Highway 21 and Highway 60, as well as groundwater discharge calculation results for the sixth differential gaging study period. Tick marks are placed at the start of each day at midnight.

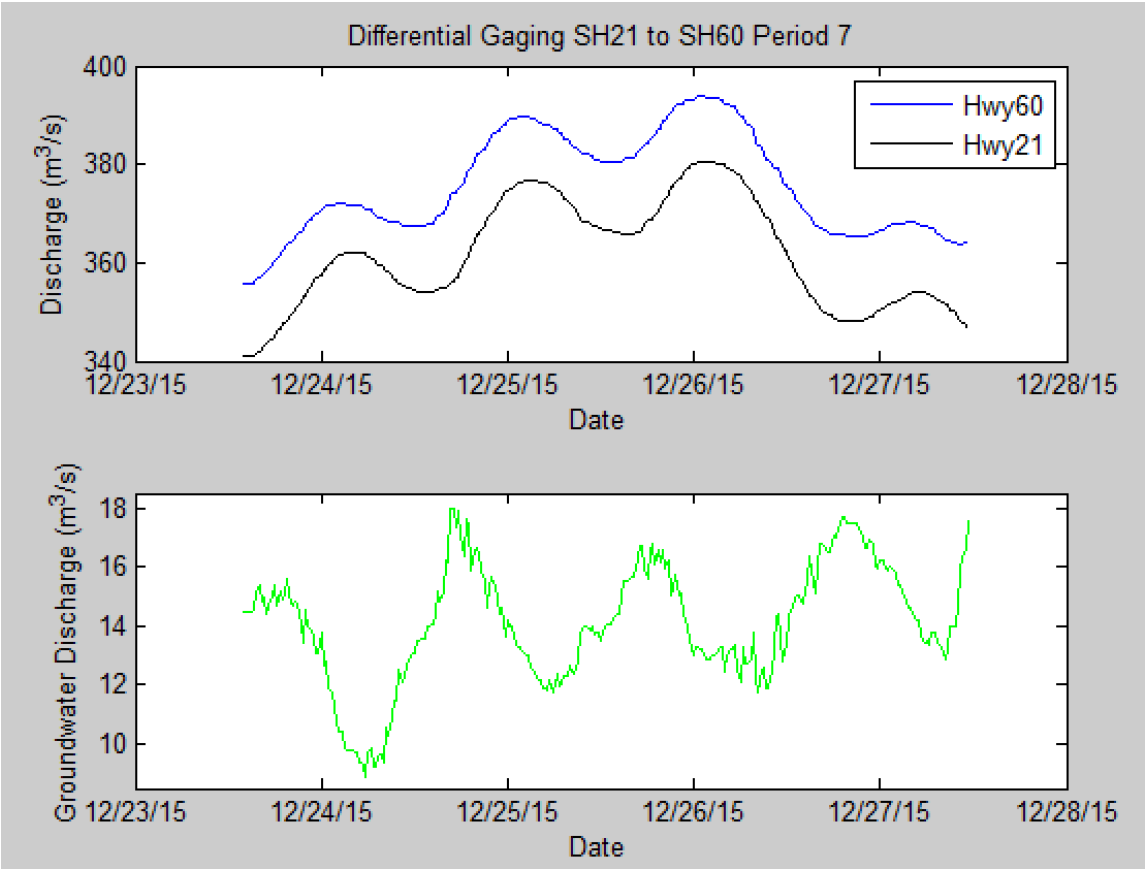

Figure 5-20: Discharges at Highway 21 and Highway 60, as well as groundwater discharge calculation results for the seventh differential gaging study period. Tick marks are placed at the start of each day at midnight.

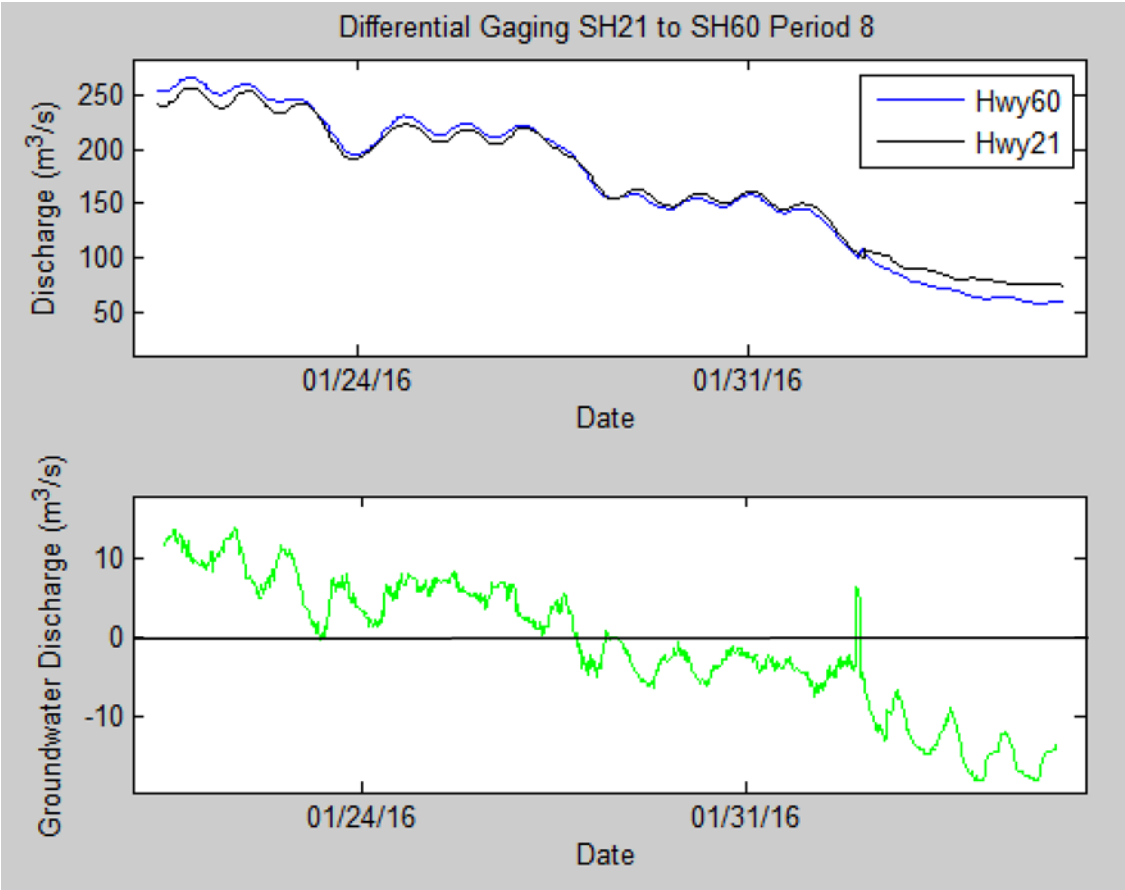

Figure 5-21: Discharges at Highway 21 and Highway 60, as well as groundwater discharge calculation results for the eighth differential gaging study period. Tick marks are placed at the start of each day at midnight.

5.1.4 Differential Gaging between SH60 and Navasota

River gage height and therefore discharge data are available from SH60 to Navasota for a shorter time period than from SH21 to SH60 because the gage was not installed at Navasota until September, 2015 (figure 5-11). For the period of available data from our Navasota gage, we performed differential gaging between SH60 and Navasota during five dry periods. The lag times found for each of these periods can be found in table 5-3. Each dry period used for groundwater discharge calculations

between these gages is shown in figure 5-22 along with the gage height and precipitation data used to help define dry periods. Even though dry periods were selected, Yegua Creek, a tributary between SH60 and Navasota (figure 5-23), discharges water from an upstream dam at Somerville Lake. It frequently continued discharging water during dry periods when all other tributaries were inactive.

Yegua Creek receives water from Davidson Creek. Both of these tributaries are gaged by the USGS, so their discharges during our study period were obtained and subtracted from our calculated Brazos River discharges at Navasota. The travel time of water from the Yegua Creek gage to our Navasota gage is known to be 1.38 days (BRA, 2014), so we incorporated this as the lag time in our calculations. The equation used in our differential gaging calculations for the stretch between SH60 and Navasota therefore was

$$Q_{gw} = Q_{Nav} - Q_{SH60} - Q_{Y+D} \qquad (5\text{-}1)$$

where Q_{gw} is groundwater discharge, Q_{Nav} is the Brazos River discharge at Navasota, Q_{SH60} is the Brazos River discharge at SH60, and Q_{Y+D} is the combined discharge of Yegua and Davidson Creeks. Discharges at Navasota before and after correction for the Yegua and Davidson Creek inflows are shown in figure 5-24. Dry periods are shown on graphs of SH60 and Navasota discharges with precipitation data in figure 5-25. This figure includes Navasota discharges corrected for tributary inflows.

Table 5-3: Periods of differential gaging and corresponding lag times used for differential gaging between SH60 and Navasota. Period start and end times are given in SH60 times, i.e. lag times were applied to Navasota data so that they matched times at SH60.

Differential Gaging Period	Date Range Start at SH60	Date Range End at SH60	Lag Time
1	10/6/15 6:20pm	10/22/15 6:00am	18 hours, 40 minutes
2	11/27/15 12:20am	11/27/15 6:20pm	12 hours
3	12/10/15 4:40pm	12/12/15 3:00pm	8 hours, 40 minutes
4	12/23/15 10:40am	12/26/15 1:40pm	23 hours
5	1/19/16 2:20pm	2/3/16 5:20pm	14 hours, 20 minutes

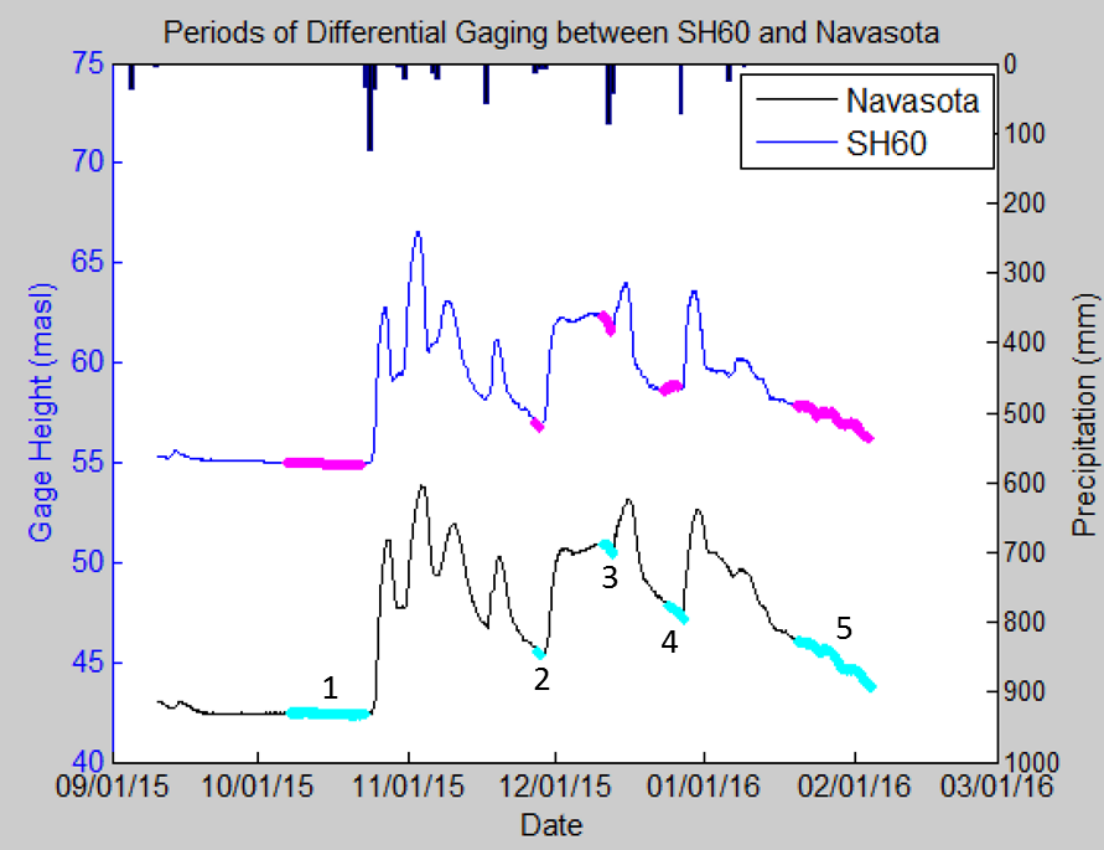

Figure 5-22: Periods of differential gaging between SH60 and Navasota are highlighted on their respective gage height graphs. The gage heights from the Navasota gage are shown in black, and those for SH60 are shown in blue. Differential gaging periods are labeled in order from 1 to 5. Precipitation data from NOAA's College Station Easterwood Airport rain gage were used to help define dry periods and are shown on the top axis.

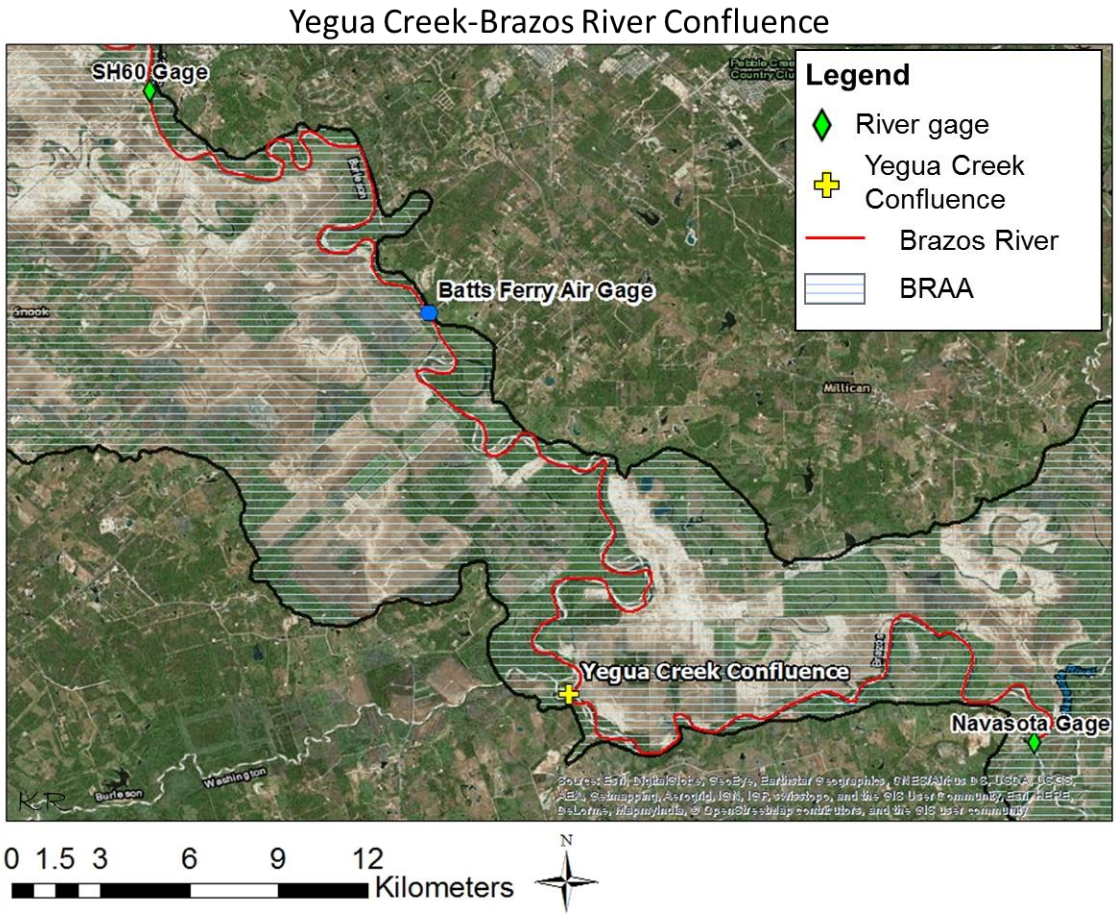

Figure 5-23: Location of the Yegua Creek confluence with the Brazos River in between our gage sites at SH60 and Navasota. Satellite imagery provided by ESRI.

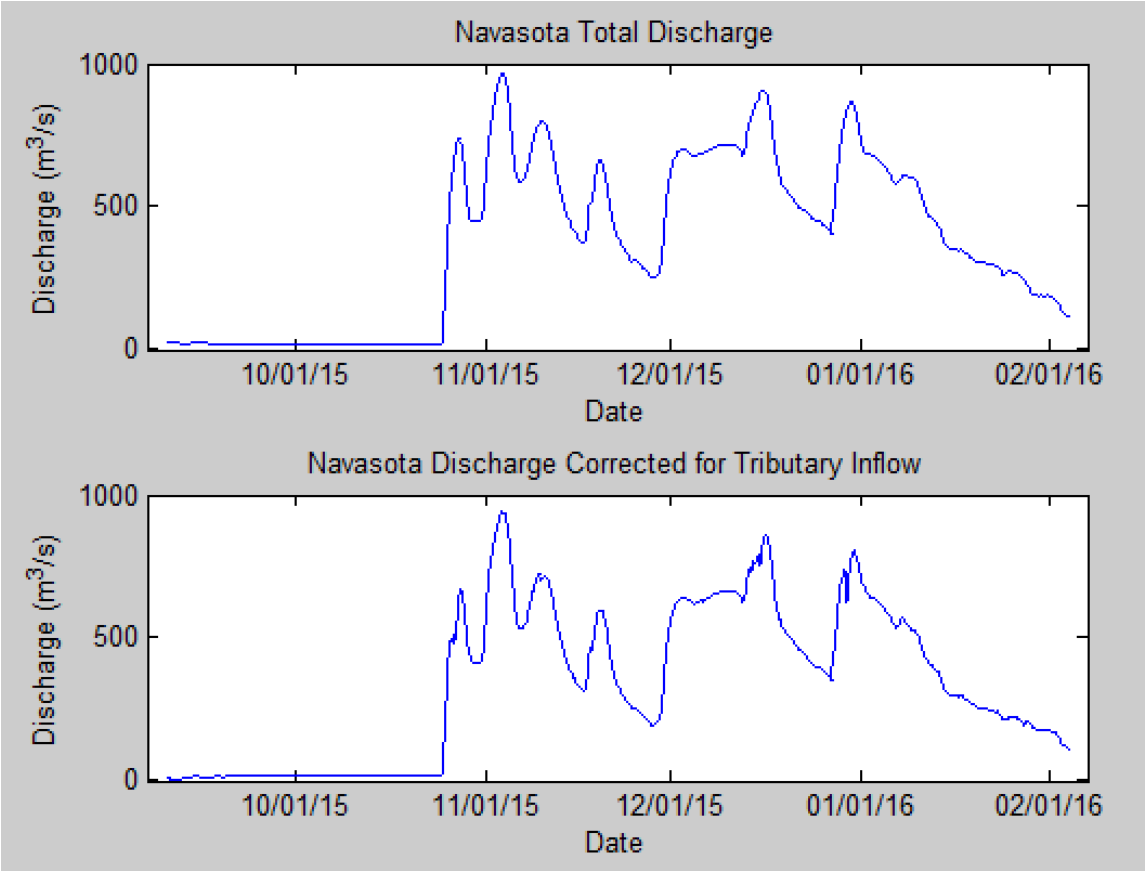

Figure 5-24: Discharge at Navasota gage before correction for known tributary discharges (top), and after correction for known tributary discharges (bottom).

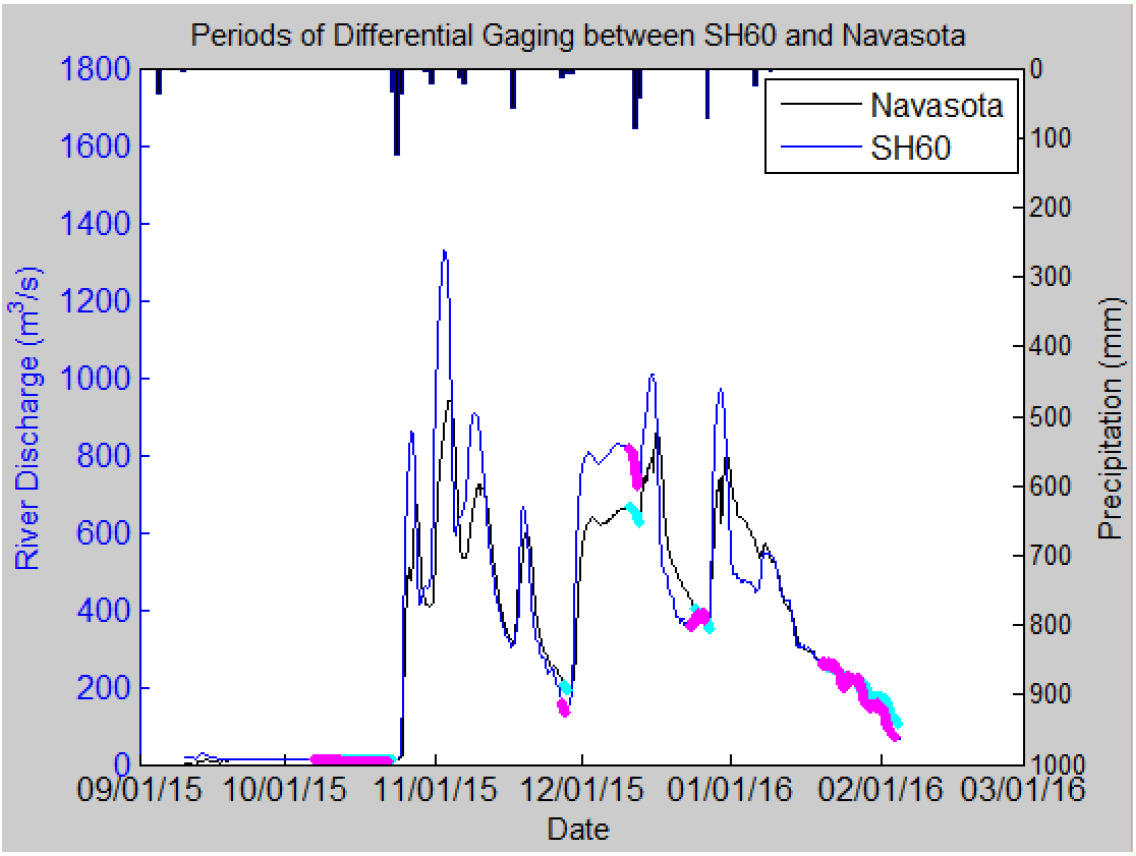

Figure 5-25: The dry periods used for differential gaging between SH60 and Navasota are shown in pink and light blue, respectively, with the calculated discharges at each site. Precipitation data from NOAA's College Station Easterwood Airport rain gage were used to help define dry periods and are shown on the top axis.

Groundwater discharge to the river derived from differential gaging calculations for each dry period are shown in figures 5-26 through 5-30. For period 1, river discharge at SH60 ranged from 10 to 12 m^3/s, and river discharge corrected for tributaries at Navasota ranged from 12 to 14 m^3/s. Groundwater discharge in this period ranged from 2 to 3 m^3/s. In period 2, river discharge at SH60 ranged from 132 to 161 m^3/s, and river discharge corrected for tributaries at Navasota ranged from 190 to 207 m^3/s. Groundwater discharge in this period ranged from 46 to 58 m^3/s. In period 3, river

discharge at SH60 ranged from 720 to 818 m^3/s, and river discharge corrected for tributaries at Navasota ranged from 626 to 664 m^3/s. Groundwater discharge in this period ranged from -154 to -94 m^3/s, indicating a net loss of water from the river to the aquifer. In period 4, river discharge at SH60 ranged from 356 to 394 m^3/s, and river discharge corrected for tributaries at Navasota ranged from 349 to 405 m^3/s. Groundwater discharge in this period ranged from -33 to 49 m^3/s. In the fifth and final period river discharge at SH60 ranged from 70 to 267 m^3/s, and river discharge corrected for tributaries at Navasota ranged from 104 to 255 m^3/s at Navasota. Groundwater discharge in this period ranged from -33 to 38 m^3/s.

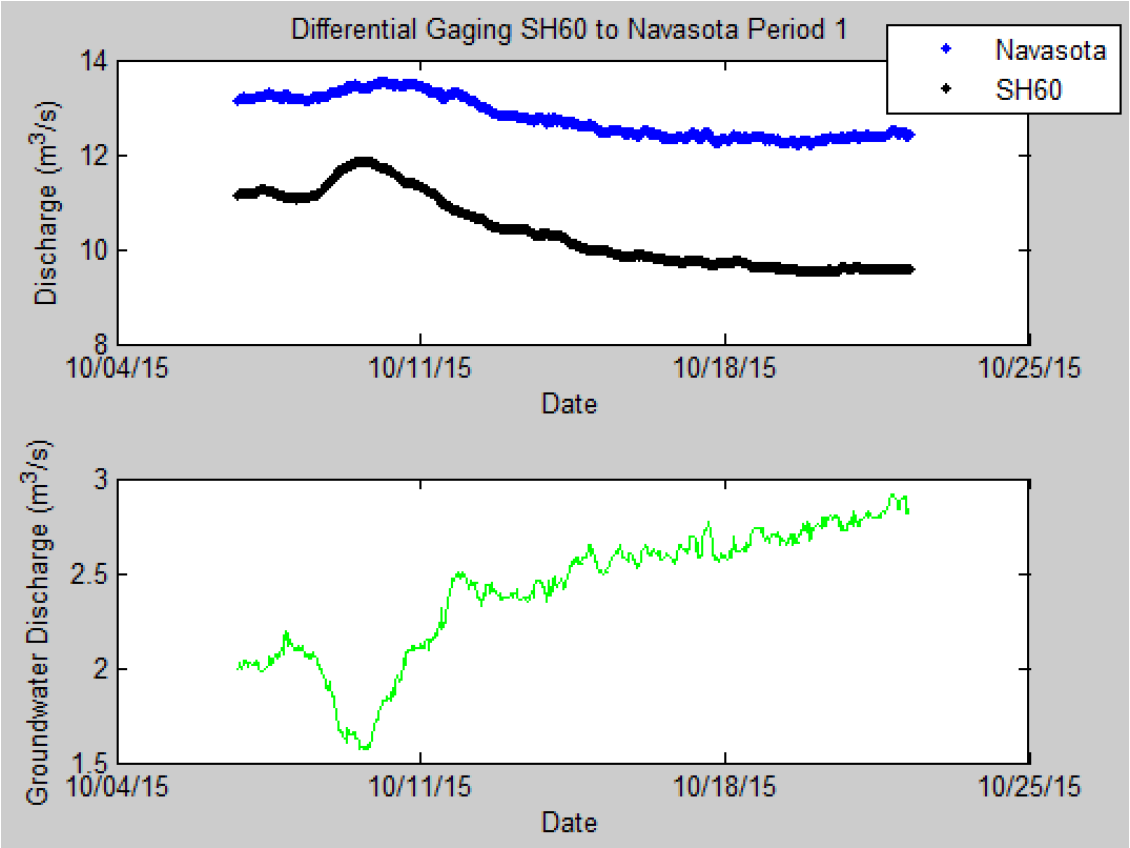

Figure 5-26: Discharges at Highway 60 and Navasota, as well as groundwater discharge calculation results for the first differential gaging study period. Tick marks are placed at the start of each day at midnight.

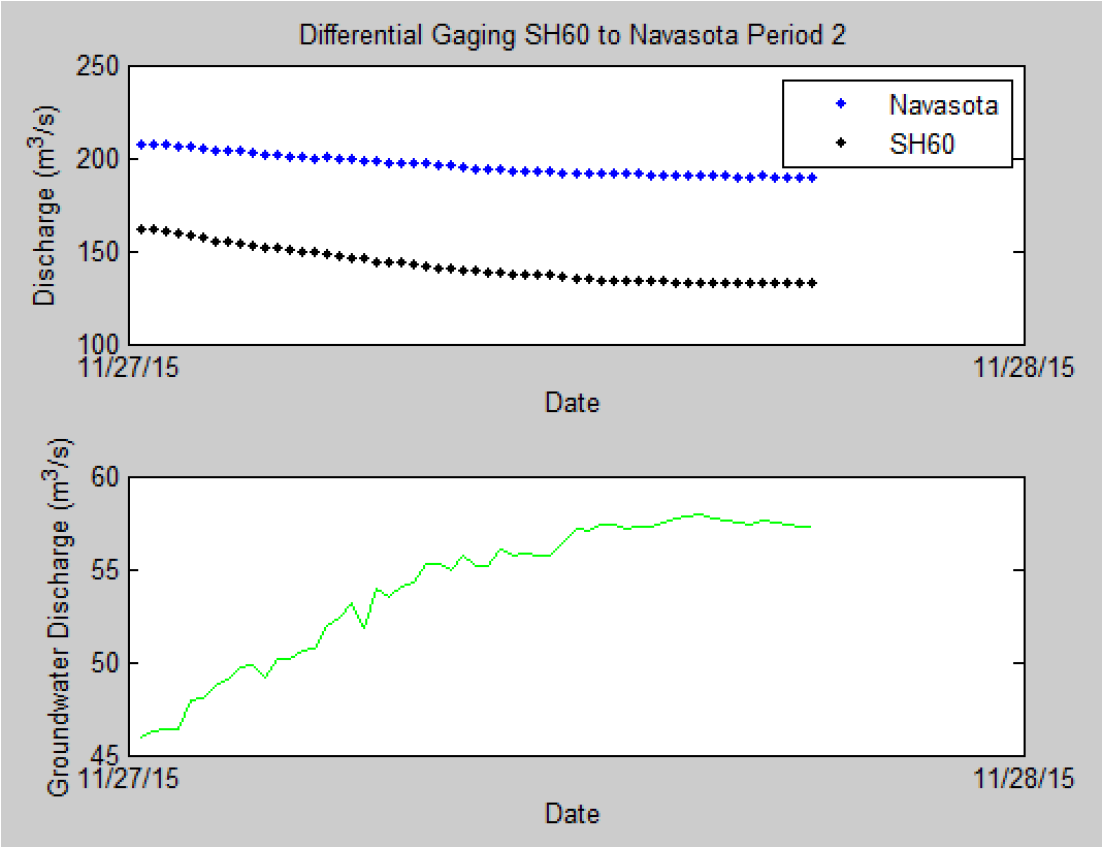

Figure 5-27: Discharges at Highway 60 and Navasota, as well as groundwater discharge calculation results for the second differential gaging study period. Tick marks are placed at the start of each day at midnight.

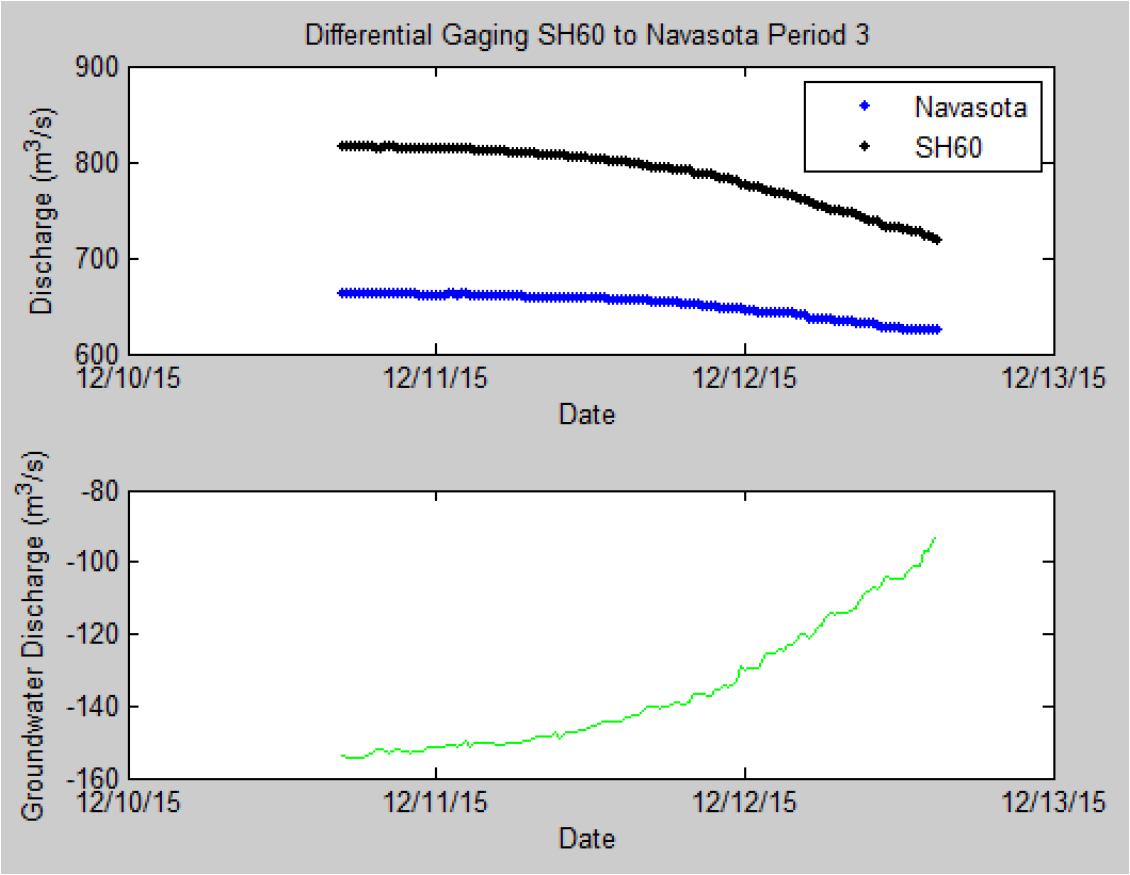

Figure 5-28: Discharges at Highway 60 and Navasota, as well as groundwater discharge calculation results for the third differential gaging study period. Tick marks are placed at the start of each day at midnight.

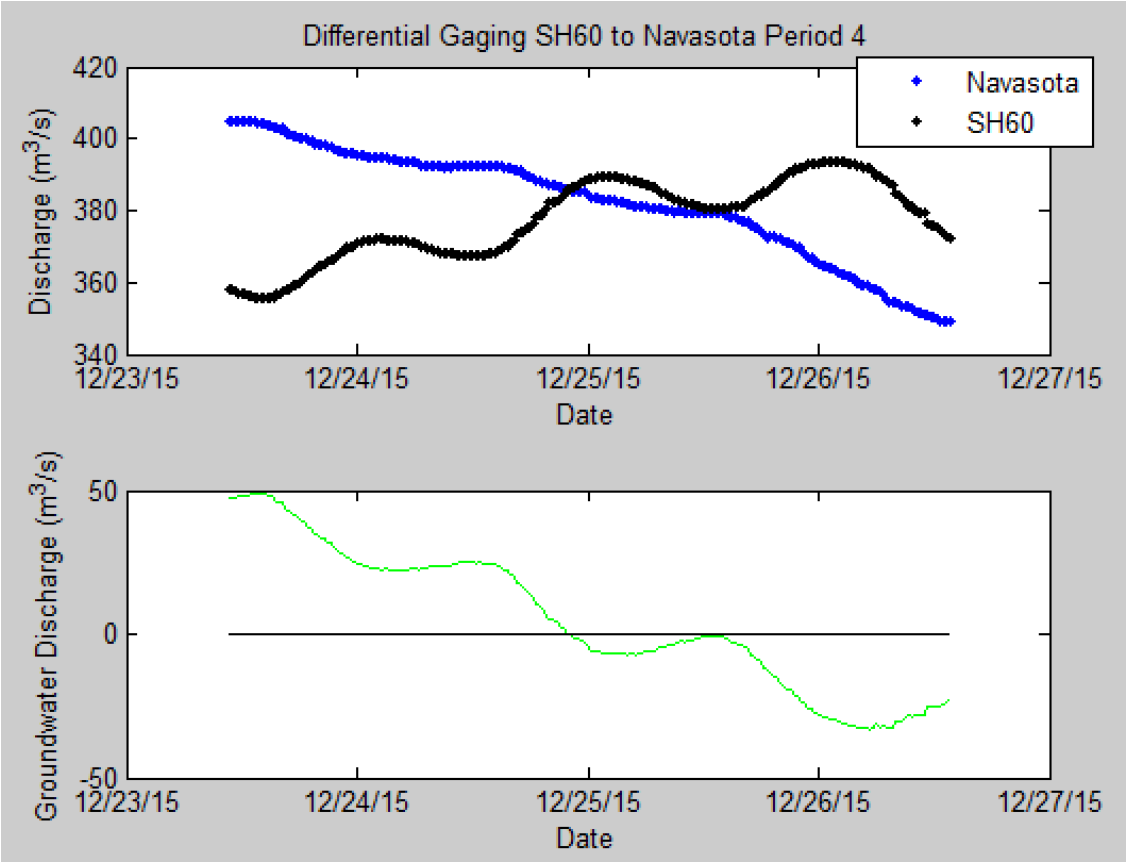

Figure 5-29: Discharges at Highway 60 and Navasota, as well as groundwater discharge calculation results for the fourth differential gaging study period. The black line in the bottom panel is the zero line. Tick marks are placed at the start of each day at midnight.

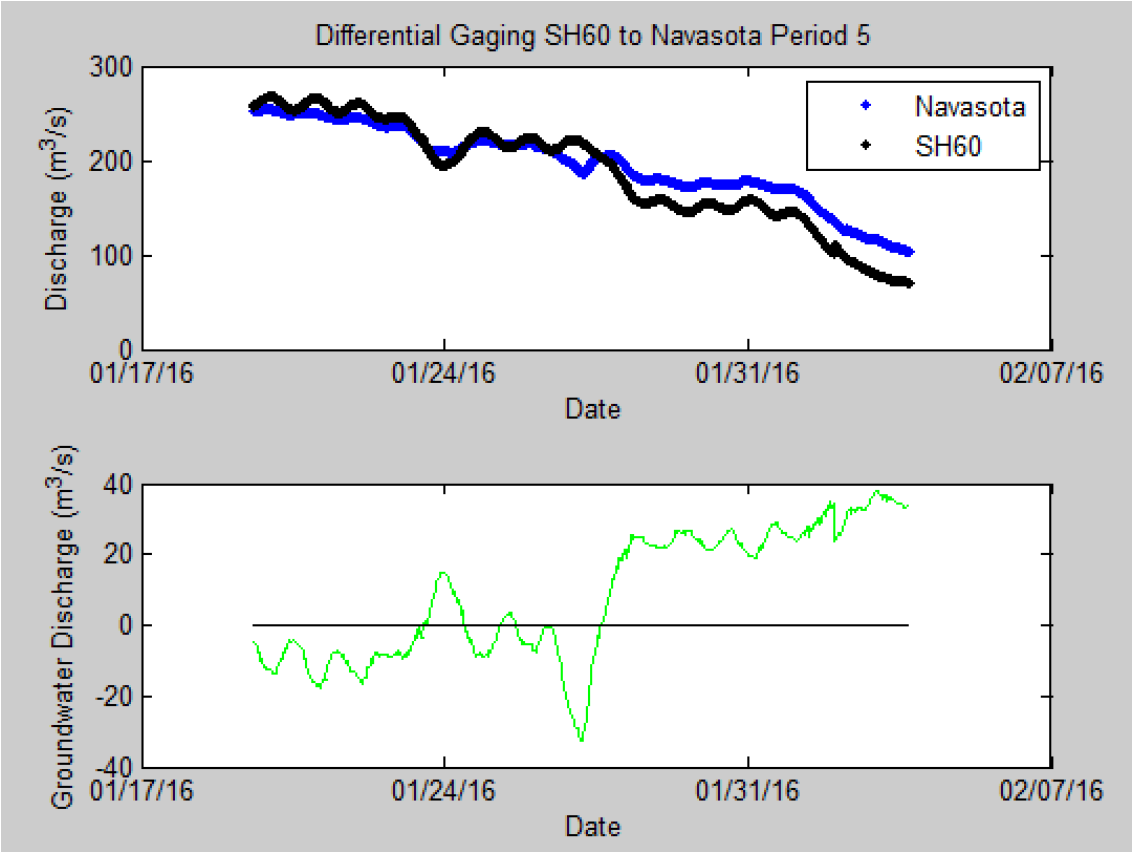

Figure 5-30: Discharges at Highway 60 and Navasota, as well as groundwater discharge calculation results for the fifth differential gaging study period. The black line in the bottom panel is the zero line. Tick marks are placed at the start of each day at midnight.

5.2 Estimating Groundwater Discharge with Specific Conductance Measurements

5.2.1 Continuous High Frequency Specific Conductance Measurements

Groundwater discharge was estimated between SH60 and Navasota using high frequency specific conductance and river discharge measurements and equation 4-5. The high frequency specific conductance and discharge data taken by our LTC pressure transducers at SH60 and Navasota are shown in figure 5-31. Specific conductance measurements taken manually at SH60 and Navasota with a YSI during this period are

shown on the same figure. The dry periods during which groundwater discharge calculations based on specific conductance mass balance were performed from SH60 to Navasota are shown on the hydrographs in figure 5-25 above. The date ranges are the same as those used for differential gaging, except for period 1, and can be found in table 5-3 above. The first period of calculation does not start at the same time as the first period of differential gaging (D days after the peak of the previous hydrograph). It does not start at the same time because the LTC pressure transducer at Navasota came partly out of the water sometime before the first SH60-Navasota dry period. The pressure reader remained in the water, allowing differential gaging measurements to continue, but the specific conductance reader came out of the water, making accurate specific conductance measurements unavailable. We re-submerged the Navasota pressure transducer completely at 1:00pm on October 7th, 2015, so that is when the first period of specific conductance measurements starts.

Specific conductance measurements and discharges at SH60 and Navasota, and groundwater discharge measurements between these two sites are shown in figures 5-32 through 5-36. Groundwater discharges calculated by differential gaging are also shown for comparison. Unlike for differential gaging, the discharge values used for the Navasota site were not corrected for tributary inflows when calculating groundwater discharge from specific conductance. They were not corrected because the estimates of groundwater discharge from specific conductance were made via mass balance (equation 4-5). The mass balance required accounting for the total mass at the upstream and downstream sites, which means the total river discharge at Navasota had to be used in

these calculations. Specific conductance data, discharge data, and a representative groundwater specific conductance value were input into equation 4-5 to calculate groundwater discharge. We obtained our groundwater specific conductance by averaging the specific conductances of nine wells in the BRAA (figure 4-6), which resulted in a value of 1267 µS/cm.

In the first period, river discharge at SH60 ranged from 9 to 12 m^3/s, and river discharge at Navasota ranged from 12 to 14 m^3/s. Specific conductance values at SH60 ranged from 162 to 235 µS/cm, and at Navasota they ranged from 815 to 1008 µS/cm. Calculated groundwater discharge in the stretch using specific conductance and the river discharges at each site ranged from 6 to 9 m^3/s, holding fairly constant. During the second period river discharge at SH60 ranged from 132 to 161 m^3/s, and river discharge at Navasota ranged from 245 to 264 m^3/s. Specific conductance values at SH60 ranged from 340 to 352 µS/cm, and at Navasota they ranged from 427 to 450 µS/cm. The calculated groundwater discharge in this period ranged from 46 to 51 m^3/s. In the third period, river discharge at SH60 ranged from 719 to 820 m^3/s, and river discharge at Navasota ranged from 676 to 719 m^3/s. Specific conductance values at SH60 ranged from 457 to 667 µS/cm, and at Navasota they ranged from 568 to 589 µS/cm. Groundwater discharge in this period ranged from -69 to 55 m^3/s. In the fourth period, river discharge at SH60 ranged from 354 to 395 m^3/s, and river discharge at Navasota ranged from 398 to 458 m^3/s. Specific conductance values at SH60 ranged from 179 to 213 µS/cm, and at Navasota they ranged from 465 to 477 µS/cm. Groundwater discharge in this period ranged from 93 to 112 m^3/s. During the fifth period, river discharge at

SH60 ranged from 70 to 268 m^3/s, and river discharge at Navasota ranged from 108 to 307 m^3/s. Specific conductance values at SH60 ranged from 274 to 608 µS/cm, and at Navasota they ranged from 469 µS/cm 573 µS/cm. Groundwater discharge in this period ranged from -1 to 58 m^3/s.

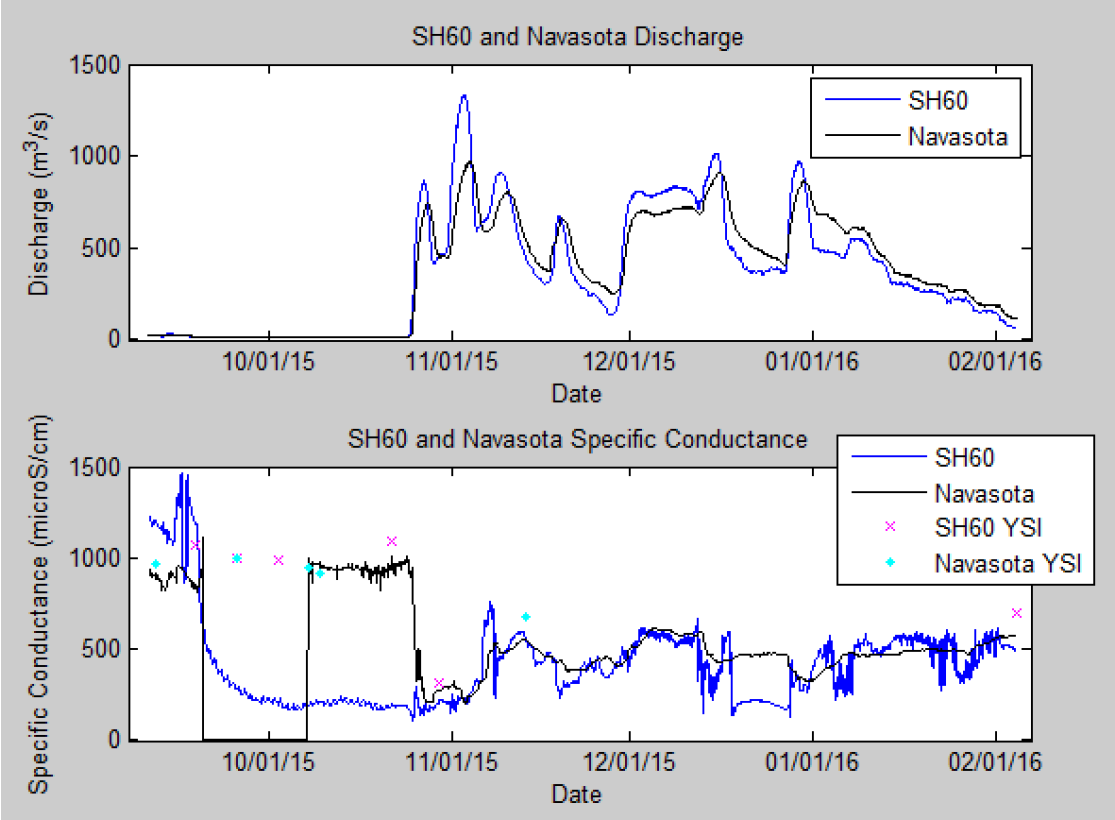

Figure 5-31: Discharges (top) and measured specific conductance values (bottom) at SH60 and Navasota gages. On-the-spot specific conductance measurements were taken with a YSI any time we visited a gage site. They are shown on the lower panel with pink Xs (SH60) and light blue dots (Navasota). YSI measurements were taken during the first dry period, but did not overlap with any other dry periods.

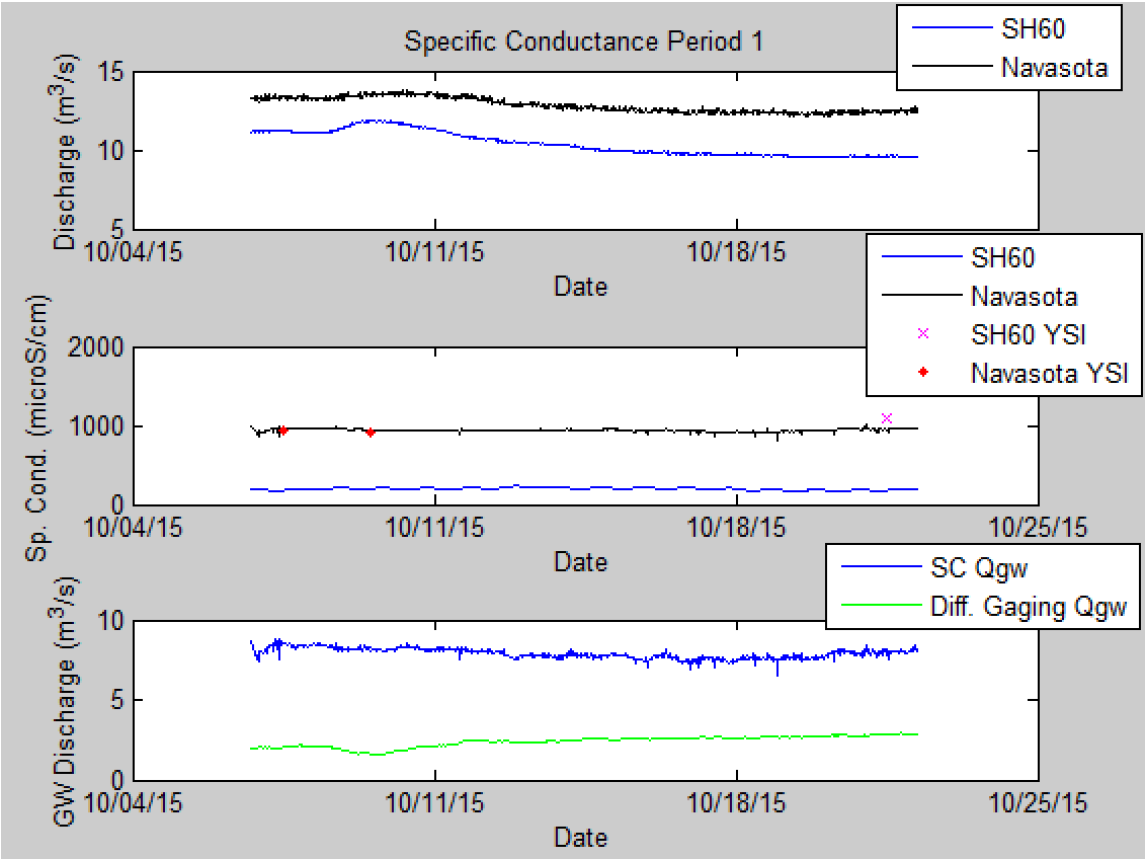

Figure 5-32: River discharge and specific conductance measurements at Highway 60 and Navasota, and calculated groundwater discharge for the first calculation period. Lag times have been incorporated into these data. Tick marks are placed at the start of each day at midnight.

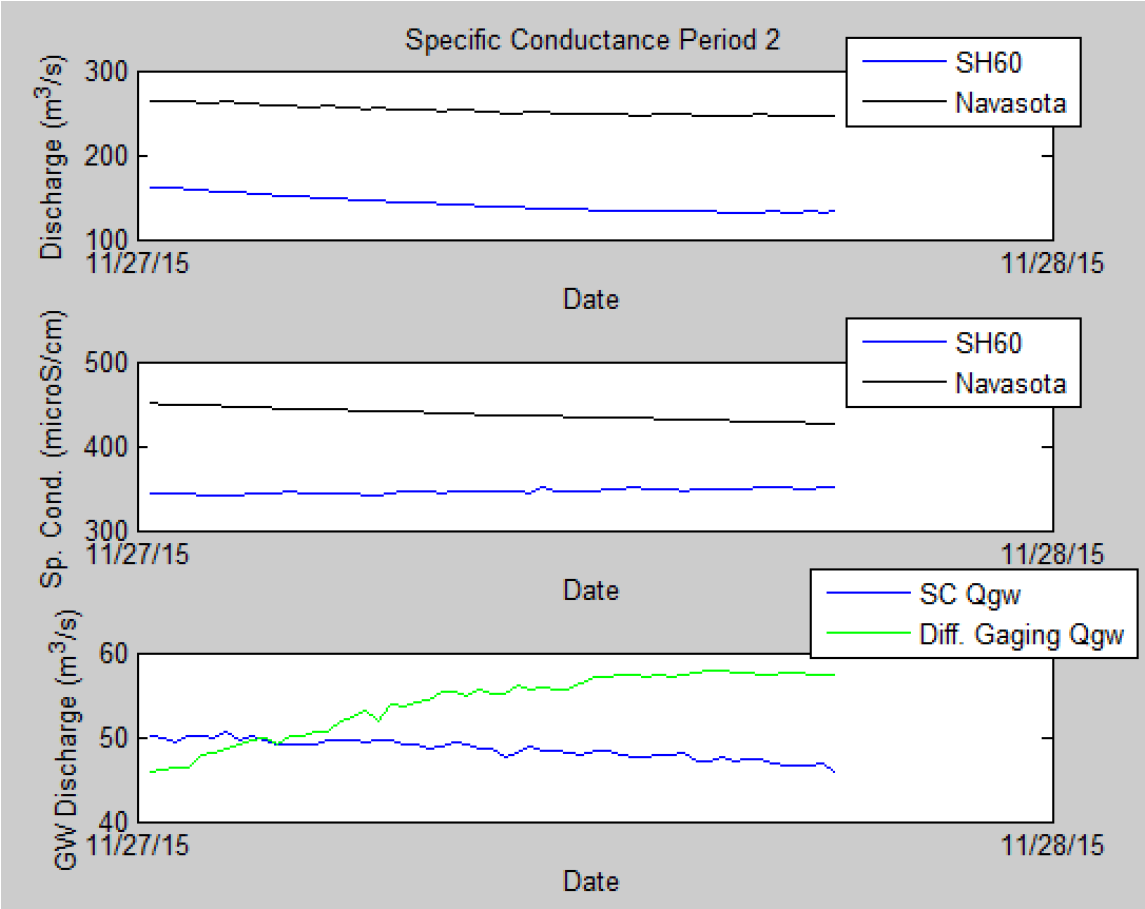

Figure 5-33: River discharge and specific conductance measurements at Highway 60 and Navasota, and calculated groundwater discharge for the second calculation period. Lag times have been incorporated into these data. Tick marks are placed at the start of each day at midnight.

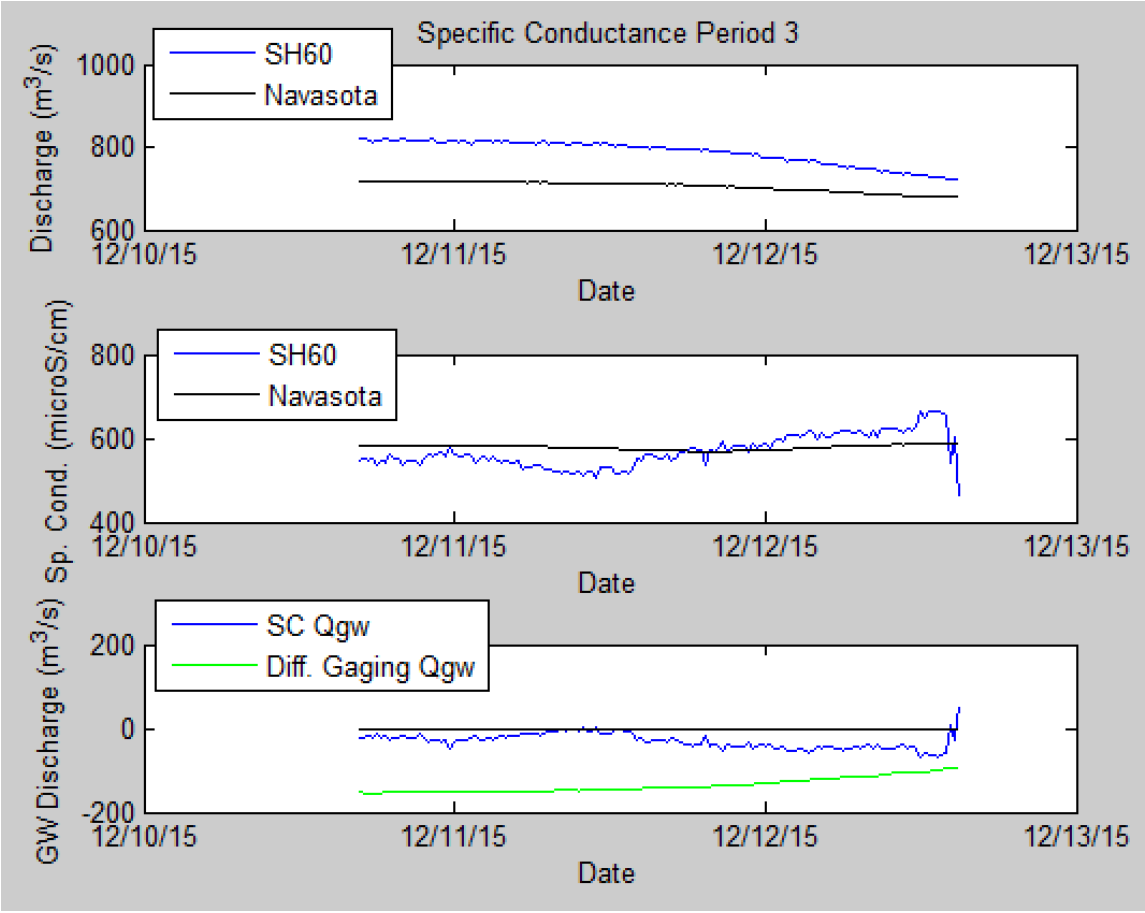

Figure 5-34: River discharge and specific conductance measurements at Highway 60 and Navasota, and calculated groundwater discharge for the third calculation period. Lag times have been incorporated into these data. The black line in the bottom panel is the zero line. Tick marks are placed at the start of each day at midnight.

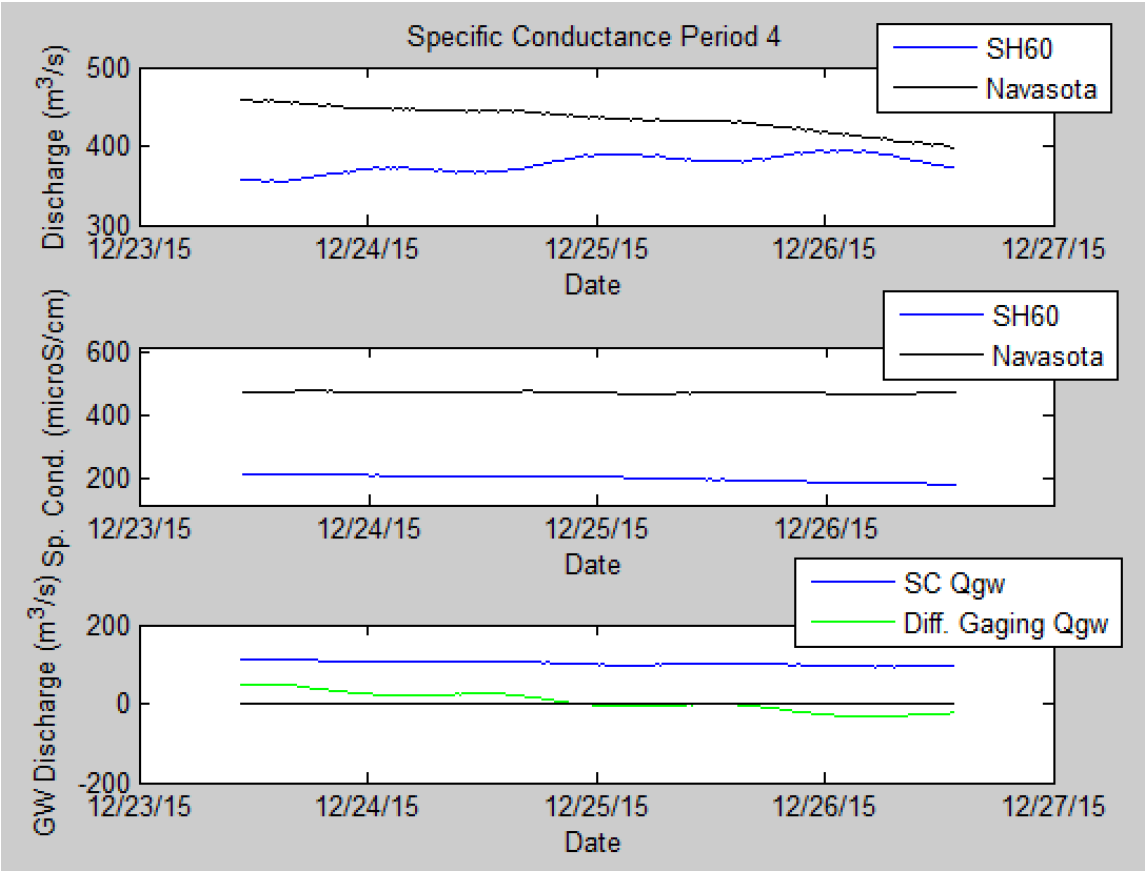

Figure 5-35: River discharge and specific conductance measurements at Highway 60 and Navasota, and calculated groundwater discharge for the fourth calculation period. Lag times have been incorporated into these data. The black line in the bottom panel is the zero line. Tick marks are placed at the start of each day at midnight.

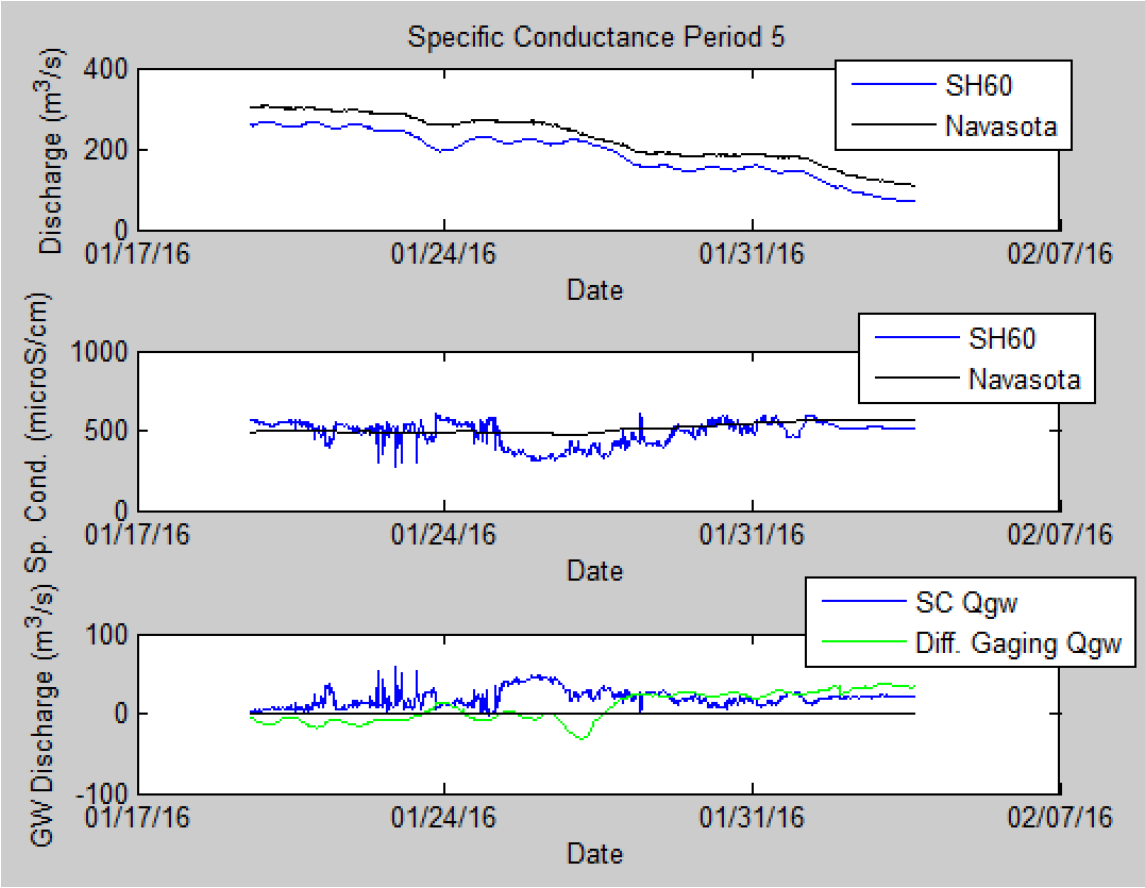

Figure 5-36: River discharge and specific conductance measurements at Highway 60 and Navasota, and calculated groundwater discharge for the fifth calculation period. Lag times have been incorporated into these data. The black line in the bottom panel is the zero line. Tick marks are placed at the start of each day at midnight.

5.2.2 Longitudinal Surveys

We conducted four different longitudinal specific conductance surveys from SH21 to SH60 on July 31, August 22, October 19, and October 21, 2015. During these surveys we collected specific conductance measurements in the river every six minutes as we paddled a canoe downstream from SH21 to SH60 over the course of each day. The measurements taken during these surveys are shown in figures 5-39 through 5-42.

We used equation 4-5 and the same representative groundwater specific conductance value that was used for our continuous high frequency specific conductance measurements (1267 µS/cm). The dates of the surveys are shown over river discharge at both SH21 and SH60 in figure 5-37. During the earliest survey conducted on July 31, 2015, specific conductance fairly constantly increased from SH21 to SH60 with values ranging from 638 to 666 µS/cm (figure 5-39). The groundwater discharge estimation from these data was 15.98 m^3/s. During the second survey conducted on August 22, 2015, specific conductance values decreased fairly continuously from SH21 to SH60 from 912 to 878 µS/cm. These values resulted in a groundwater discharge estimate of 5.70 m^3/s.

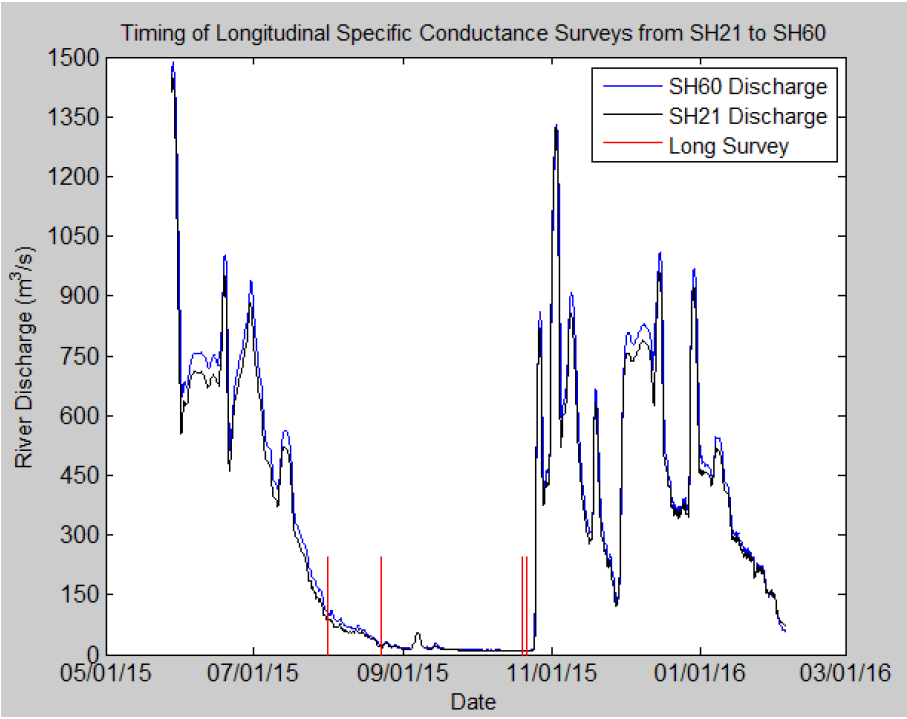

Figure 5-37: The timings of the four longitudinal surveys are indicated by vertical red lines on this graph of river discharges at SH21 and SH60.

The specific conductance surveys completed on October 19 and 21, 2015, can be seen to stop at the inflow of a tributary in figures 5-41 and 5-42. This tributary is Thompsons Creek (figure 5-38), and it discharges treated wastewater from the nearby Thompsons Creek Wastewater Treatment Plant at some times during the year, but not all year. The specific conductance values spiked by approximately 100 µS/cm downstream of the influent point of this stream, so the survey data below that point were suspected to be influenced by treatment plant discharges and were not used.

Excluding the values affected by the wastewater treatment plant outflow, the specific conductance on October 19, 2015, fluctuated between 901 and 916 µS/cm. Groundwater discharge was calculated to be -1.01 m^3/s. This method, however, is a mass balance that can only measure positive groundwater discharges, so the groundwater discharge on this day can be considered 0 m^3/s. Specific conductance decreased fairly continuously on October 21, 2015, from 1006 to 981 µS/cm. The calculated groundwater discharge from this survey was 1.70 m^3/s. The values input into equation 4-5 to obtain these groundwater discharge estimates can be found in table 5-4.

Table 5-4: This table summarizes the values used to calculate groundwater discharge from four separate longitudinal specific conductance surveys conducted from SH21 to SH60.

Date	Q_{us} (m3/s)	Q_{ds} (m3/s)	C_{gw} (mg TDS/L)	C_{us} (mg TDS/L)	C_{ds} (mg TDS/L)	Q_{gw} (m3/s)
7/31/2015	89	116	823.55	414.7	431.6	15.98
8/22/2015	25	34	823.55	592.8	573.95	5.70
10/19/2015	7.2	5.8	823.55	590.85	590.2	-1.01
10/21/2015	5.97	8.3	823.55	653.25	638.95	1.70

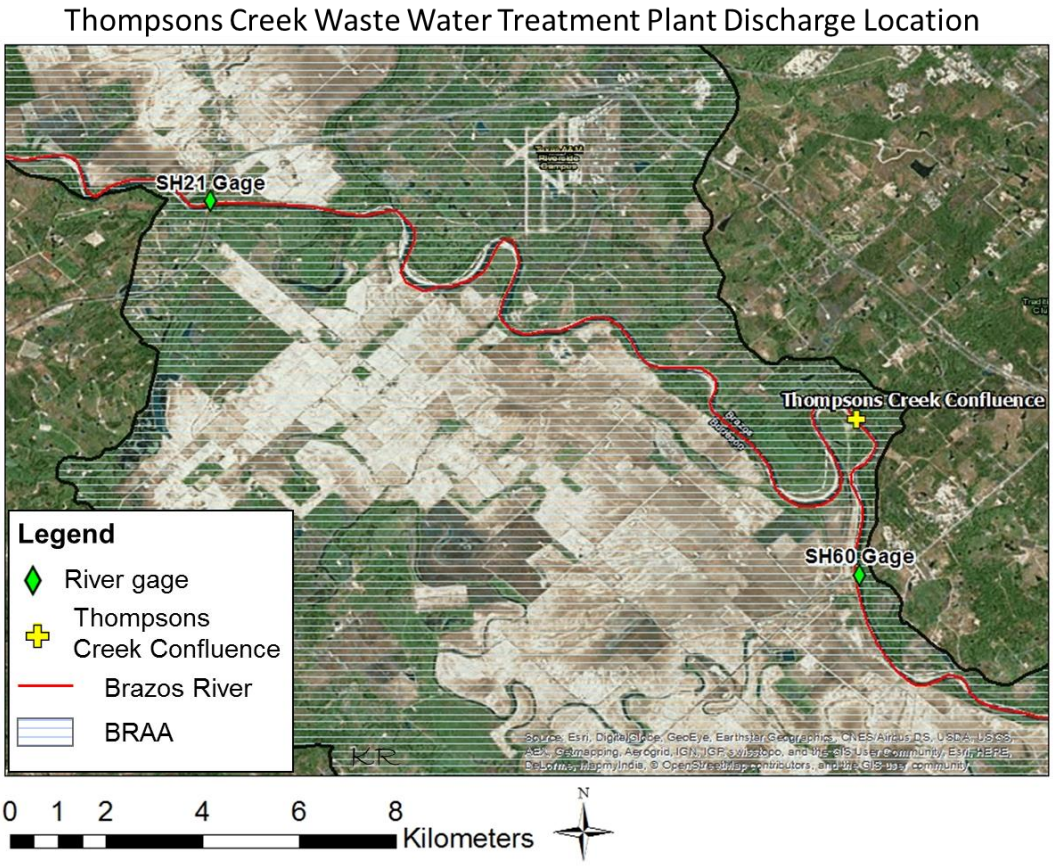

Figure 5-38: Location of the discharge from the Thompsons Creek Waste Water Treatment Plant. Satellite imagery provided by ESRI.

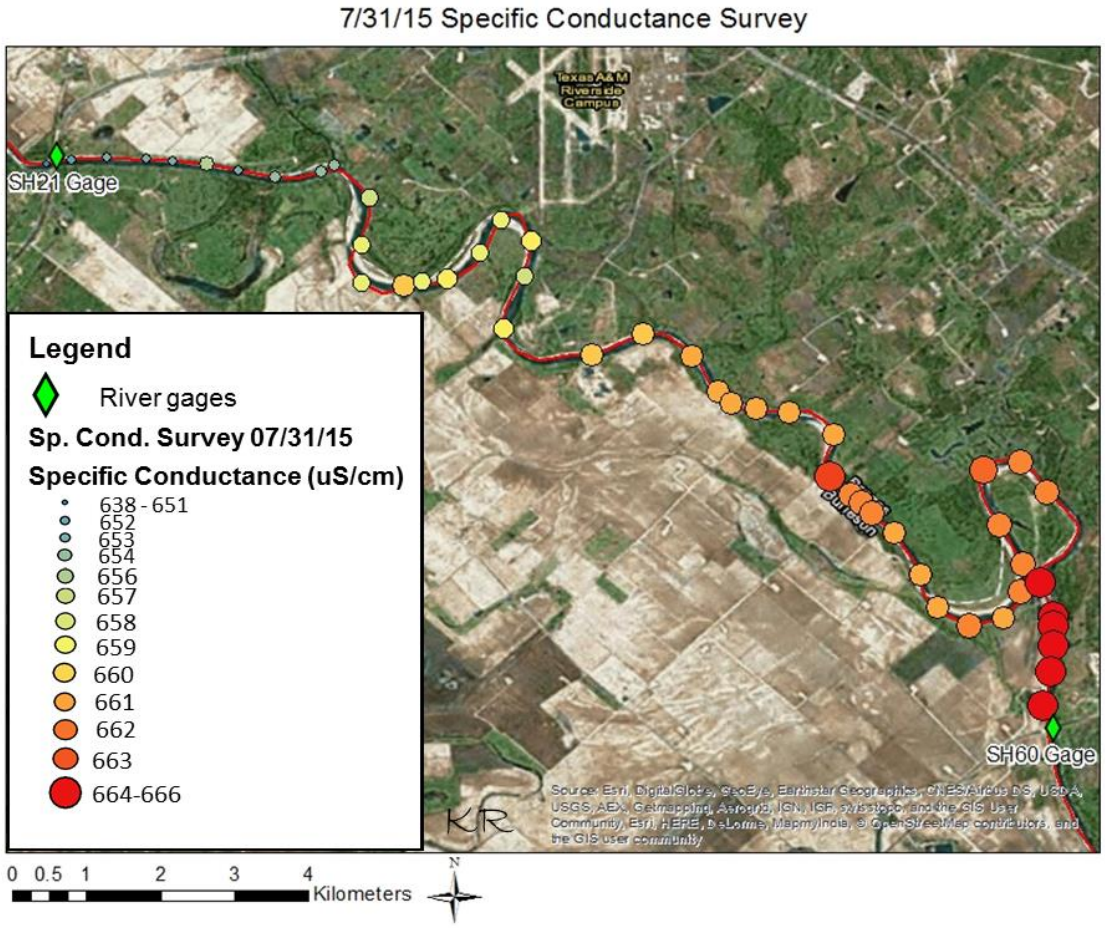

Figure 5-39: Longitudinal specific conductance survey from 7/31/15. The specific conductance increases nearly continuously from 638 to 666 µS/cm. Satellite imagery provided by ESRI.

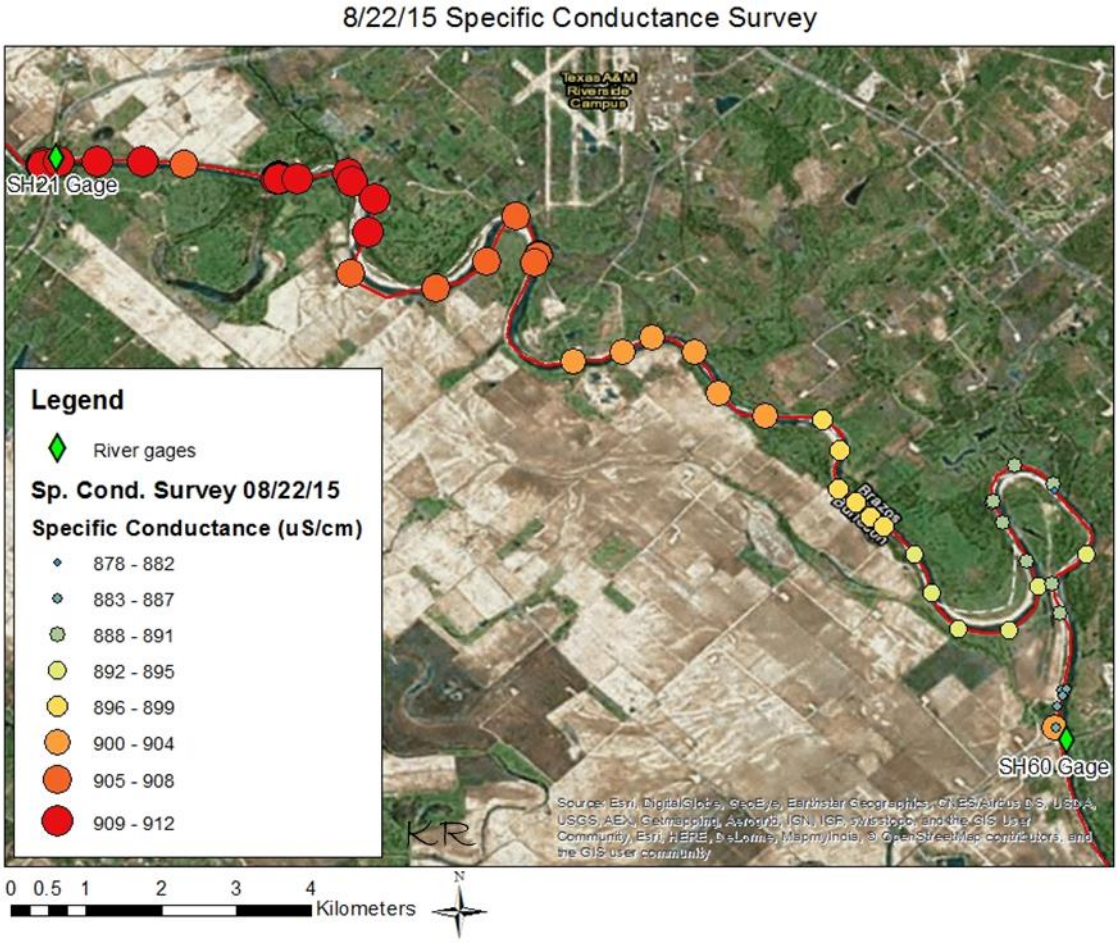

Figure 5-40: Longitudinal specific conductance survey from 8/22/15. The specific conductance decreases nearly continuously from 912 to 878 µS/cm. Satellite imagery provided by ESRI.

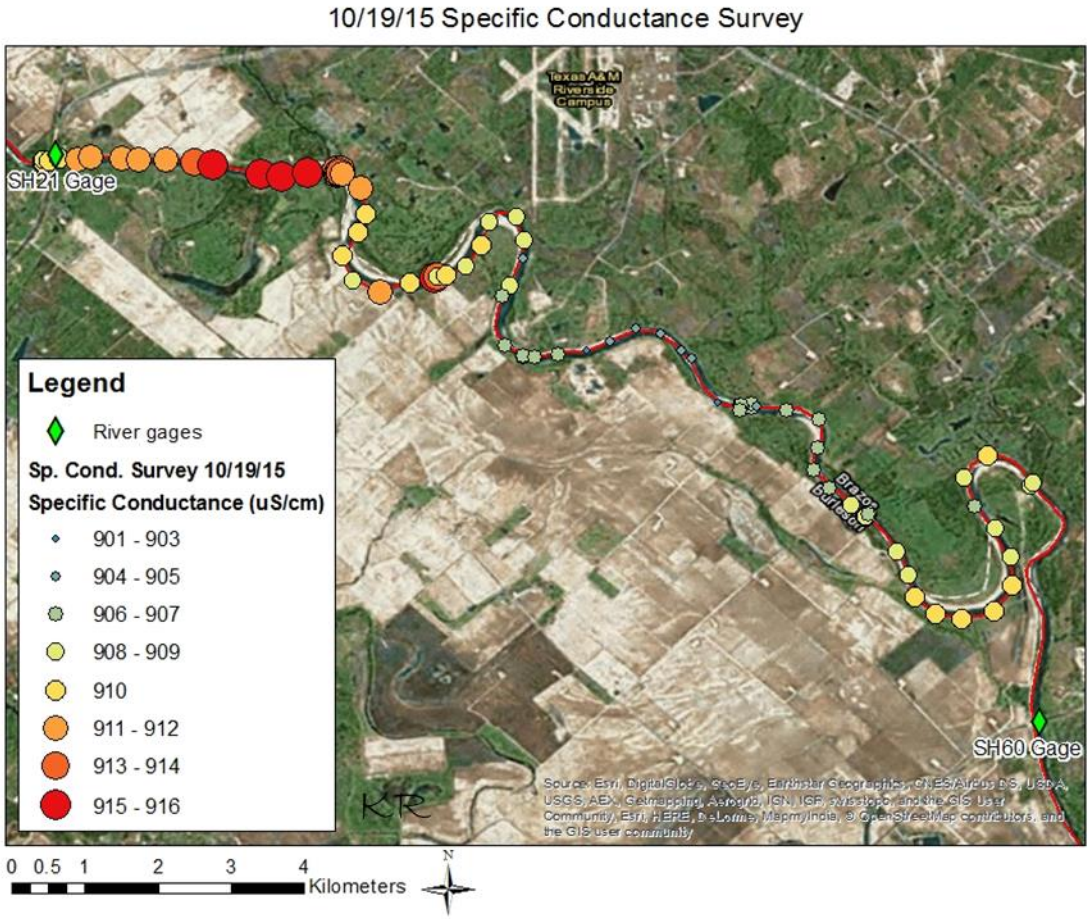

Figure 5-41: Longitudinal specific conductance survey from 10/19/15. The specific conductance fluctuates between 901 and 916 µS/cm. Satellite imagery provided by ESRI.

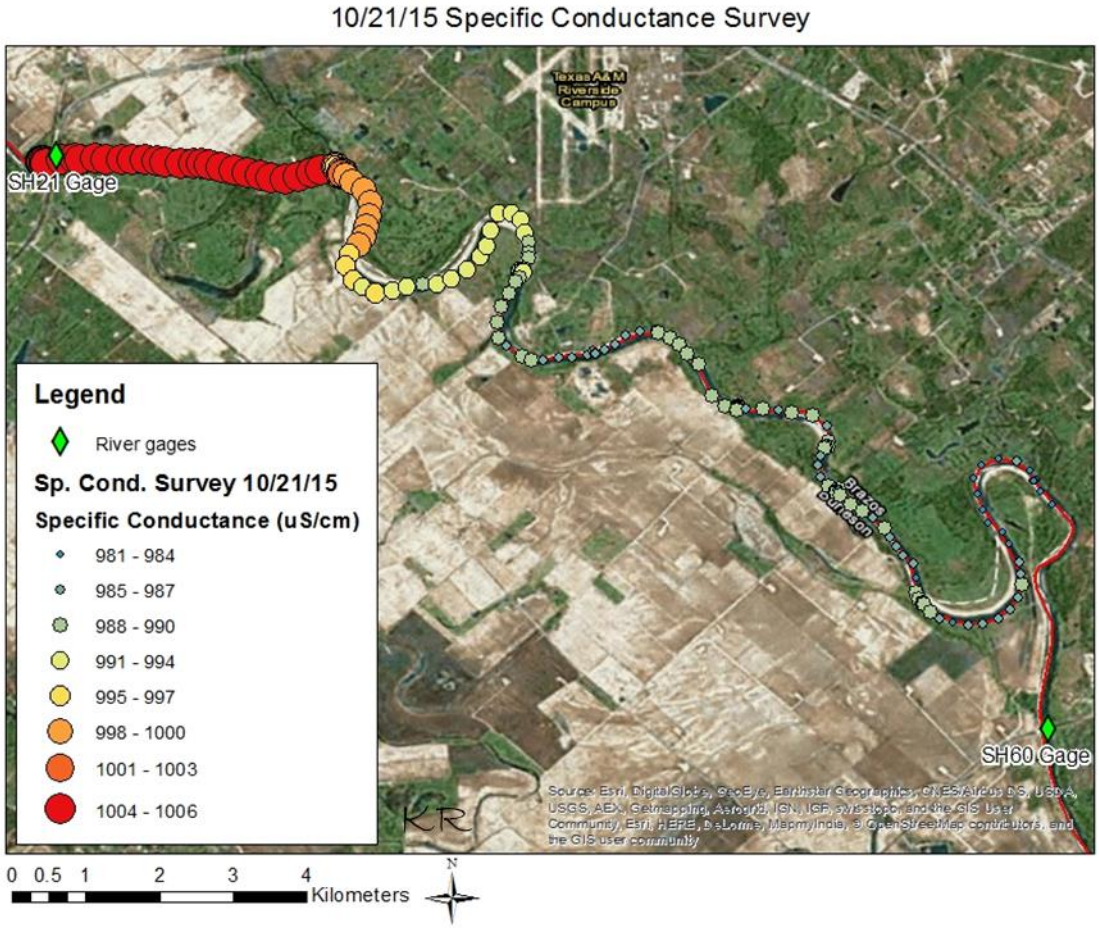

Figure 5-42: Longitudinal specific conductance survey from 10/21/15. The specific conductance fluctuates, but generally decreases from 1006 to 981 µS/cm. Satellite imagery provided by ESRI.

5.3 Estimating Groundwater Discharge using Major Ions and EMMA

We measured major ion concentrations on 31 river samples and 10 groundwater samples taken throughout our study period. From the ion concentrations of these samples and an assessment of our study site, we identified four endmember water bodies that we expected to contribute water to the Brazos River. The four endmembers we identified are 1) Lake Whitney, the lake 266 river-km upstream of our study area,

formed by a dam that releases water to help maintain minimum flows in the Brazos River. 2) Brazos River Alluvial Aquifer. 3) Groundwater on the eastern side of the river, possibly from the Yegua formation. 4) A combination of bank storage and runoff as sampled from the river immediately following five separate large rain events. The ion chemistry from Lake Whitney was obtained from a separate study (van Plantinga et al., in review), and the chemistry assumed for the bank storage/runoff component is an average of the samples taken from the river following the five rain events.

We performed a principal component analysis (PCA) to ensure the samples we had identified as endmembers indeed were good representative components of our Brazos River samples. Before PCA could be conducted, the major ions appropriate to include in the PCA had to be identified. They were found by plotting the concentrations of each ion against every other ion for every sample. Those results are shown in figure 5-43. Ions that had endmember concentrations (represented by the dark blue, green, red, and light blue circles in figure 5-43) that encapsulated the river sample concentrations (represented by pink circles) were selected for inclusion in PCA. The ions we included were sodium, magnesium, calcium, chloride, sulfate, and bicarbonate because the endmember values encapsulated the river sample values well (figure 5-43).

The results of PCA, performed on Z-scores of sample concentrations (i.e. standardized concentrations), are shown in figures 5-44 through 5-50. The scree plot, which shows the amount of variability explained by PC1, PC2, and PC3, is shown in figure 5-44. Plots of PC1 vs. PC2, PC2 vs. PC3, and PC1 vs. PC3 are shown in figures 5-45 through 5-47 with scores of each sample plotted against each other. The scores of

samples show where they lie in principal component space, as opposed to where they lie in terms of concentrations of single ions. The loadings of the principal components, or the weight of each ion for that PC, are shown in figures 5-48 through 5-50. These loadings figures show the importance of each ion for each PC. The scree plot in figure 5-44 shows that PC1 explains 62% of the variability in our ion data, and PC2 explains 27%. Combined, PC1 and PC2 explain 89% of the variability in the data. PC3 explains only 8.35% of the variability.

The plot of PC1 vs. PC2 (figure 5-45) shows the river sample PC scores are well encapsulated within the endmember PC scores. This shows that these are likely good endmember values. They are well encapsulated in the graph of PC1 vs. PC3 (figure 5-46), as well, which is more evidence of good endmember values. The river sample values are not encapsulated by endmember values as well in the plot of PC2 vs. PC3 (figure 5-47), likely because PC2 and PC3 do not describe enough of the variability on their own to provide good results.

The graphs of loadings describe the primary ions that make up each principal component. From figure 5-48 it can be inferred that PC1 has fairly equal influence from sodium, magnesium, calcium, chloride, and sulfate as they all have similar positive scores between 0.4 and 0.5. PC2 is most influenced by alkalinity, or bicarbonate, followed by magnesium with scores near 0.8 and 0.6, respectively (figure 5-48). PC3 does not describe much of the variability and therefore is not as important as PC1 or PC2, but it is most influenced positively by calcium, and influenced negatively by

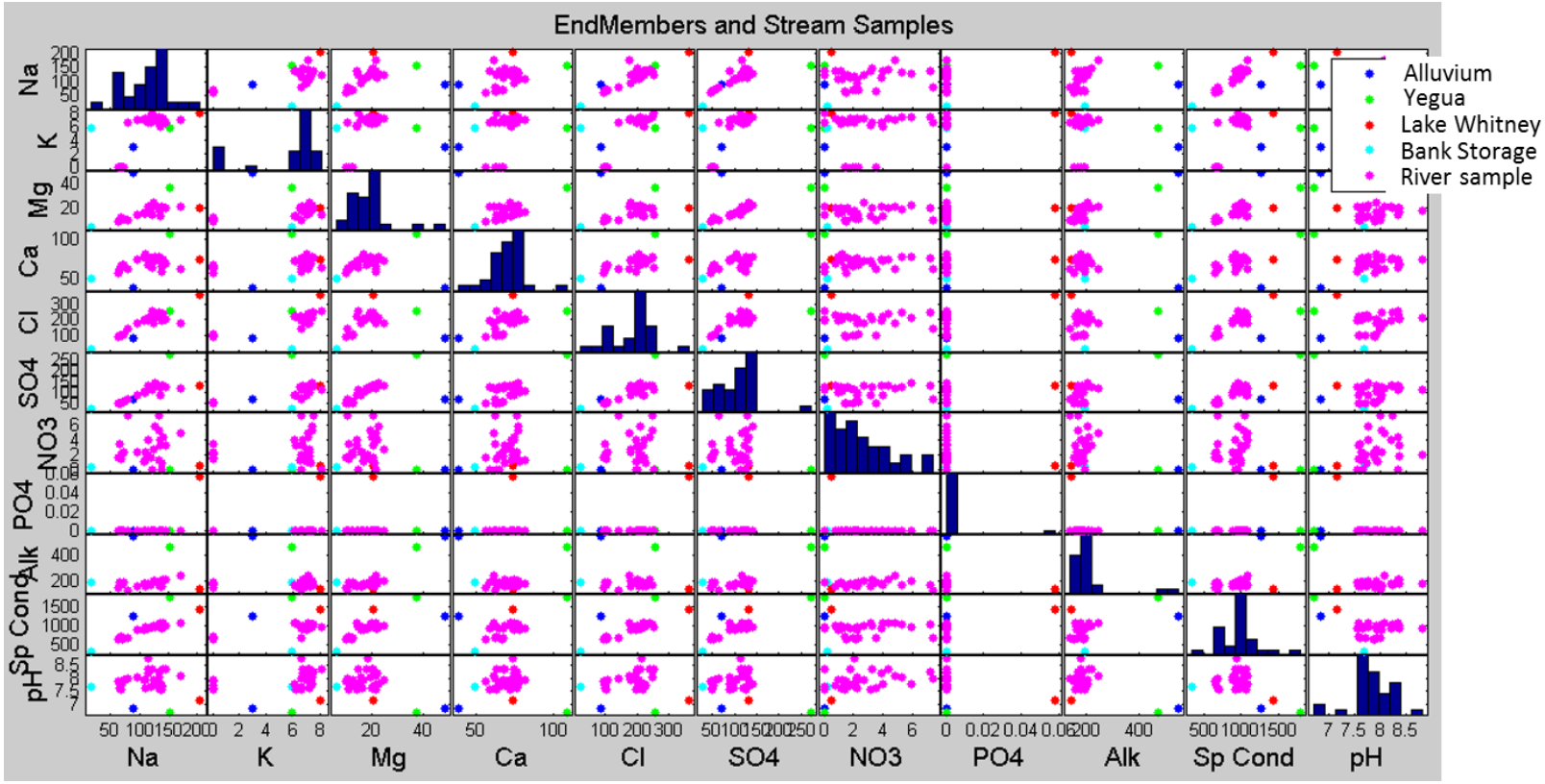

Figure 5-43: Ion concentrations in river samples and endmember samples plotted against each other. Ions in which the endmember values form a polygon around the river sample values were selected for PCA.

sodium, though calcium has the highest absolute value score near 0.8 (figure 5-49). Sodium has a score near -0.5 (figure 5-49).

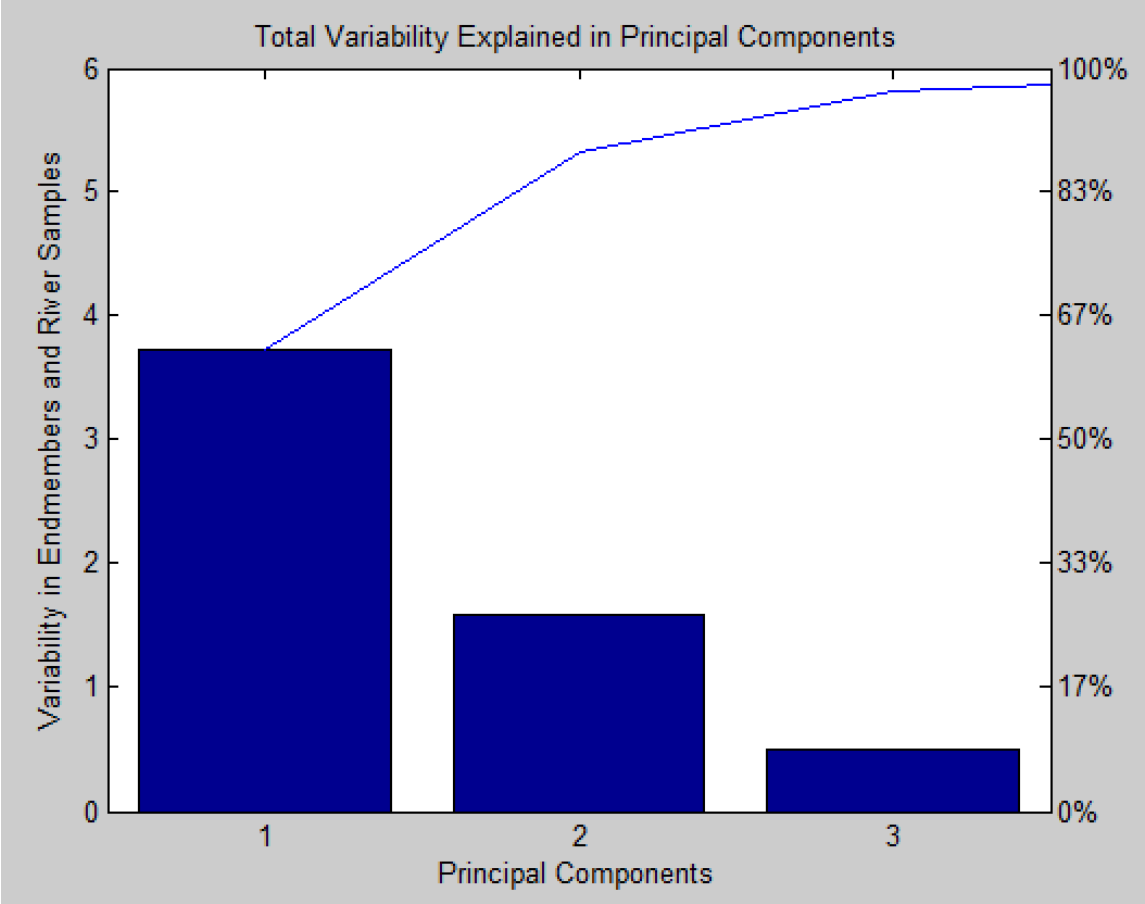

Figure 5-44: Scree plot showing the variability in our water sample data described by each principal component. PC3 describes only 8.35% of the variability, while PC1 explains 62% of the variability and PC2 explains 27%.

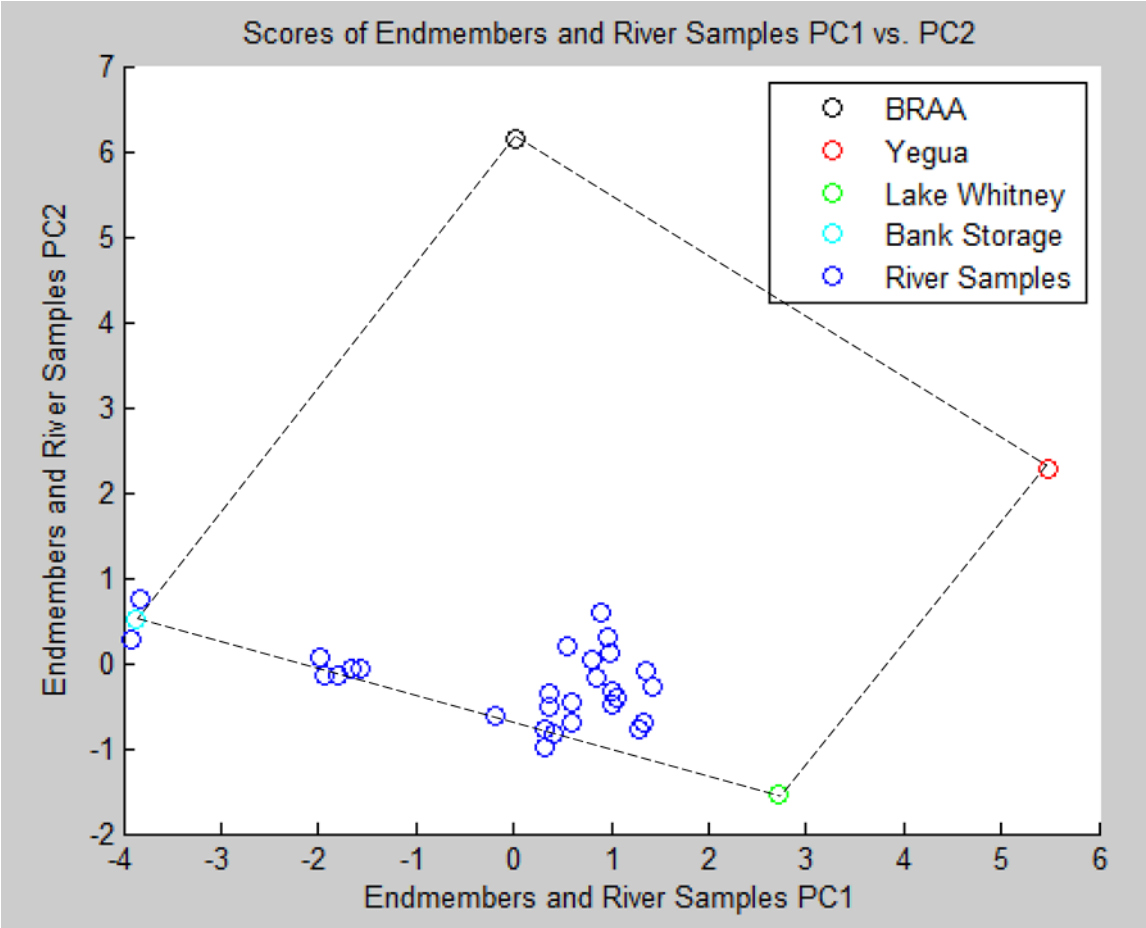

Figure 5-45: This figure shows the scores of the endmember samples and river samples on PC1 and PC2. The river samples are within the polygon formed by the endmember values, showing that their composition is some combination of the endmembers.

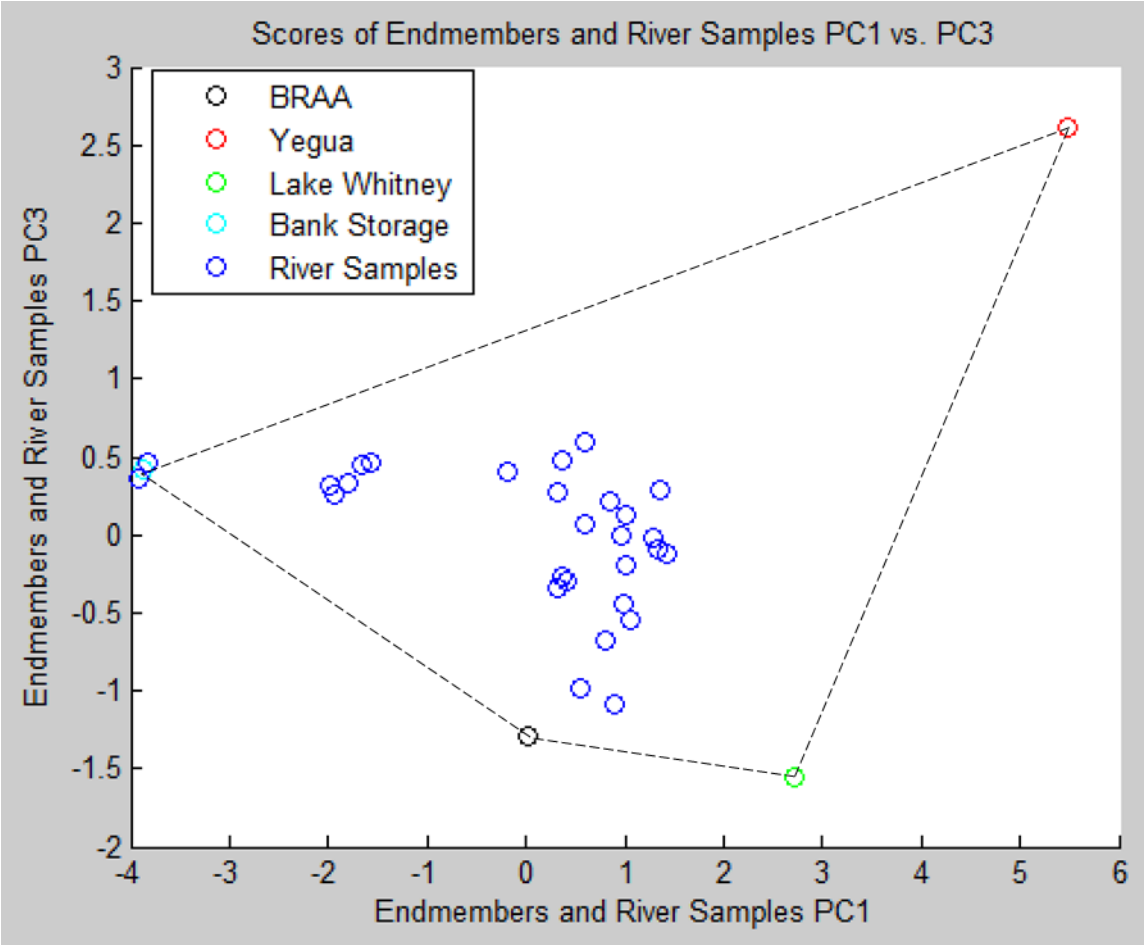

Figure 5-46: This figure shows the scores of the endmember samples and river samples on PC1 and PC3. The river samples are within the polygon formed by the endmember values, showing that their composition is some combination of the endmembers.

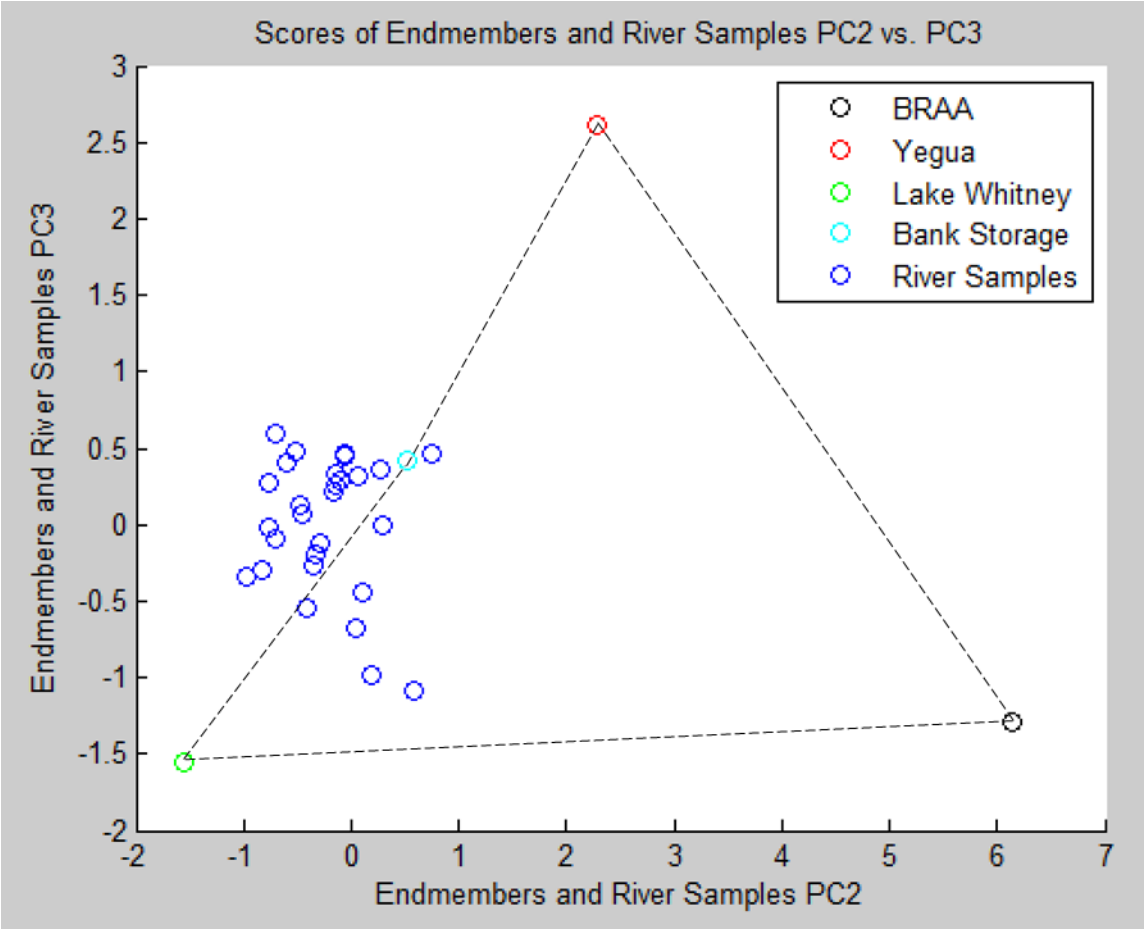

Figure 5-47: This figure shows the scores of the endmember samples and river samples on PC2 and PC3. The river samples are not enclosed within the polygon formed by the endmember values as well as for PC1 vs. PC2 and PC1 vs. PC3. That is likely because the variability is not explained as well by PC2 and PC3 as by PC1 and either PC2 or PC3.

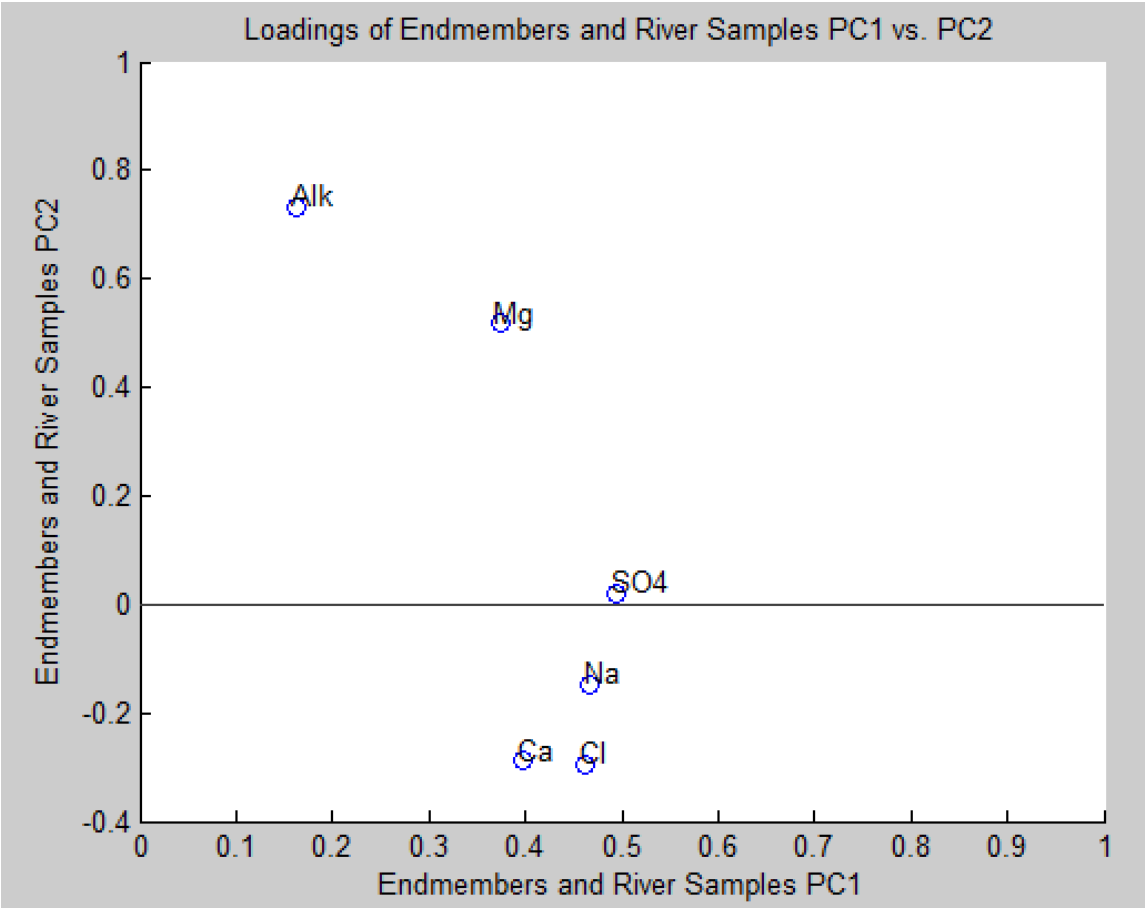

Figure 5-48: This figure shows the loadings of PC1 and PC2. PC1 is affected almost equally by calcium, chloride, sodium, sulfate, and magnesium. PC2 is affected strongest by alkalinity, and second strongest by magnesium.

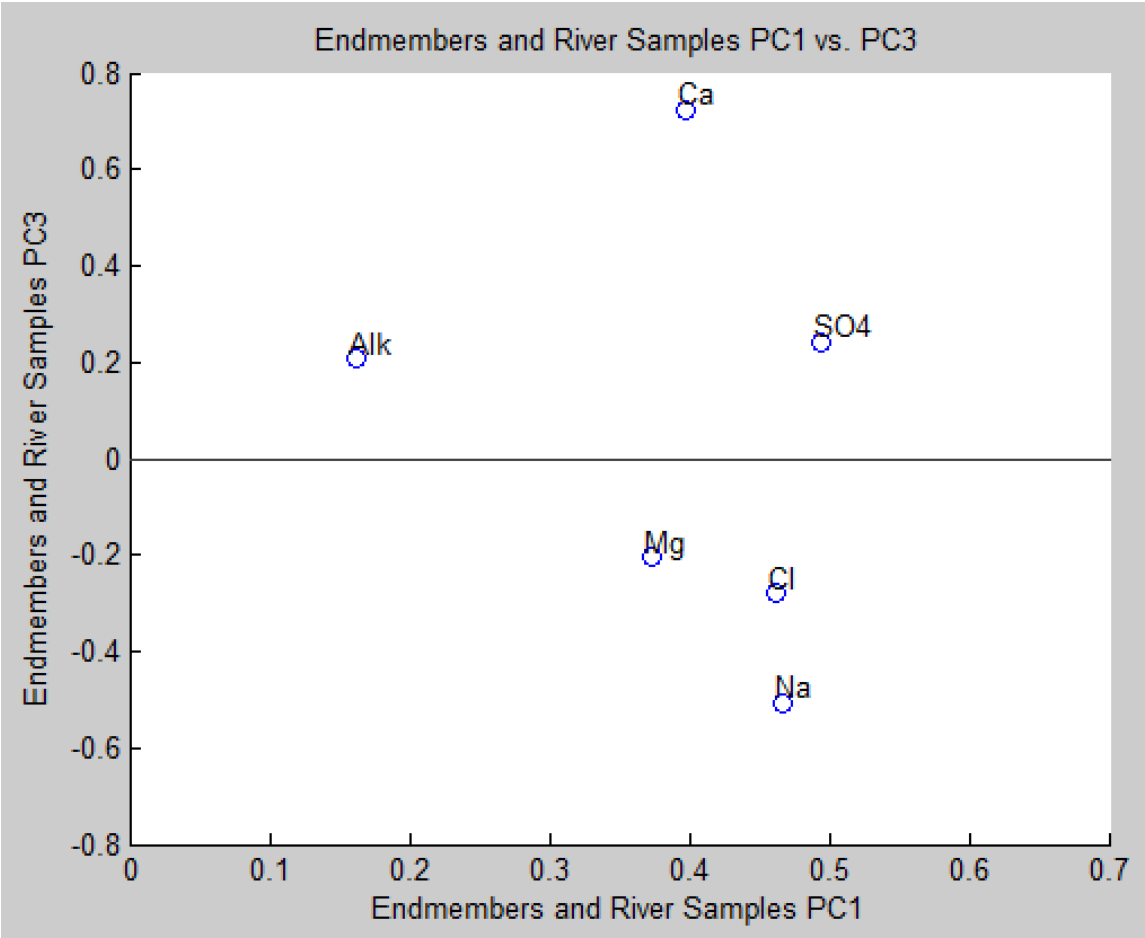

Figure 5-49: This figure shows the loadings of PC1 and PC3. PC1 is affected almost equally by calcium, chloride, sodium, sulfate, and magnesium. PC3 is affected most strongly by calcium.

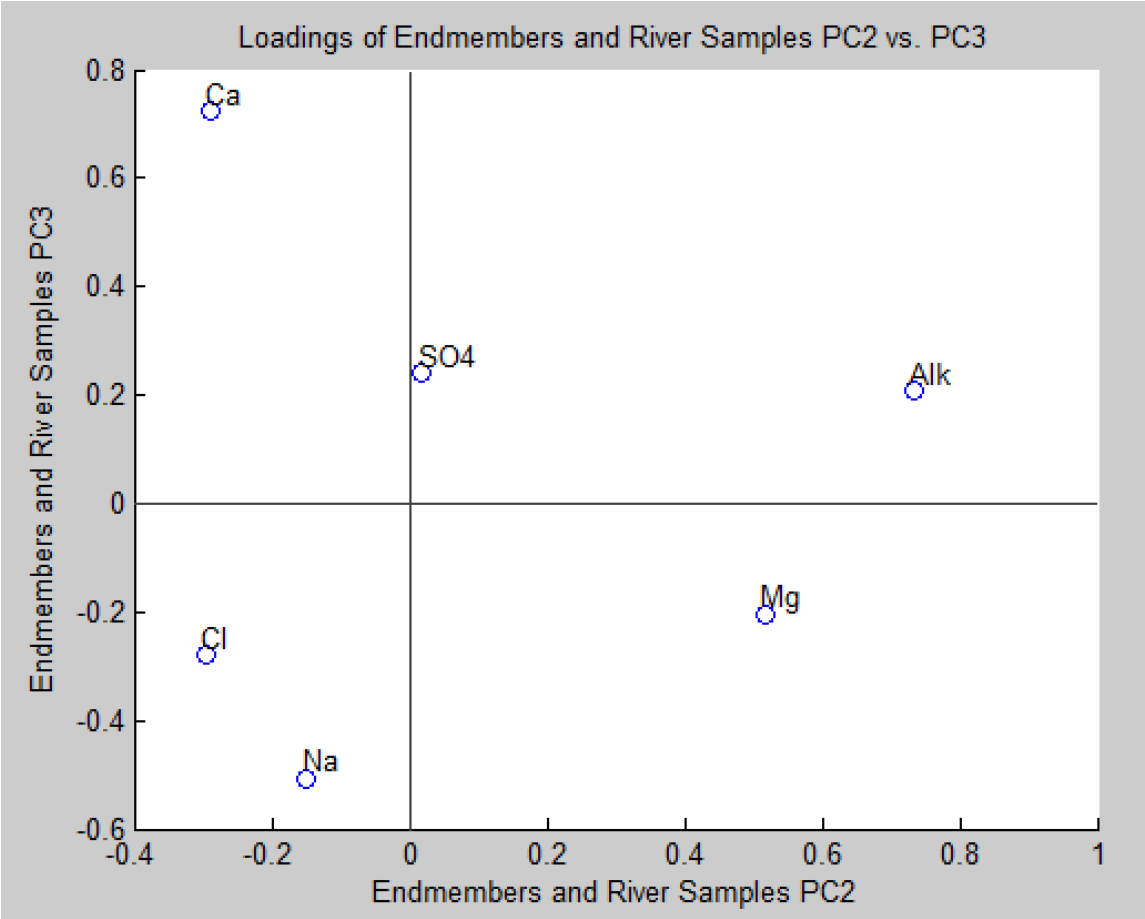

Figure 5-50: This figure shows the loadings of PC2 and PC3. PC2 is affected strongest by alkalinity, and second strongest by magnesium. PC3 is affected most strongly by calcium.

After ensuring that our identified endmembers were appropriate through PCA, we determined the percent of each endmember contained in our river water samples through Endmember Mixing Analysis (EMMA) (Hooper et al., 1990). From these endmember percentages we were able to calculate groundwater discharge between two gage sites on days that we had river water samples taken from consecutive gages, either both SH21 and SH60, or both SH60 and Navasota. We were able to check the high

frequency measurements taken using our methods of differential gaging and in-situ specific conductance recordings using this method.

Brazos River samples were collected most days during construction of rating curves from May 28, 2015, to November 13, 2015. We have samples from at least one of the sets of consecutive gages on nine separate days. The results of EMMA are shown in figures 5-51 and 5-52 for all river water samples analyzed. The proportion of stream discharge made up of each endmember at each consecutive site are shown in figures 5-53 through 5-62. Table 5-5 contains the groundwater discharge estimates derived from these EMMA results, with BRAA water, Yegua water, and bank storage/runoff all considered groundwater.

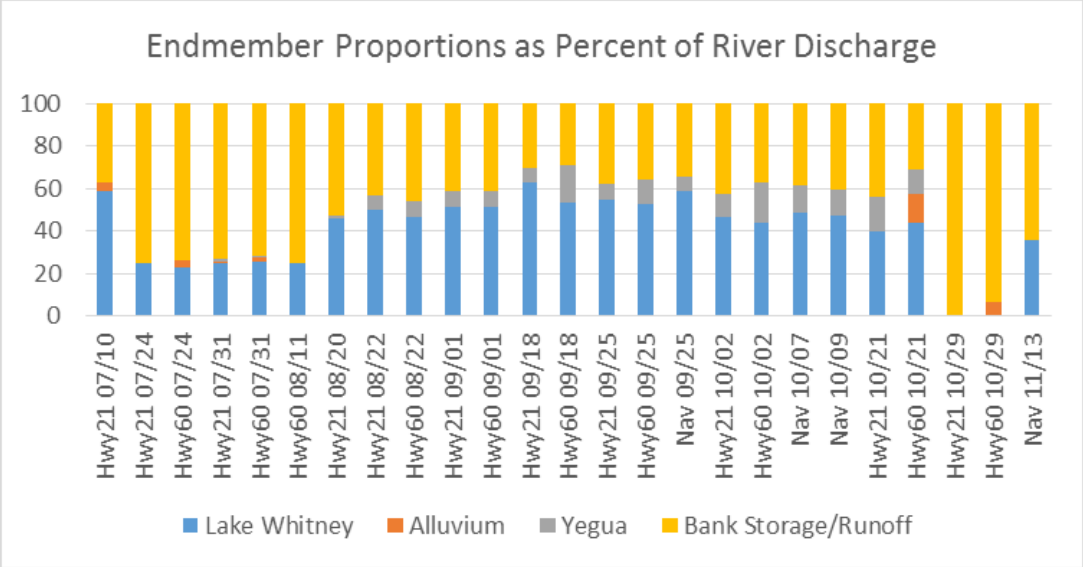

Figure 5-51: The percent makeup of each endmember is shown for each river water sample taken at one of our gage locations. Most samples are made up of primarily Lake Whitney water or bank storage/runoff.

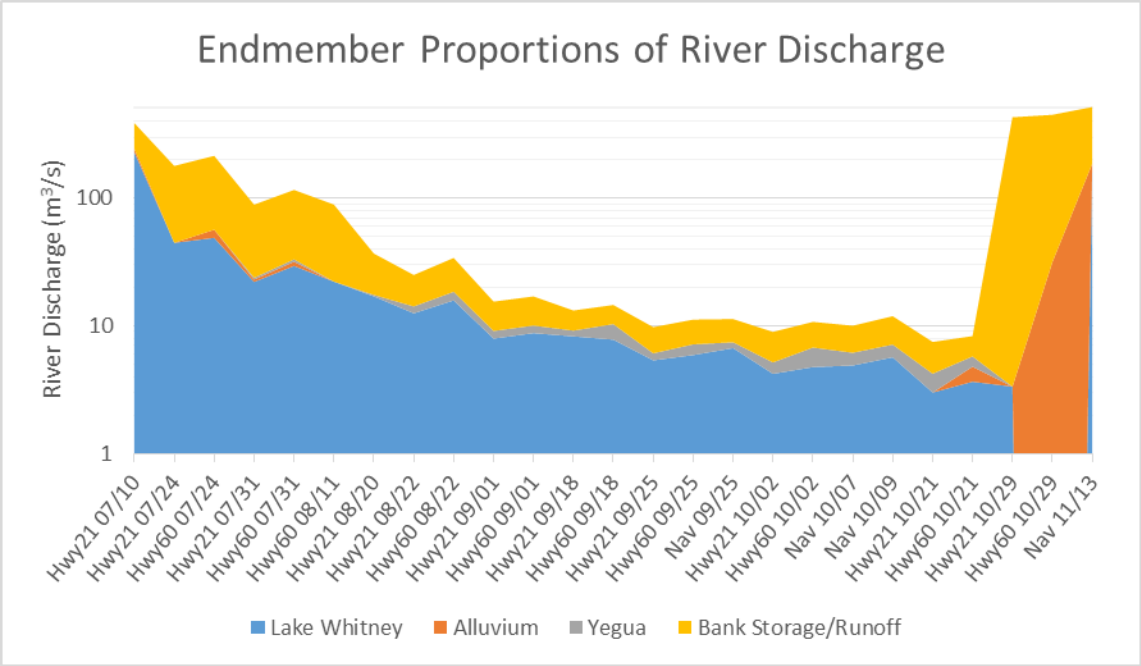

Figure 5-52: The endmembers that made up the largest proportions of river discharge tended to be Lake Whitney and bank storage/runoff. Yegua and Alluvium water often made up 0% of flow.

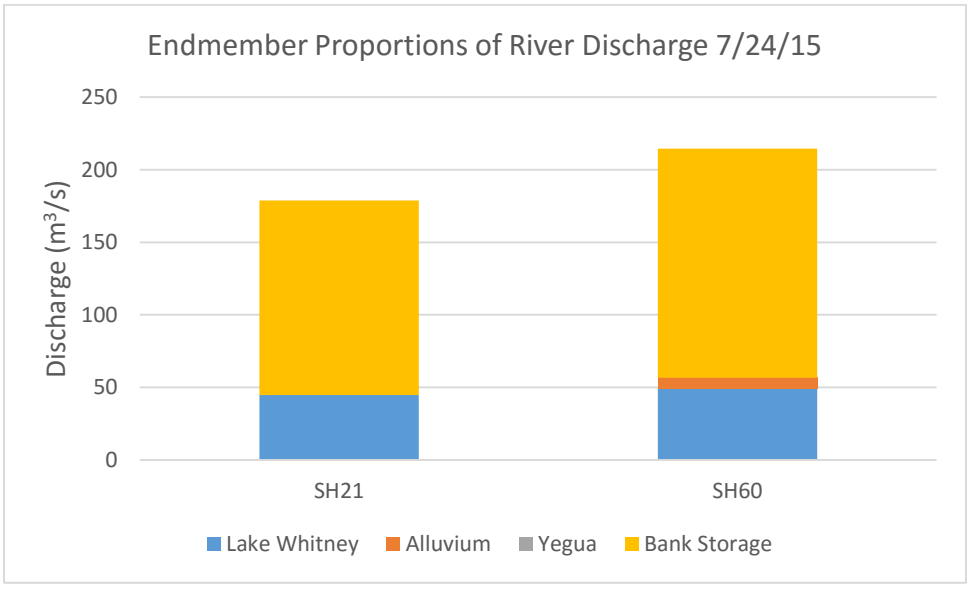

Figure 5-53: The amounts of Lake Whitney water, BRAA water, Yegua formation water, and bank storage/runoff are shown as proportions of total river discharge at SH21 (upstream) and SH60 (downstream).

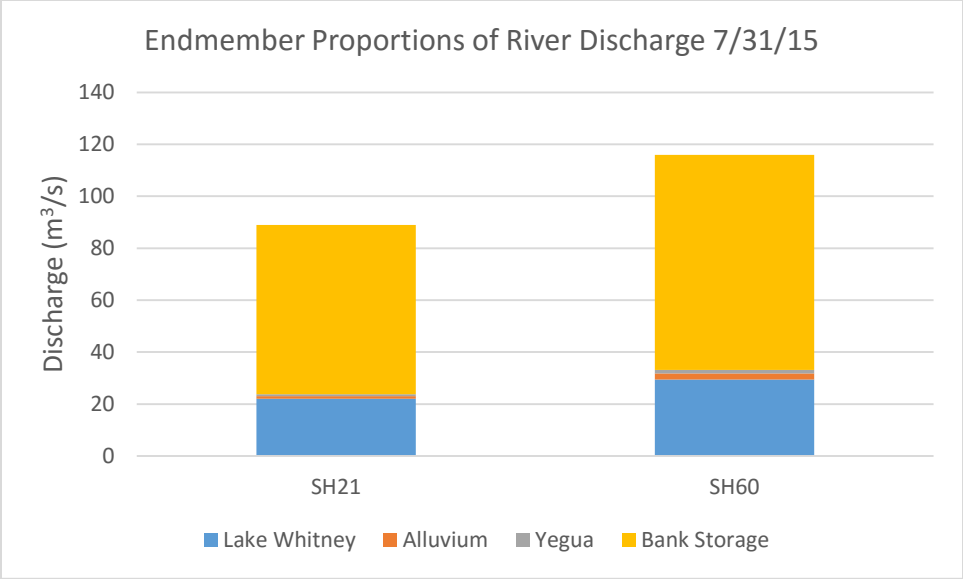

Figure 5-54: The amounts of Lake Whitney water, BRAA water, Yegua formation water, and bank storage/runoff are shown as proportions of total river discharge at SH21 (upstream) and SH60 (downstream).

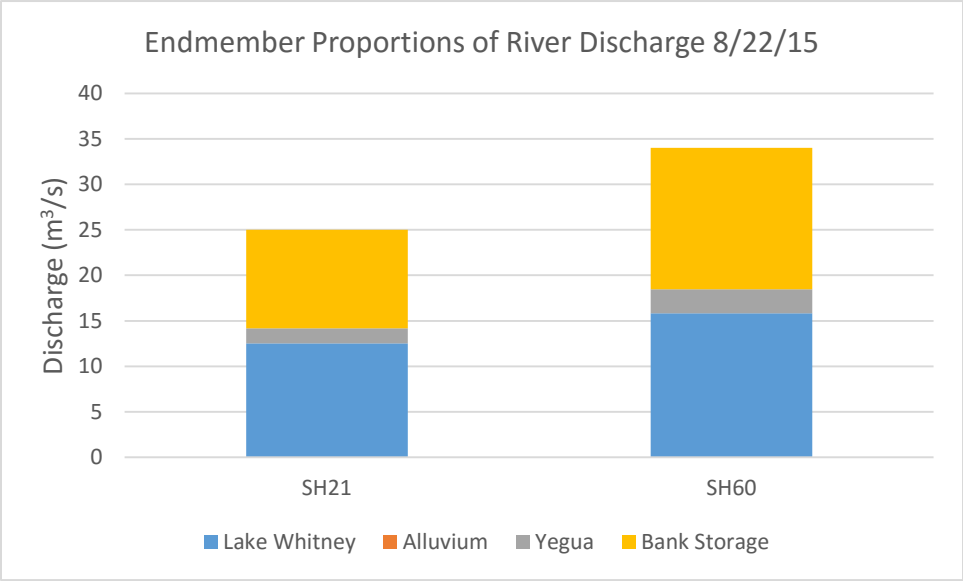

Figure 5-55: The amounts of Lake Whitney water, BRAA water, Yegua formation water, and bank storage/runoff are shown as proportions of total river discharge at SH21 (upstream) and SH60 (downstream).

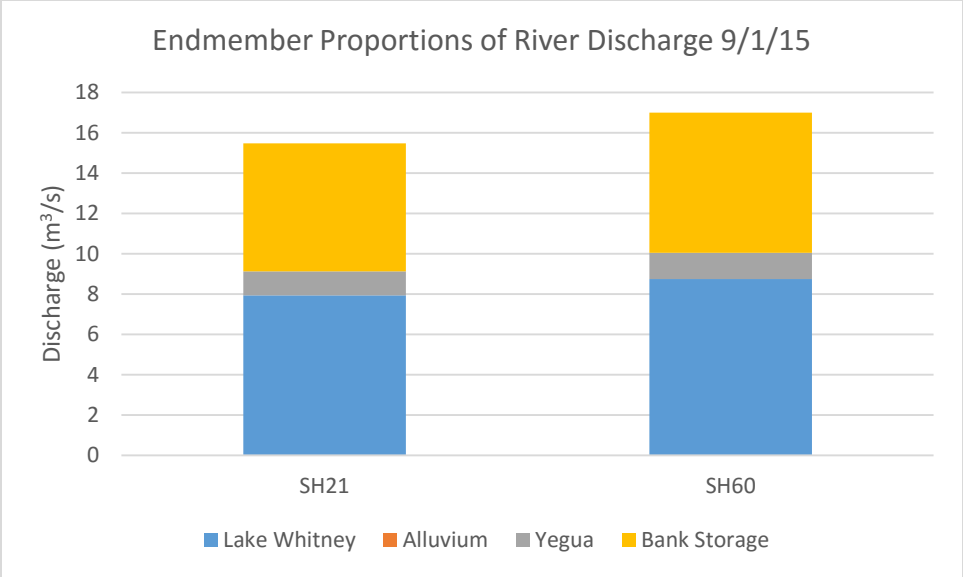

Figure 5-56: The amounts of Lake Whitney water, BRAA water, Yegua formation water, and bank storage/runoff are shown as proportions of total river discharge at SH21 (upstream) and SH60 (downstream).

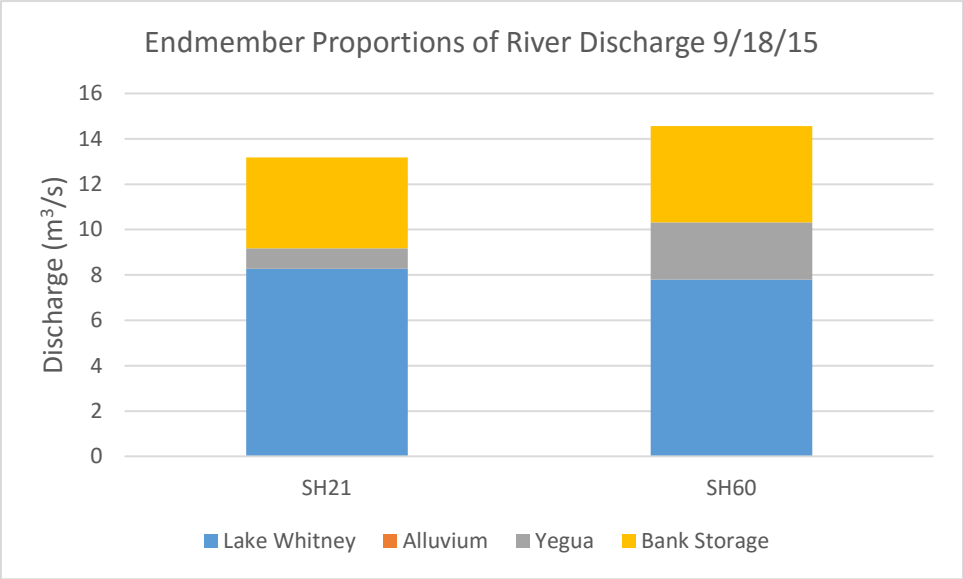

Figure 5-57: The amounts of Lake Whitney water, BRAA water, Yegua formation water, and bank storage/runoff are shown as proportions of total river discharge at SH21 (upstream) and SH60 (downstream).

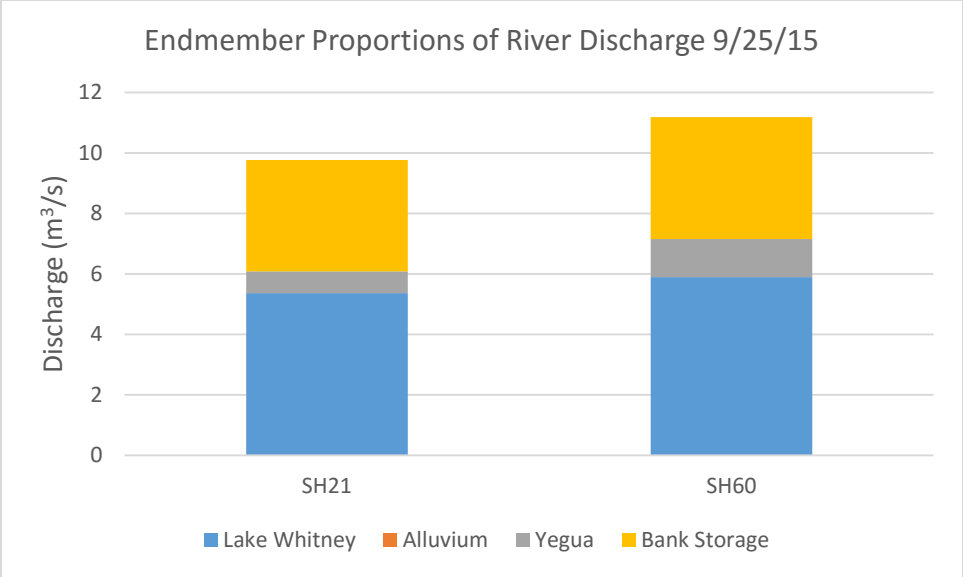

Figure 5-58: The amounts of Lake Whitney water, BRAA water, Yegua formation water, and bank storage/runoff are shown as proportions of total river discharge at SH21 (upstream) and SH60 (downstream).

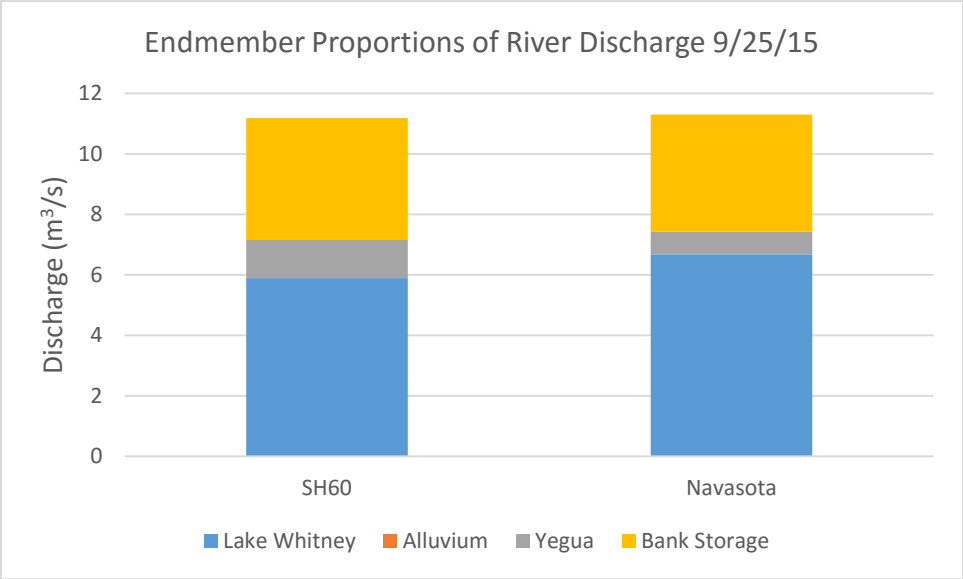

Figure 5-59: The amounts of Lake Whitney water, BRAA water, Yegua formation water, and bank storage/runoff are shown as proportions of total river discharge at SH60 (upstream) and Navasota (downstream).

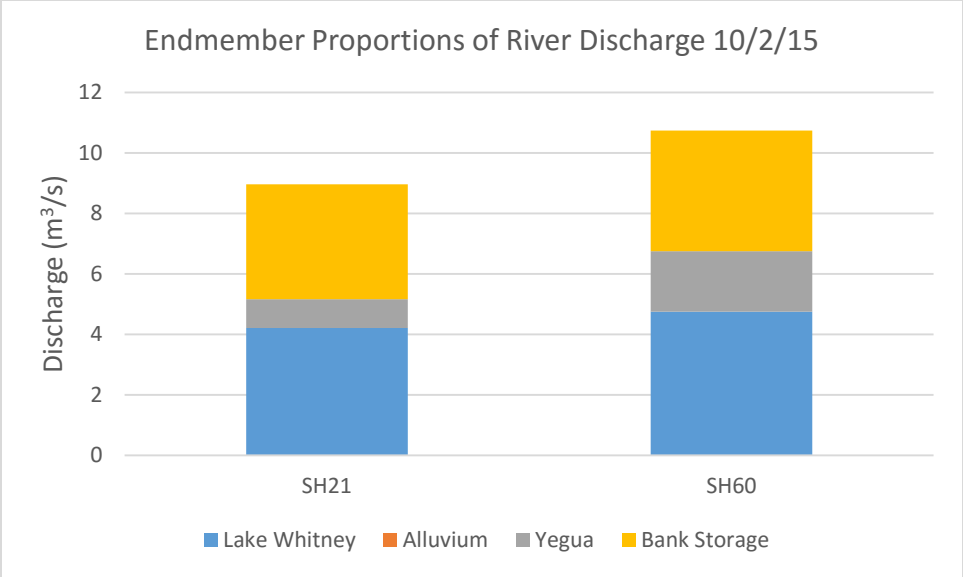

Figure 5-60: The amounts of Lake Whitney water, BRAA water, Yegua formation water, and bank storage/runoff are shown as proportions of total river discharge at SH21 (upstream) and SH60 (downstream).

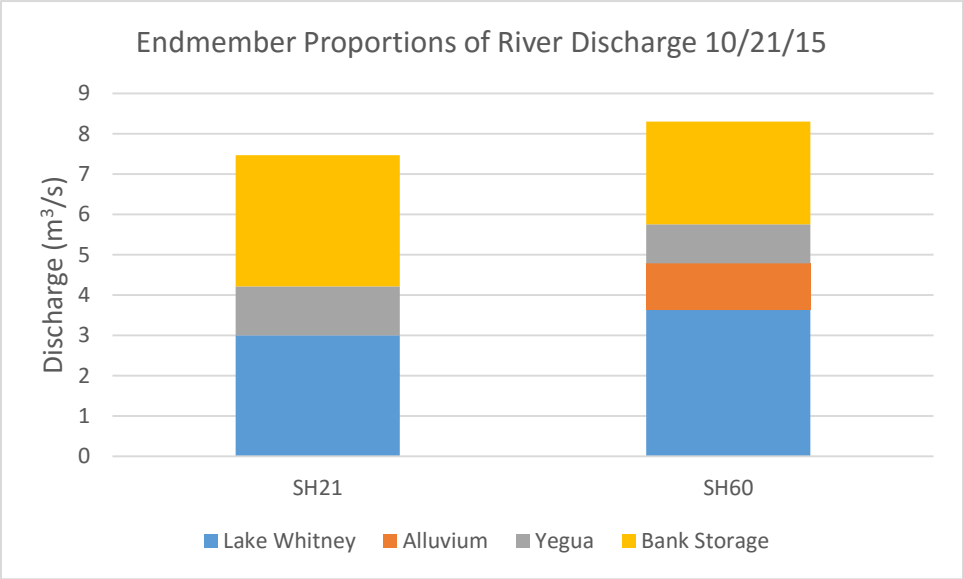

Figure 5-61: The amounts of Lake Whitney water, BRAA water, Yegua formation water, and bank storage/runoff are shown as proportions of total river discharge at SH21 (upstream) and SH60 (downstream).

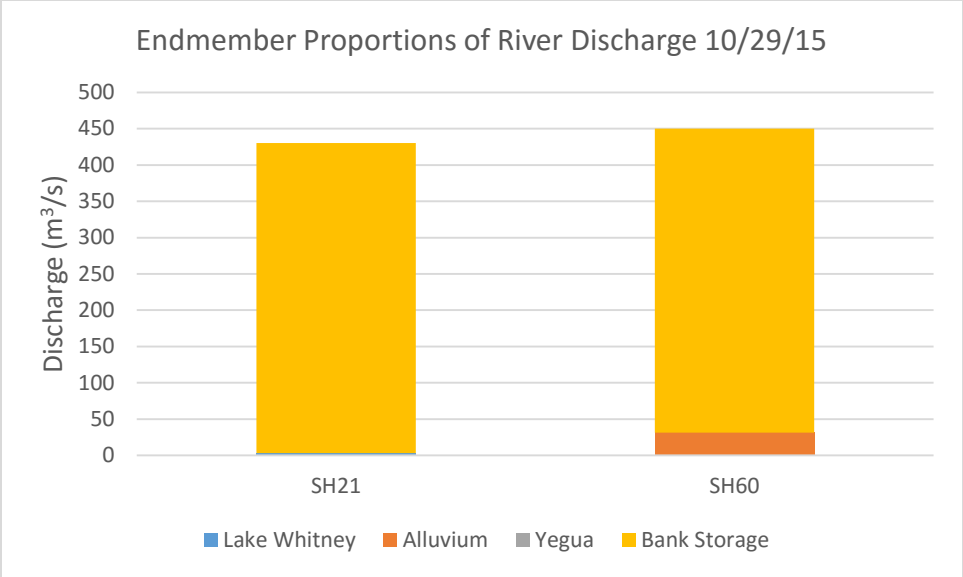

Figure 5-62: The amounts of Lake Whitney water, BRAA water, Yegua formation water, and bank storage/runoff are shown as proportions of total river discharge at SH21 (upstream) and SH60 (downstream). Note that total river discharge is much higher for this day than many of the other days on which river samples were taken.

Table 5-5: Groundwater discharges calculated from EMMA-derived percentages of groundwater at consecutive river gage sites. Groundwater in these calculations includes BRAA water, Yegua water, and bank storage/runoff water.

River Stretch	Date	ADCP or gage-based river discharge used?	Q_{gw} (m^3/s)
SH21 to SH60	7/24/2015	Gage	31.5
SH21 to SH60	7/31/2015	ADCP	19.6
SH21 to SH60	8/22/2015	ADCP	5.7
SH21 to SH60	9/1/2015	ADCP	0.7
SH21 to SH60	9/18/2015	ADCP	1.8
SH21 to SH60	9/25/2015	ADCP	0.9
SH60 to Navasota	9/25/2015	ADCP	-0.7
SH21 to SH60	10/2/2015	ADCP	1.2
SH21 to SH60	10/21/2015	ADCP	0.2
SH21 to SH60	10/29/2015	Gage	23.1

5.4 Estimating Groundwater Discharge using Aquifer Hydraulic Gradients

5.4.1 SH21 to SH60

We input continuous high frequency BRAA water table levels and SH60 river levels into the Dupuit equation (equation 4-4) to calculate groundwater discharge over the time period in which we had both aquifer and river level data. The results of the Dupuit equation-calculated groundwater discharge from SH21 to SH60 are shown in figure 5-63. These calculations cover the period from May 28, 2015 through January 29, 2016, though one small section is missing when gage data at SH60 is not available. The maximum calculated groundwater discharge over this period was 11 m^3/s, and the minimum was -30 m^3/s. This assumed that the observed hydraulic gradients and aquifer hydraulic conductivity were similar along the entire 13.8 km linear length of river from SH21 to SH60. Groundwater discharge estimated with the Dupuit equation is compared to river discharge at SH60 in figure 5-64. When river discharge was low, groundwater discharge was generally high. When river discharge was high, groundwater discharge was generally strongly negative. This suggests that the river recharges the aquifer during high flow events. The aquifer and river water levels over this period, in meters above sea level (masl), are shown in figure 5-65. The fact that river water surface elevation rises above the aquifer water table suggests that the river recharges the aquifer during high flows.

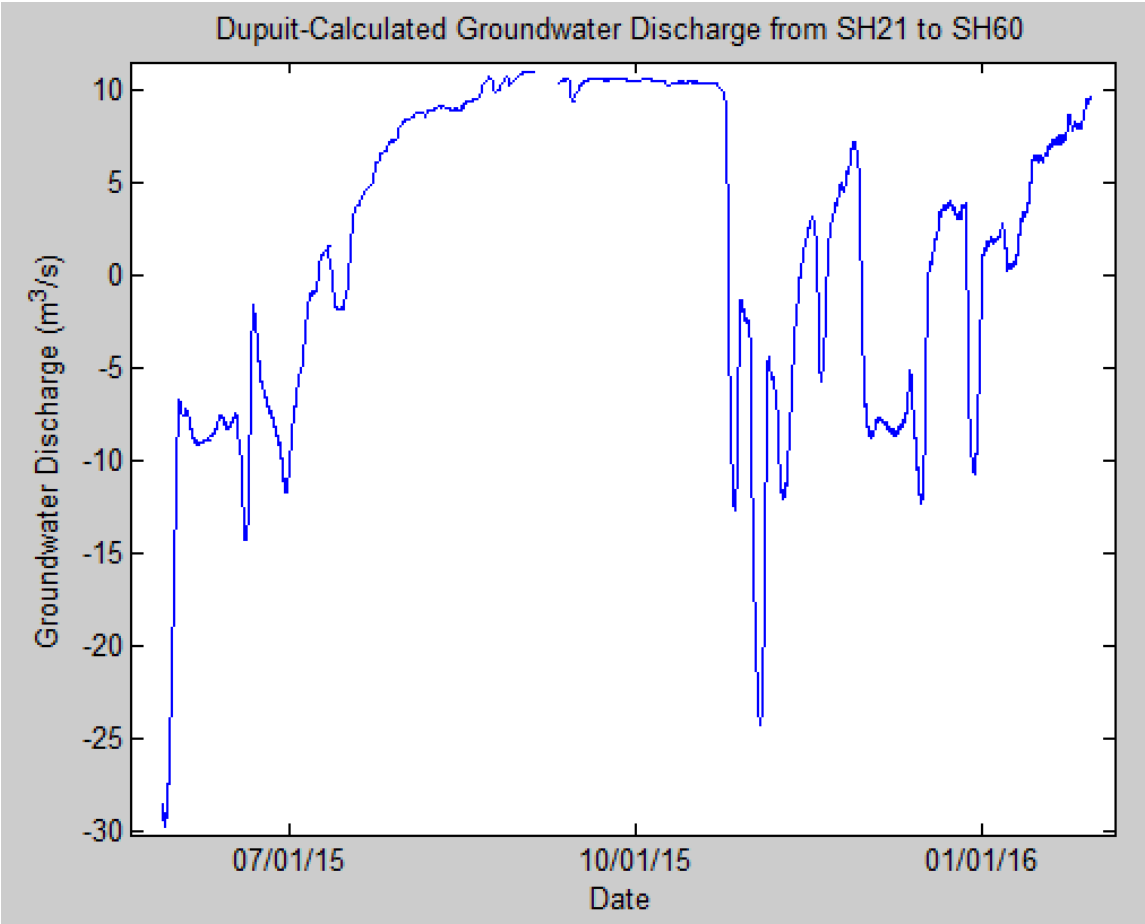

Figure 5-63: Groundwater discharge to the Brazos River from the BRAA in the stretch from SH21 to SH60 as calculated by the Dupuit equation.

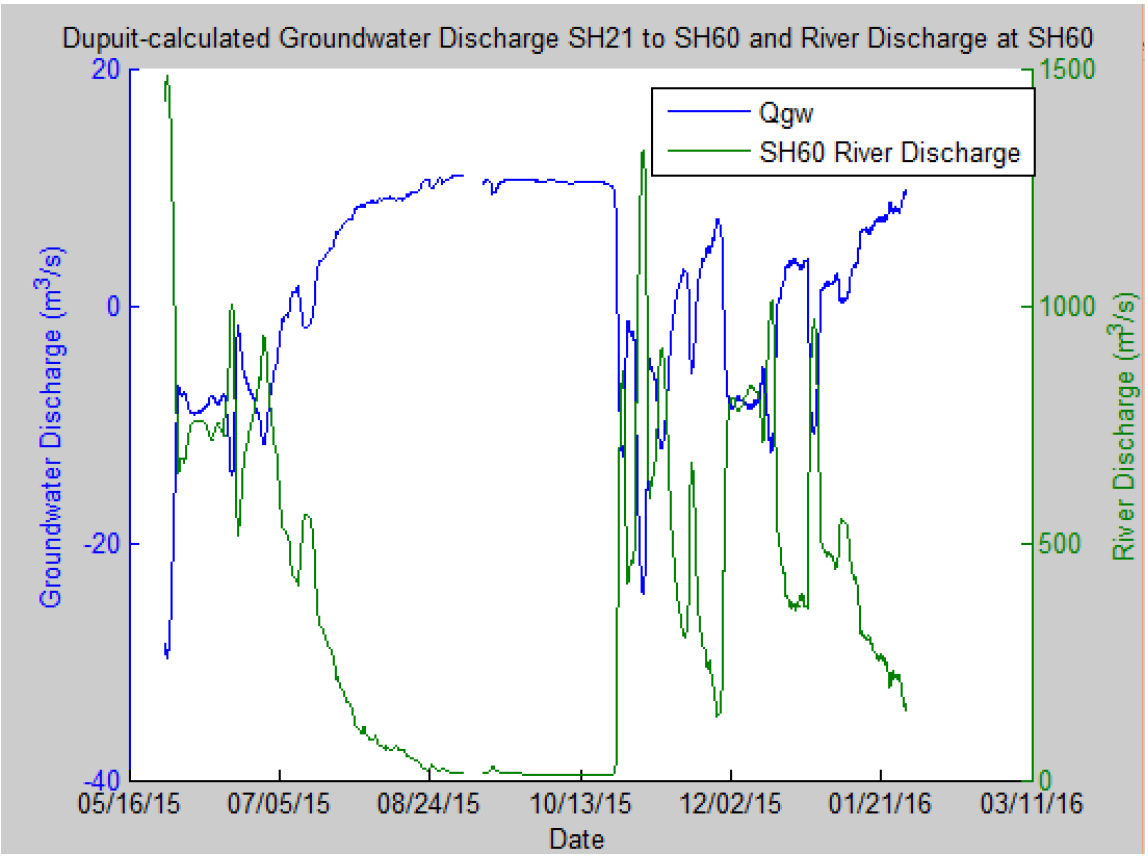

Figure 5-64: Groundwater discharge to the Brazos River from the BRAA in the stretch from SH21 to SH60 as calculated by the Dupuit equation, as well as river discharge at SH60 over the same time period.

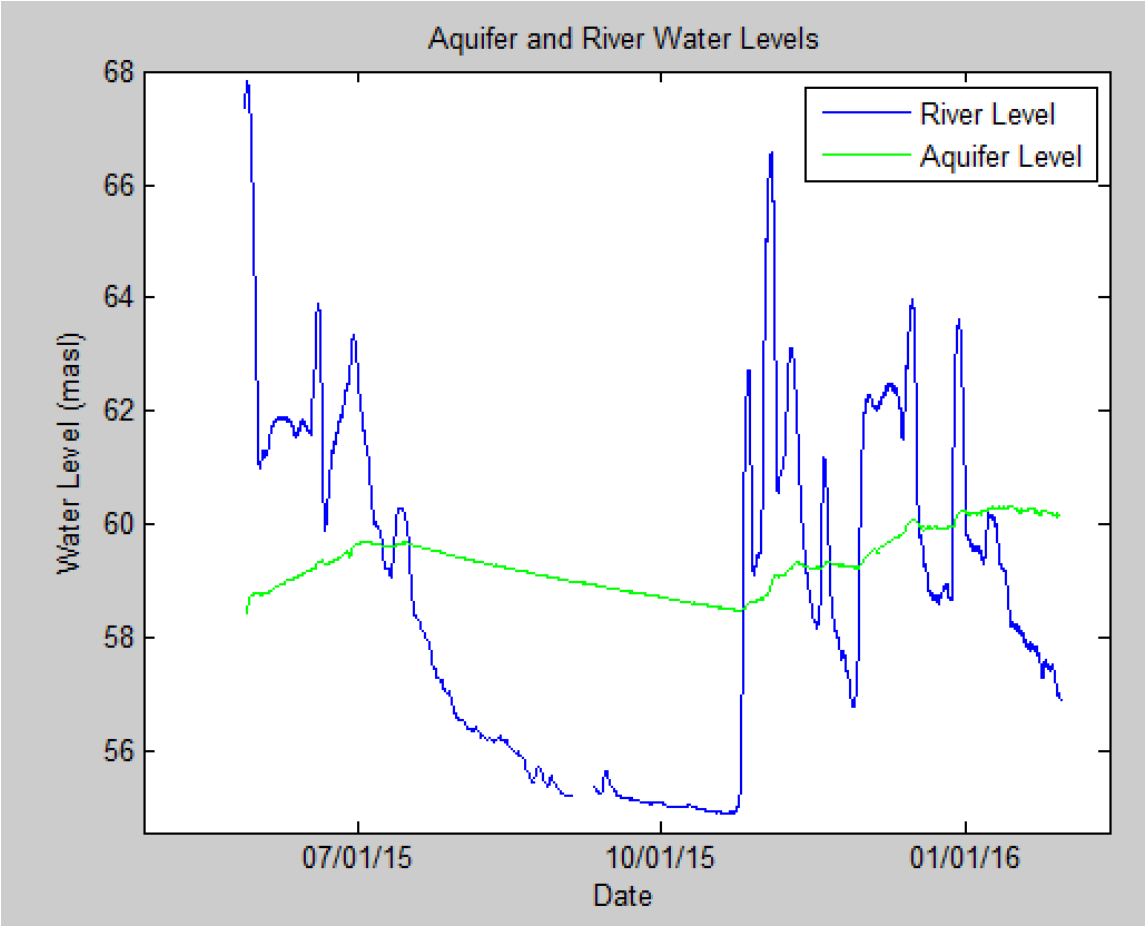

Figure 5-65: This figure shows Brazos River and BRAA relative water surface elevations. During major storm events, the surface of the Brazos River usually reached elevations above that of the aquifer water, but during dry periods the river level usually dropped below the aquifer level.

5.4.2 SH60 to Navasota

The results of calculating groundwater discharge between SH60 and Navasota using the Dupuit equation are shown in figure 5-66. These results are shown relative to river discharge at SH60 in figure 5-67. The river levels and aquifer levels shown in figure 5-65 were used for these calculations, but applied to the stretch south of SH60. Groundwater discharge was found to have a maximum value of 27 m^3/s, and a minimum

value of -73 m^3/s. For these calculations we again made the assumption that observed hydraulic gradients and aquifer hydraulic conductivity were similar along the entire linear length of river, 33.9 km from SH60 to Navasota. As in the stretch from SH21 to SH60, the negative groundwater discharge values suggest aquifer recharge from the river during high flows. Groundwater discharge is also highest when the river is lowest, and lowest when the river is highest.

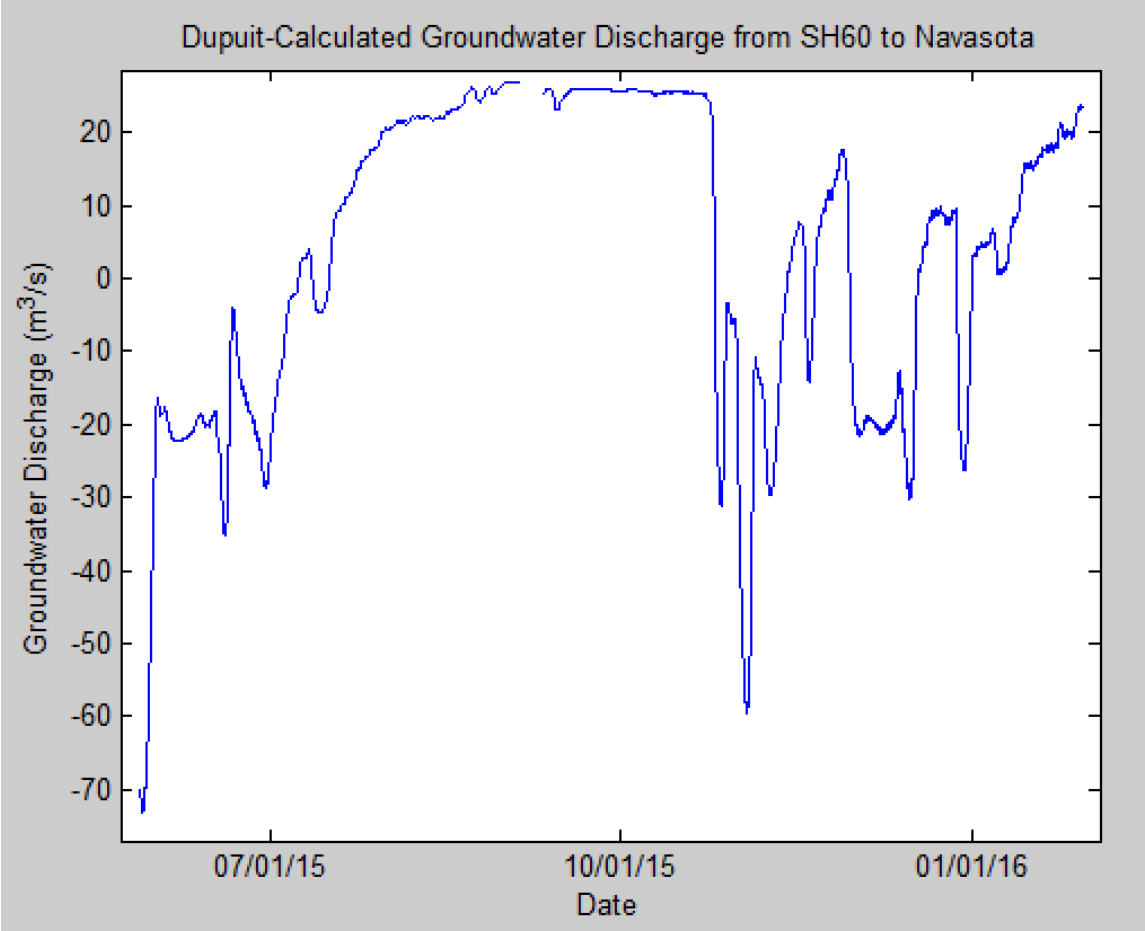

Figure 5-66: Groundwater discharge to the Brazos River from the BRAA in the stretch from SH60 to Navasota as calculated by the Dupuit equation.

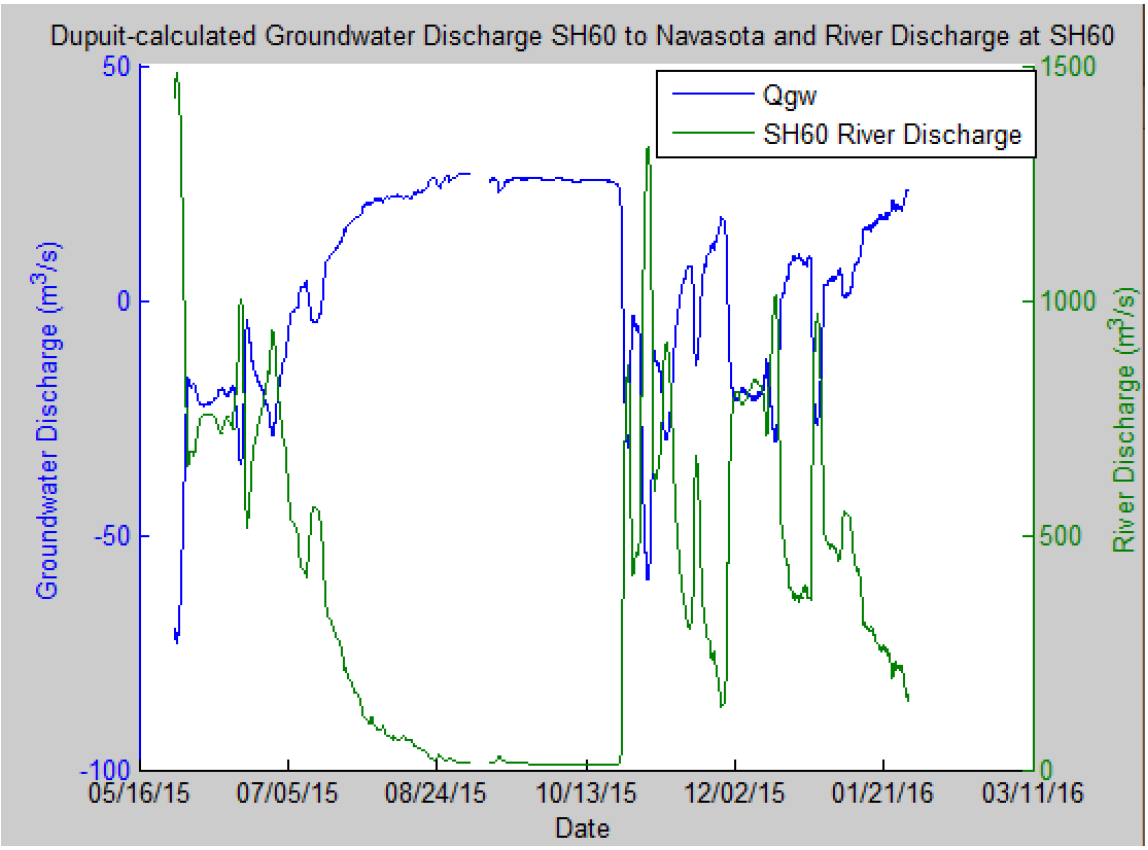

Figure 5-67: Groundwater discharge to the Brazos River from the BRAA in the stretch from SH60 to Navasota as calculated by the Dupuit equation, as well as river discharge at SH60 over the same time period.

5.5 Baseflow Separation

The following figures show the results of baseflow separation completed in the USGS GW Toolbox. The Navasota discharges were corrected for Yegua and Davidson Creek discharges prior to being input into the program. This method found a maximum baseflow at SH21 over the study period to be 579 m^3/s, and a minimum baseflow of 9 m^3/s (figure 5-68). The maximum baseflow percent at SH21 was found to be 100, which is the same as a BFI of 1. The minimum baseflow percent found at SH21 was 2.8,

corresponding to a BFI of .028. At SH60 the maximum baseflow was found to be 720 m^3/s, and the minimum was 10 m^3/s (figure 5-69). The maximum baseflow percent was 100 (equal to a BFI of 1), and the minimum was 3 (the same as a BFI of .03). At Navasota the largest baseflow was found to be 641 m^3/s and the minimum was found to be 0 m^3/s (figure 5-70). The greatest baseflow percent was 100 (equivalent to a BFI of 1), and the lowest was 0 (the same as a BFI of 0).

From these results the groundwater discharge between gage sites could be calculated for each day. To do so, the baseflow values at SH21 were subtracted from the baseflow values at SH60 to find groundwater discharge between SH21 and SH60. The baseflow values at SH60 were subtracted from the baseflow values at Navasota to find the groundwater discharge between SH60 and Navasota. The results from these calculations are shown in figure 5-71 for SH21 to SH60, and in figure 5-72 for SH60 to Navasota. The first few days were left out of these calculations because the dummy 0-values input for days with missing data affected the baseflow estimates for the first few days of the calculations.

The major spikes in groundwater discharge seen on figures 5-71 and 5-72 are artifacts of the method and should not be considered actual groundwater discharge values. They resulted from certain storm peaks on 6/12/15 between SH21 and SH60, and on 12/12/15 between SH60 and Navasota being treated differently by the program at each respective gage. When those spikes are ignored as artifacts from inconsistent storm peak calculations, the groundwater discharge between SH21 and SH60 remained quite constant with a maximum value of 40 m^3/s and minimum value close to 1 m^3/s (figure 5-

71). The largely negative, erratic values starting January 7, 2016, are likely artifacts of the program missing storm peaks at SH21 that it identified correctly at SH60.

The values for groundwater discharge between SH60 and Navasota are likely most accurate in the beginning period of calculations before the large peak near December 12, 2015, starts (figure 5-72). During this beginning period, groundwater discharge ranged from -5 to 13 m^3/s from September 20 to November 16, 2015, and ranged from 13 to 68 m^3/s from November 16 through November 27, 2015.

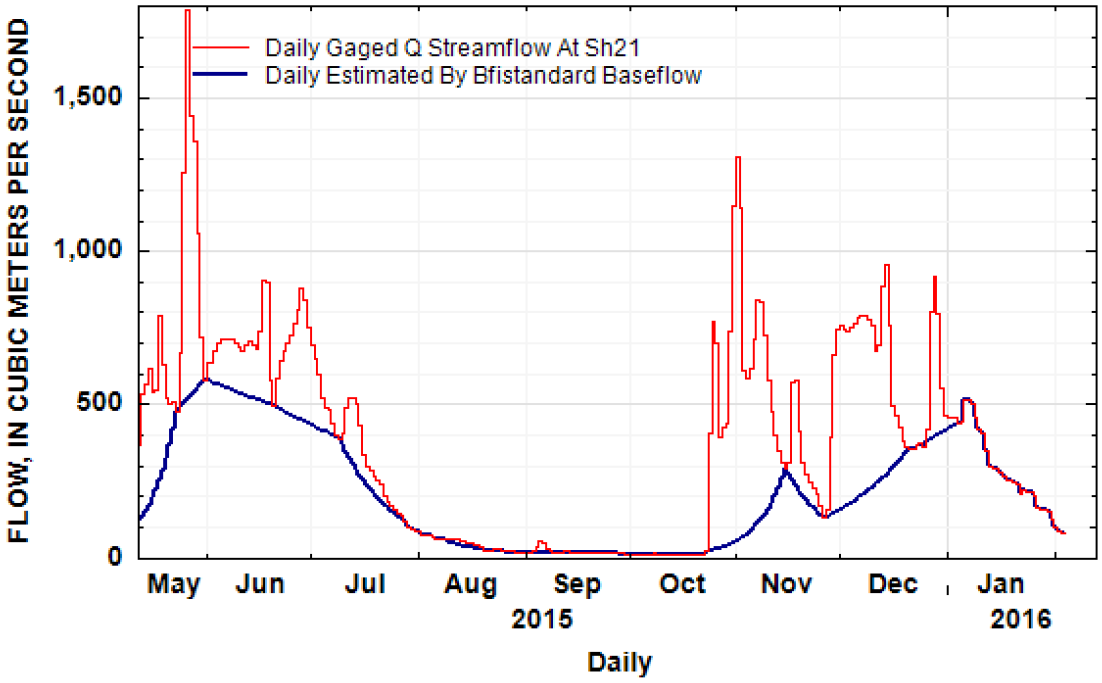

Figure 5-68: Results of baseflow separation at SH21 using the Standard BFI method in the USGS GW Toolbox.

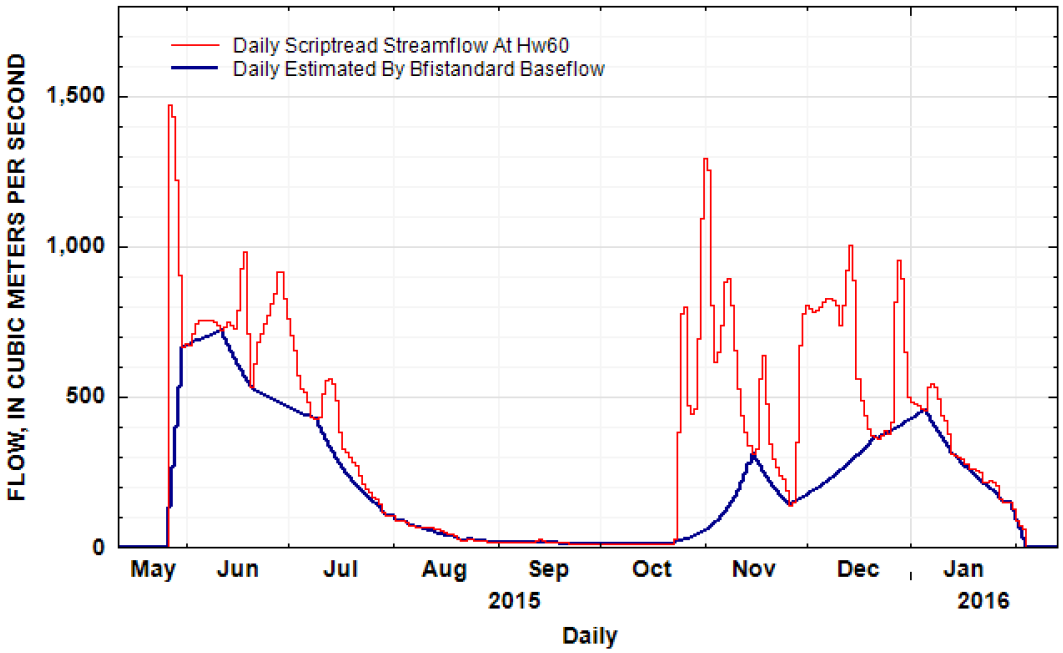

Figure 5-69: Results of baseflow separation at SH60 using the Standard BFI method in the USGS GW Toolbox.

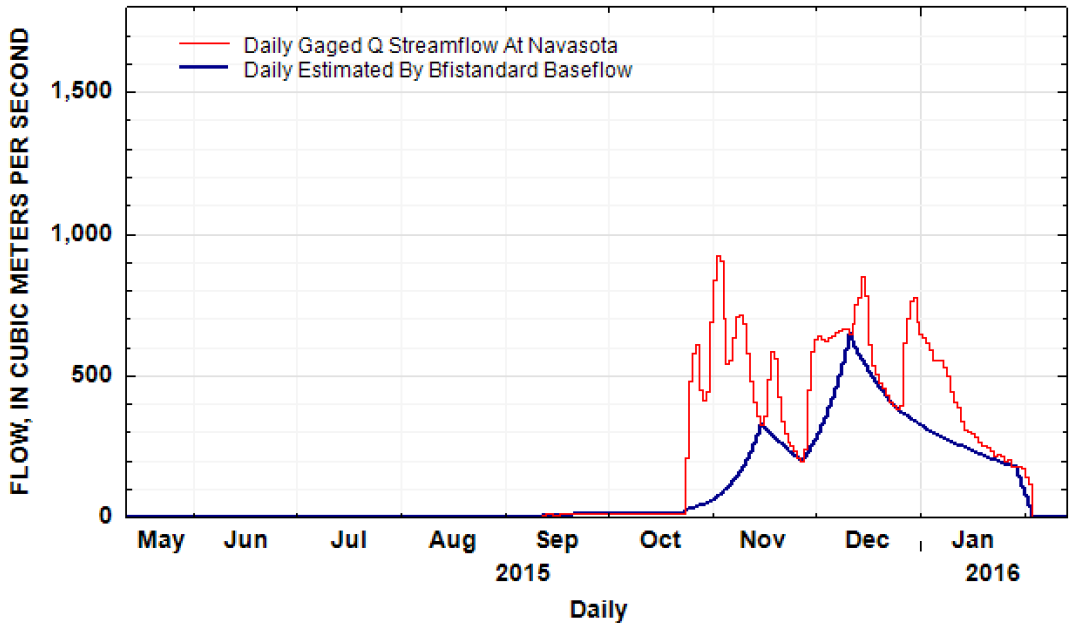

Figure 5-70: Results of baseflow separation at Navasota using the Standard BFI method in the USGS GW Toolbox. Tributary inflows were subtracted from Navasota discharge before data was imported and used for baseflow separation.

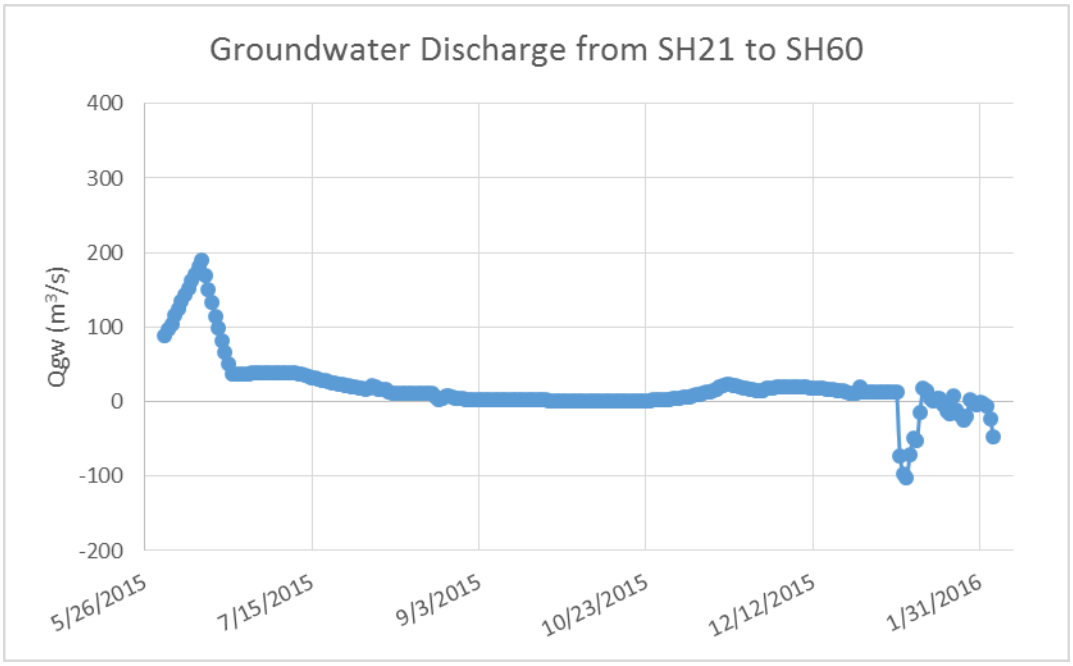

Figure 5-71: Estimated groundwater discharge between SH21 and SH60 based on baseflow separation.

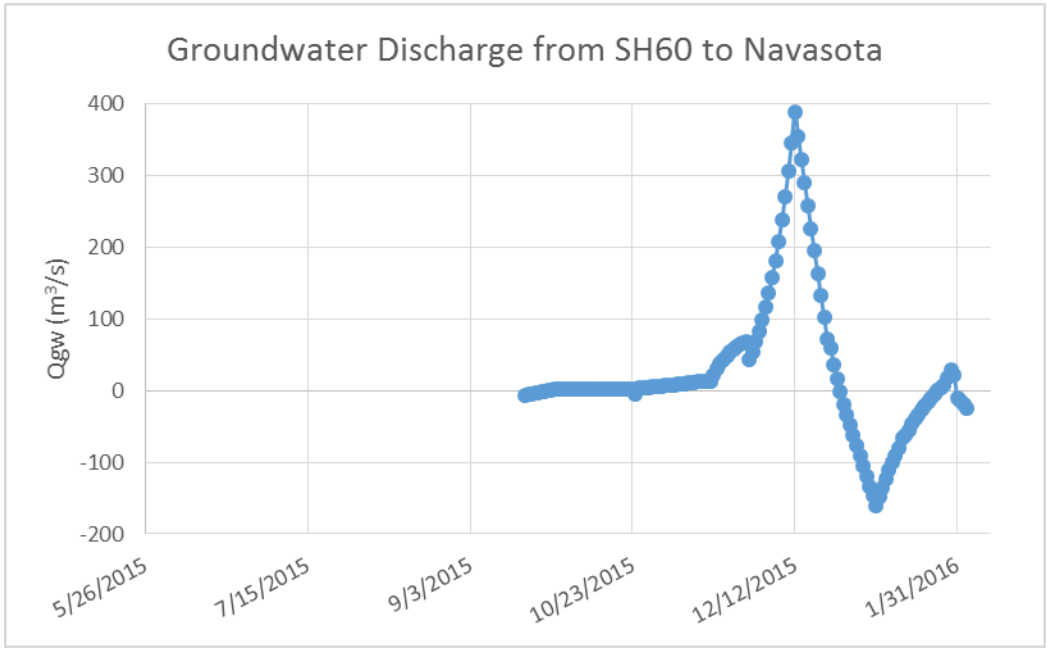

Figure 5-72: Estimated groundwater discharge between SH60 and Navasota based on baseflow separation.

6. DISCUSSION

6.1 Groundwater-Surface Water Interactions SH21 to Navasota

Figure 6-1 summarizes the results from all five methods used to estimate groundwater discharge to the Brazos River in the northern stretch from SH21 to SH60. Figure 6-2 summarizes the groundwater discharge estimates derived from all five methods used in the southern stretch from SH60 to Navasota. Hydrograph separation estimates that were artificially high or low due to the GW Toolbox assigning storm peaks differently at each gage (figures 5-71 and 5-72) were excluded from both figures.

The stretch from SH21 to SH60 was found to be gaining for most of the year, with higher groundwater discharges at high river flows and lower groundwater discharges at low river flows. As river discharge slowly decreases, groundwater discharge also decreases in this stretch (figure 6-1, periods 2, 6, and 8, all methods except Dupuit). The EMMA method indicated that bank storage made up a large proportion of river discharge (71 to 99%) soon after rain events, with the highest proportions of bank storage observed in the river at flows above 80 m^3/s before and after the dry summer (August to late October) (figure 5-52). This finding of bank storage discharge after rain events and the finding by Chakkah and Munster (1997) and Chowdhury et al. (2010) that there is little correlation between rainfall and aquifer levels in the BRAA have implications for the Brazos River-BRAA system. These findings suggest that the aquifer is mainly recharged by the river during rain events, then the

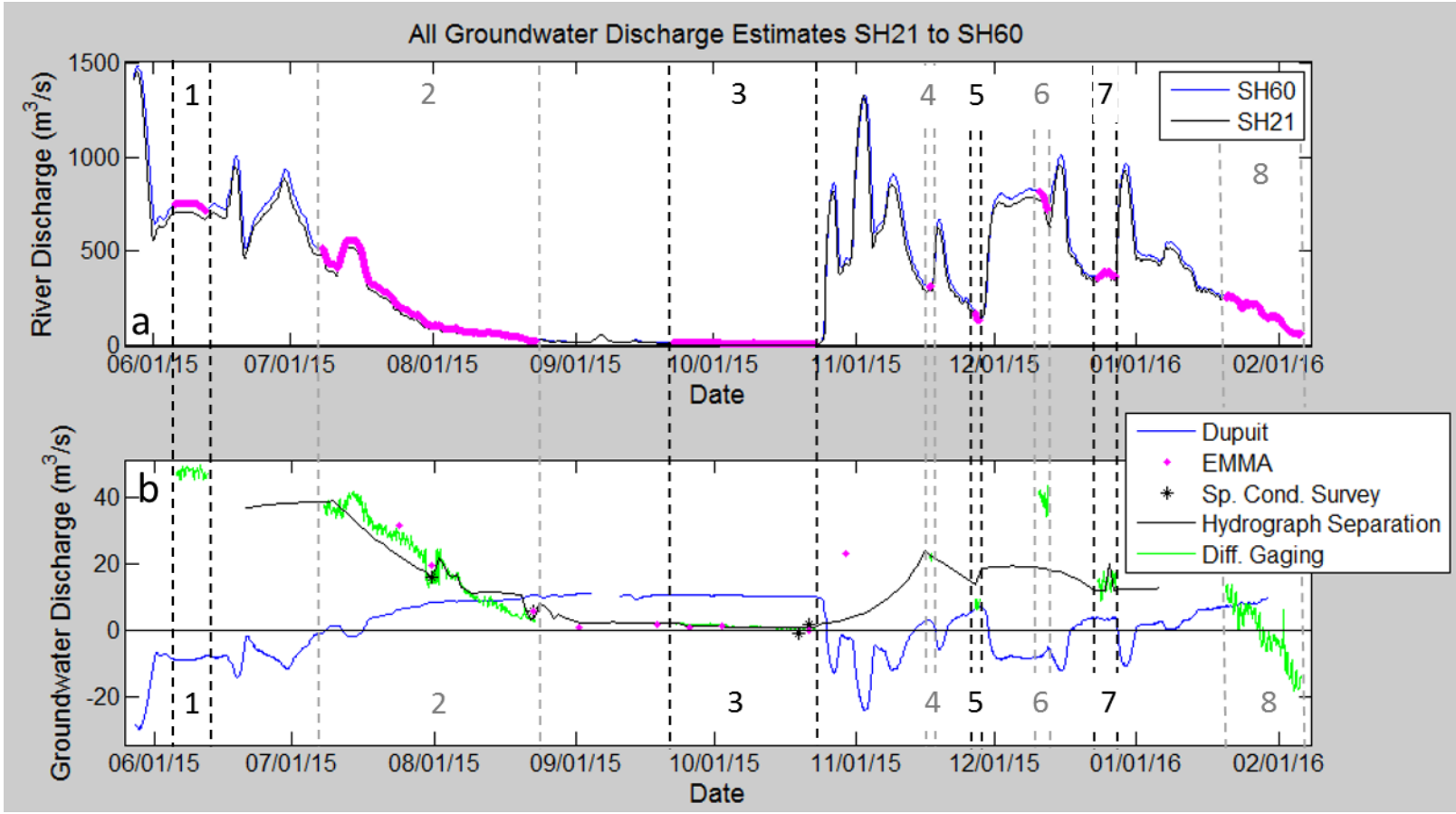

Figure 6-1: The river discharges at SH21 and SH60 are shown for the entire study period. Dry periods over which differential gaging was performed are shown on the SH60 hydrograph in pink and labeled with numbers 1-8 (a). Estimates from all five methods used to estimate groundwater discharge are shown for the entire study period with each dry period labeled 1-8 (b).

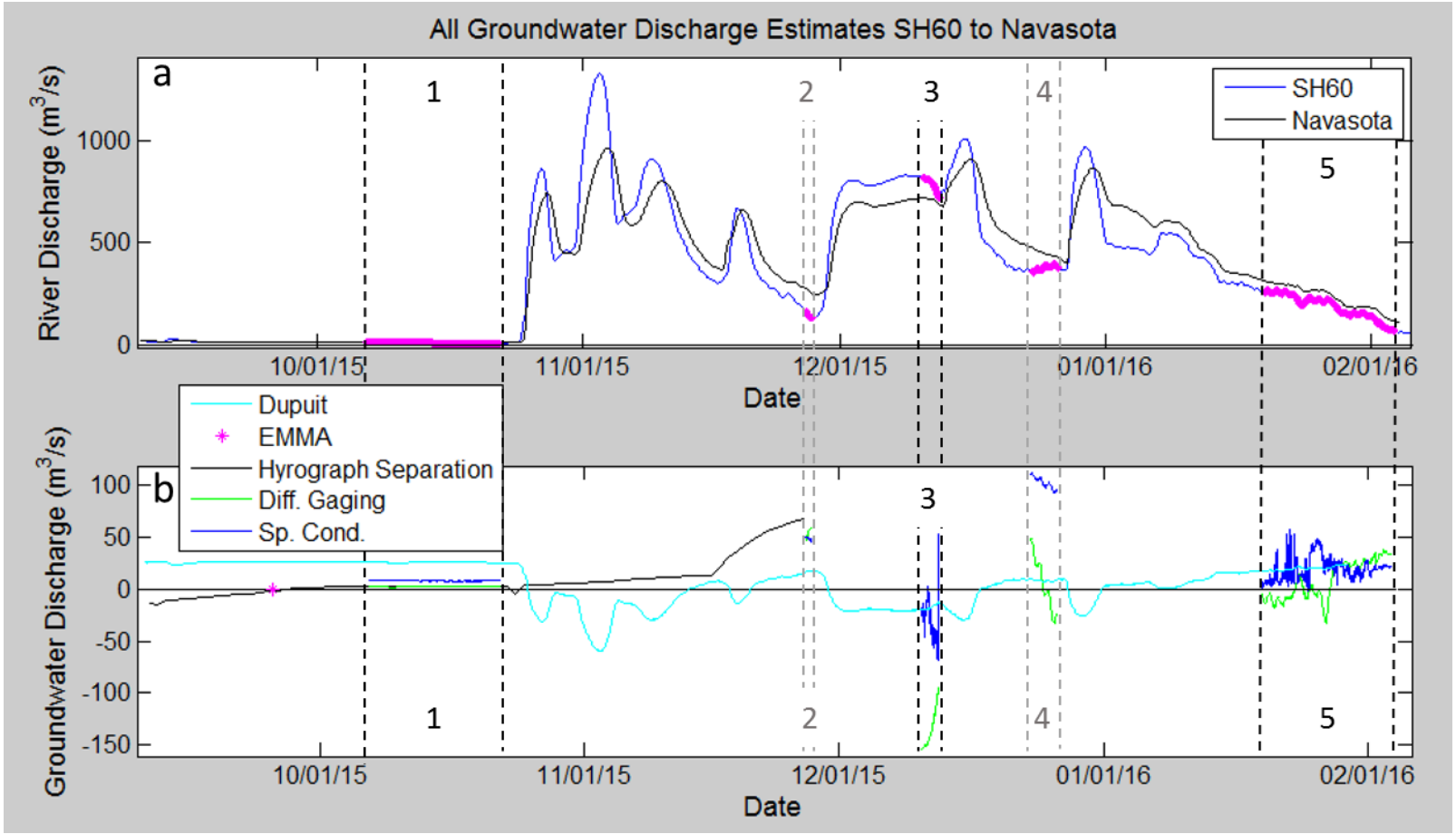

Figure 6-2: The river discharges at SH60 and Navasota are shown for the entire study period of this stretch. Dry periods are shown on the SH60 hydrograph in pink and labeled with numbers 1-5 (a). Estimates from all five methods used to estimate groundwater discharge are shown for the entire study period with each dry period labeled 1-5 (b).

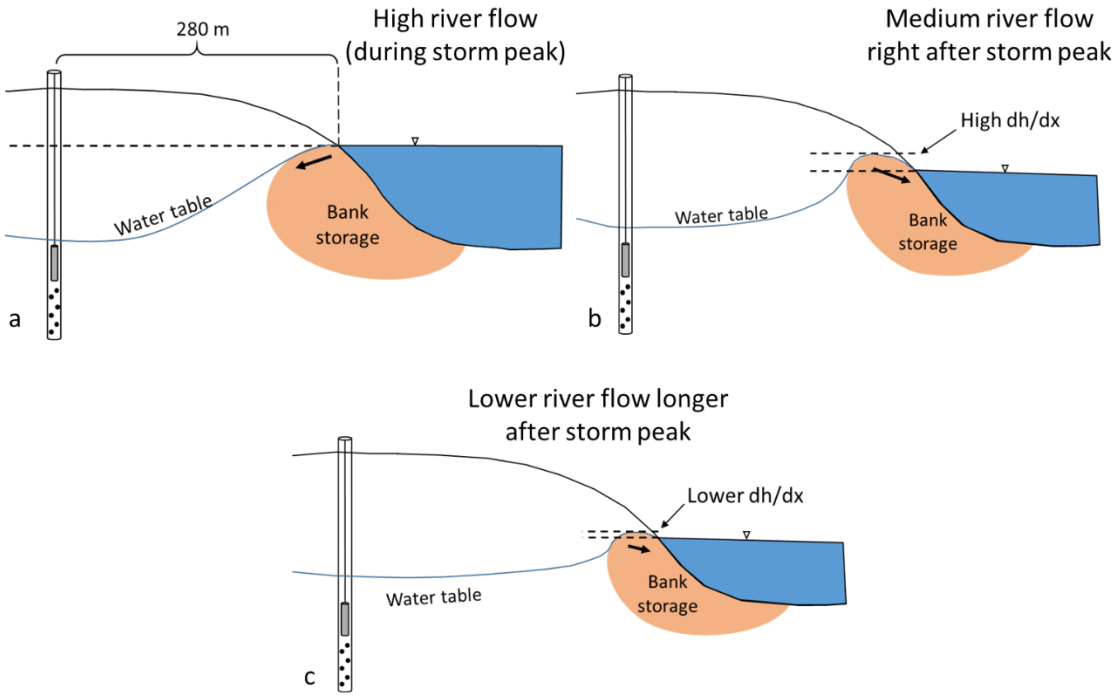

Figure 6-3: Conceptual diagram of bank storage and hydraulic gradients. The river recharges the aquifer and creates bank storage during high flows (a). Soon after a storm event the hydraulic gradient (dh/dx) between the bank storage and river is at its highest (b). The hydraulic gradient between bank storage and the river decreases as bank storage drains out of the aquifer (c).

recharge slowly returns to the river starting soon after the rain event ends. The slow decrease in groundwater discharge after storm events indicated by our differential gaging, specific conductance, EMMA, and hydrograph separation methods (figure 6-1) also suggests that the hydraulic gradient between the aquifer and river is highest immediately following rain events, and decreases as bank storage drains out of the river banks. Figure 6-3 provides a depiction of this process. The Dupuit equation method did not indicate the same results, we think largely because our well was too far away from the river to detect major changes in aquifer level caused by changes in river level.

Adding on to these findings, EMMA also showed that the proportion of regional groundwater observed in the river is highest long after storm events once river discharge drops below 25 m^3/s (6% to 26% of flow long after storm events compared to 0% to 7% of flow soon after storm events) (figures 5-51 and 5-52). Total groundwater discharge is lowest during these periods when regional groundwater is the main source of groundwater discharge, likely because the hydraulic gradient between the river and aquifer continues to decrease as bank storage drains out of the aquifer (figure 6-3). The increase in regional groundwater percentage of river water as time after storm event increases suggests that regional groundwater mainly only discharges into the river after bank storage has drained out of the aquifer. Figure 6-4 shows how regional groundwater percentage may increase with time since a storm event.

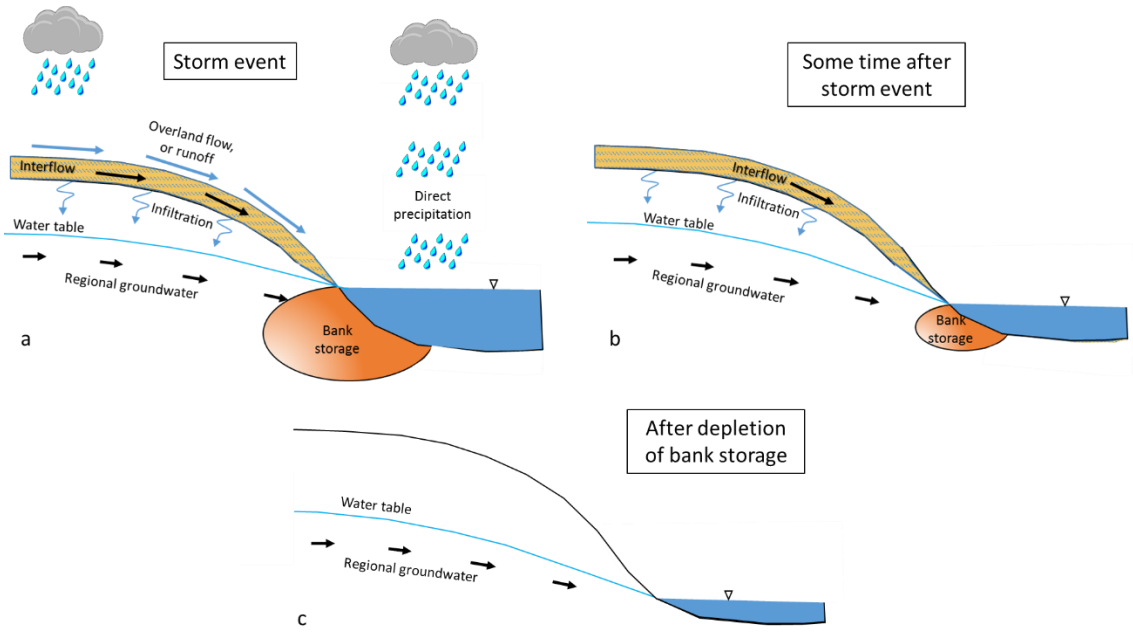

Figure 6-4: The volume of bank storage stored in the river banks is highest during and immediately following rain events (a). Bank storage starts getting depleted after the end of the rain event (b). Bank storage must get depleted from the aquifer before mainly regional groundwater is discharging into the river (c).

Endmember mixing analysis made some additional valuable contributions to our understanding of the Brazos River-BRAA system. EMMA found that Lake Whitney water is consistently a large component of Brazos River water (23% to 63%) at low to intermediate flows, though it is a smaller component (0% to 36%) at high river flows following rain events when bank storage/runoff make up most of the flow (figures 5-51 and 5-52). At low flows (< 30 m^3/s) EMMA found Lake Whitney water to make up 40% to 60% of flow. This shows that the suggestion by hydrograph separation that river flow is completely groundwater-derived baseflow (BFI = 1) during the dry summer months (figures 5-68, 5-69, and 5-70) is incorrect, highlighting the weaknesses of hydrograph separation in characterizing regulated rivers. Hydrograph separation

assumes the lowest flows during the summer are attributable to only groundwater discharge, but this is not the case when an upstream dam is discharging water to maintain river flows.

Another important contribution made by EMMA was showing that Yegua aquifer water is discharging into the Brazos River in this stretch, making up a maximum of 19% of flow at SH60 on October 2, 2015 (figures 5-51, 5-52, and 5-60). This agrees with past qualitative suggestions made by Turco et al. (2007) that Yegua water discharges to the Brazos River in this stretch. A past study by Chowdhury et al. (2010) argued that the Queen City, Sparta, and Evangeline aquifers do not contribute flow to the Brazos River, but they did not investigate possible discharges from the Yegua aquifer.

Though the SH21 to SH60 stretch was found to be gaining through most of our study period, it did switch to losing in January-February of 2016 (figure 6-1, period 8). The river conditions were similar to earlier during our study period (late July in dry period 2, and late November in dry period 5) with discharge at ~160 m^3/s and decreasing. The groundwater-surface water interactions, however, differed between these three periods. The difference may lie in the fact that the river was first at a flow of ~160 m^3/s in July with a water temperature (as measured by our YSI) of 30-35˚ C. At this time of year the river was still gaining, though very little, and discharge had been receding for nearly a month (figure 6-1, period 2). In January-February we measured the water temperature to be 11-14˚ C. At this time of year the river was losing. These temperature differences may have caused differences in biological behavior in the river, with more activity and growth during the warm summer months. Biofilms may have

formed on the bottom sediments of the river during the summer, clogging the bottom and sides (Battin and Sengschmitt, 1999) and greatly reducing the amount of water exchange between the Brazos River and BRAA. There were likely fewer biofilms in January-February due to the low temperatures and reduced biological activity, so the bottom of the river was not clogged, allowing water to be lost to the aquifer. Figure 6-5 depicts this process. The similar river discharge in late November likely did not result in losing water to the aquifer because only a few days had passed since the last precipitation event and the bank storage was likely still discharging into the river. Three to four weeks had passed between precipitation events and the late July and early February river discharges of ~160 m^3/s, so bank storage may have already drained from the aquifer.

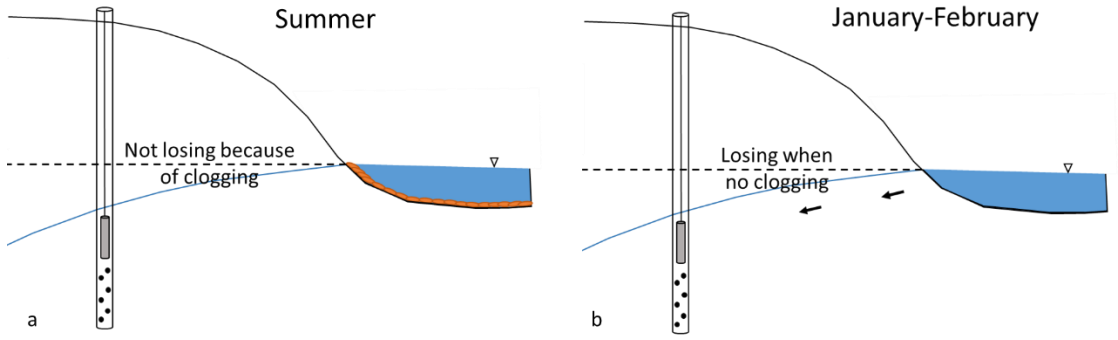

Figure 6-5: In the summer there were likely biofilms clogging the river bottom, reducing interaction between the Brazos River and BRAA (a). In the winter, when water temperatures were ~20˚ lower than in the summer, fewer biofilms may have formed, allowing river water losses to the aquifer (b).

Compared to the stretch from SH21 to SH60, we observed different groundwater-surface water interaction dynamics in the southern stretch from SH60 to

Navasota. This stretch was not consistently gaining water from the aquifer, but often was losing water (figure 6-2, periods 3, 4, and 5). In the northern stretch from SH21 to SH60 groundwater discharge was observed to start immediately following rain events. The southern stretch, in contrast, was observed to lose water at high flows and only gain water below certain threshold river discharges. In late December the southern stretch only gained water when river discharge dropped below 386 m^3/s, and in late January it started gaining after river discharge dropped below 212 m^3/s (figure 6-2).

We suspect the reason for this difference between stretches, with the northern stretch primarily gaining and the southern stretch switching between gaining and losing, is related to the location of the Brazos River within the BRAA and its floodplain. In nearly the entire northern study stretch, the Brazos River flows diagonally across the alluvium (figure 3-3). The river does not abut the elevated Eocene formations that bound the BRAA except for over a very short segment near the end of the stretch. In the southern study stretch, the Brazos River abuts the sides of the BRAA for nearly its entire length (figure 3-3). This location along the side of the floodplain brings the river into contact with the elevated Eocene formations beyond the BRAA, allowing interactions to occur. These interactions include possible losses of water from the river to the deposits. The threshold value at which the river switches from losing to gaining water must therefore be dependent on antecedent aquifer conditions in both the BRAA and the other formations bordering the alluvium. The difference in groundwater discharge dynamics between two stretches with varying connection to the deposits outside the alluvium

suggests that the processes shown in figures 6-3, 6-4, and 6-5 apply primarily to the BRAA, and not the other formations beyond the Brazos River floodplain.

We learned from EMMA that the Brazos River recharges bank storage in the BRAA during high flow events, then regains the water lost starting immediately after the high flow event ends (figure 6-3). If much of the water sent into the banks of the river during high flow events goes into formations outside of the BRAA in the southern stretch, it may not be returned to the river the way it is from the BRAA. As much as half of the water that flows into the banks could be lost because one side of the river flows up against formations external to the BRAA, allowing interaction with and loss of water to peripheral formations, while the other side of the river sends bank storage into the alluvium that likely returns to the river eventually. If this is the case, hydraulic gradients in the formations bordering the BRAA must slope away from the river at high flows, and may or may not slope towards it during low flows. It is possible that there is little interaction between the Brazos River and the Eocene formations beyond the BRAA during low flows when the river is not losing water to its banks. The observed groundwater discharge may be from the BRAA and not these external formations.

The relations between river level and aquifer hydraulic gradient are likely different for the BRAA and neighboring deposits. The northern stretch of river would be most affected by hydraulic gradients between the Brazos River and BRAA, while the southern stretch would be affected on one side of the river by hydraulic gradients between the river and the Eocene deposits on the border of the BRAA (and Brazos River

floodplain). This may explain why we observed the northern stretch to be mostly gaining and the southern stretch to often be losing.

A past study by Turco et al. (2007) suggested that the section of Brazos River overlying the Yegua-Jackson (Yegua) aquifer should be gaining due to contributions from that aquifer. Both of our study stretches, however, overlie the Yegua-Jackson outcrop (figure 3-2), and only the northern stretch is primarily gaining. Our EMMA results indicated that water likely from the Yegua formation can be found in the river at all three of our gage sites (figures 5-51 and 5-52), confirming the suggestion that the Yegua aquifer contributes flow to the Brazos River in this area. Both of our studied stretches are located above the outcrop of the Yegua-Jackson aquifer (figure 3-2), however, and the southern stretch was often losing water. These water losses above a major aquifer outcrop mean that the river position over aquifer outcrops is not the only driving factor behind water gains and losses in the Brazos River. We have found that the location of the river in the alluvium, either in the middle of the alluvium or abutting the side of it, is even more important.

6.2 Groundwater Discharge between SH21 and SH60

6.2.1 Comparing All Methods of Estimating Groundwater Discharge

Differential gaging, longitudinal specific conductance surveys, EMMA, and hydrograph separation methods tended to give similar Q_{gw} estimates from SH21 to SH60. The Dupuit equation-based estimates differed most from our other methods' estimates throughout the entire study period. EMMA estimates were within 4.5 m^3/s of differential gaging and specific conductance-based estimates on all but one day, October

29 (figure 6-1). In terms of groundwater percent of river discharge, EMMA, specific conductance, differential gaging and hydrograph separation had very similar results in periods 2 and 3, the only periods when all methods overlapped. The differences between all methods during these periods were always less than 7% of river discharge, except on September 1 for EMMA, and at the end of period 2. On September 1, EMMA estimated that groundwater made up 4% of flow, and hydrograph separation estimated that it made up 15%. Estimates from the other methods are not available on this day. This was within a week after a precipitation event, when tributaries may have still been active and the river was not steady, which may explain the greater difference between estimates. At the end of period 2 the difference between differential gaging and hydrograph separation increased from 1 percentage point on August 9 to a maximum of 18 percentage points on August 20 before converging again.

Continuous hydrograph separation estimates were within 10 m^3/s of continuous differential gaging estimates, point estimates made with EMMA, and specific conductance survey estimates during five of the six differential gaging periods that overlapped with good hydrograph separation estimates (figure 6-1). The periods where all the methods produced similar groundwater discharge estimates were 2, 3, 4, 5, and 7. There may have been greater differences between the differential gaging and hydrograph separation estimates during period 6 (~18 m^3/s, figure 6-1) because the hydrograph separation program assumed a dam-release river peak was a storm event during this period, whereas we were able to treat it as a non-storm event in our differential gaging calculations. In terms of groundwater percent of river flow, hydrograph separation

estimates were within 7% of differential gaging during periods 3, 4, 5, and 6, and 0 to 18% different during period 2 as stated above.

On October 29, the EMMA-derived groundwater discharge estimate was considerably higher than the hydrograph separation method's estimate (the only other estimate available on that date besides from the Dupuit equation), with 23 m^3/s (5% of river discharge) compared to 3 m^3/s (1% of river discharge), respectively. These different results from EMMA may be a result of the river being in less steady conditions on October 29, 2015, than on the other days when EMMA samples were taken (figure 6-1). The samples taken upstream and downstream on this day may have been taken from very different bodies of water because of the travel time of water from upstream to downstream. The river flow was quite steady when most of our EMMA samples were taken from July 24 to October 21, 2015, making incorporation of the travel time into sampling times less significant. Accommodation of travel times may have been more important when the river flow was less steady on October 29, 2015. It is also likely that tributaries to the Brazos River were still active on this day as it had rained only four days before on October 25. The October 29 SH21 and SH60 river samples appeared to have large amounts of bank storage/runoff (figure 5-62). On this day this endmember was probably more runoff than bank storage, unlike in the other samples taken during dry periods when there was little runoff and tributary discharge occurring.

The Dupuit equation-based estimates tended to have a negative relationship between river discharge and groundwater discharge, while our four other estimate methods had a positive relationship in terms of total groundwater discharge (figure 6-1).

The Dupuit method also suggested the river was often recharging the aquifer at high flows as evidenced by negative groundwater discharge estimates. It estimated that groundwater discharge increased as river level decreased. This is not what we observed from our more direct river-based measurements of major ions, specific conductance, and differential gaging, however, that indicated decreasing groundwater discharge with decreasing river level. The Dupuit equation-based estimates have the most assumptions of all our methods, including that K and hydraulic gradient between the aquifer and river were the same over both entire study stretches, and that Q_{gw} was the same from both sides of the river. This method should therefore be the least trusted of our methods used to estimate groundwater discharge.

In terms of groundwater percent of river flow, differential gaging estimated 2% to 22% of river flow during gaining periods. The highest percentage of river flow (22%) occurred on August 2 when the river was at a flow of ~108 m^3/s during dry period 2. During period 2 the percent of river discharge made up of groundwater generally increased from ~7% to 17% according to EMMA, specific conductance, hydrograph separation, and differential gaging, though there was a small peak in the middle of the period when the differential gaging estimate reached 22%. All four of these methods also showed that the percentage of river water made up of groundwater decreased through period 3 from ~17% to 6%. Dupuit estimates of groundwater percent of river flow were mostly within 2 to 12% of hydrograph separation estimates during period 2, but jumped to 100 percentage points greater during period 3. Dupuit groundwater

percent estimates reached 109% during period 3, which is impossible and shows that this method did not work during that period.

6.2.2 Longitudinal Surveys

In most gaining rivers, specific conductance would be expected to increase in the downstream direction since in most regions groundwater typically has higher specific conductance than surface water (Pai et al., 2015). During three out of four of our longitudinal specific conductance surveys, however, specific conductance actually decreased in the downstream direction. Other studies have seen this occur in the Brazos River before (Wurbs et al., 1993; Dawson et al., 2015). They attributed this mainly to river basin geology upstream of Lake Whitney causing naturally high salt loads that get diluted downstream with inputs from tributaries and increasingly less saline groundwater (Wurbs et al., 1993). Evaporation of water in Lake Whitney can cause further concentration of salt loads in the Brazos River upstream of our study stretch (van Plantinga et al., in review).

Lake Whitney has been found by other studies to receive water with 1426 µS/cm (Wurbs and Lee, 2009). For this study we assumed a value of 1427 µS/cm for Lake Whitney water from data from van Plantinga et al. (in review). We found the BRAA endmember to have a value of 1267 µS/cm based on our well samples. It is possible that on July 31, 2015, the day that we saw specific conductance increase in the river from 638 (± 3.2) to 666 (± 3.3) µS/cm, we were catching up to a slug of high specific conductance water from Lake Whitney as we paddled toward SH60 from SH21. The specific conductance values we observed in the river on this day show that the river was

diluted between Lake Whitney and SH21 as suggested by Wurbs et al. (1993) and Dawson et al. (2015), possibly by tributaries, but likely also by dilute bank storage from recent flood events. Our EMMA calculations found that bank storage was a large component of river flow on July 31, making up 73% of river flow at SH21 and 71% of river flow at SH60 (figures 5-51 and 5-52).

Even though specific conductance generally decreased in the downstream direction during three of our four surveys (figures 5-40 through 5-42), the values calculated for groundwater discharge from this method agree well with the values from our other methods. It seems that the mass balance for total dissolved solids estimates groundwater discharge well both when dissolved solids are being contributed and diluted. We are not sure why positive groundwater discharge values were calculated from our August 22, 2015, and October 21, 2015, surveys even when the groundwater endmember value of specific conductance (mean 1267 µS/cm ± 6.3) was higher than the specific conductance values observed in the river (between 878 ± 4.4 and 1006 ± 5.0 µS/cm). If groundwater discharge was positive, the higher specific conductance value of the groundwater relative to the river water would have been expected to cause the specific conductance in the river to increase in the downstream direction. We observed the opposite during two surveys, though groundwater discharge was still estimated to be positive (table 5-4). On August 22, 2015, specific conductance in the river decreased from 912 ± 4.6 to 883 ± 4.4 µS/cm, and on October 21, 2015, specific conductance in the river decreased from 1005 to 983 µS/cm.

6.2.3 Dupuit Equation Estimates

The Dupuit equation estimates differed the most from estimates from all four of our other methods. This is likely because of the many assumptions that went into this method. Those assumptions included that the hydraulic gradient between the BRAA and Brazos River was the same over the entire 14 km straight stretch from SH21 to SH60. This assumption implies that the aquifer is homogeneous over the entire stretch, which is clearly not true from Shah et al.'s (2007) map of aquifer thickness and Proffitt's (2015) map of aquifer transmissivity that, combined, show that aquifer K ranges from ~2.3 x 10^{-5} to 1.4 x 10^{-3} m/s in our study area. The K we used in our Dupuit calculations, and assumed for the entire study stretch, was 5.13 x 10^{-4} m/s based on pumping tests performed at our monitoring well site during a separate study (Shuai et al., 2014). The actual hydraulic conductivities observed across the study stretch range two orders of magnitude, and 4% to nearly 300% of the K value we used in our calculations. This great variability in K shows the difficulty in scaling the Dupuit method up to the entire study stretch. The other major assumption we made to obtain our Dupuit estimates was that Q_{gw} was the same from both sides of the river. In this study stretch that assumption was likely acceptable because the river flows through the middle of the alluvium for nearly this entire stretch. It was not a good assumption for the southern stretch, however, as will be described below.

Our Dupuit data is the same shape as our river stage data, but flipped upside down (figure 6-1). These Dupuit results simply come from the aquifer water table 280 m from the river, the location of our well, remaining relatively stable while the river

level fluctuated. Our well therefore was not close enough to the river to detect fluctuations in bank storage levels. A closer well may have captured finer fluctuations in aquifer level that only occur more immediately adjacent to the river and are more representative of the level of bank storage. It is possible that the levels in a closer well would show a stronger relationship between aquifer and river level, and would predict bank storage discharge better than our well that is 280 m away (figure 6-6). Dupuit estimates from a closer well may match our EMMA bank storage discharge estimates better.

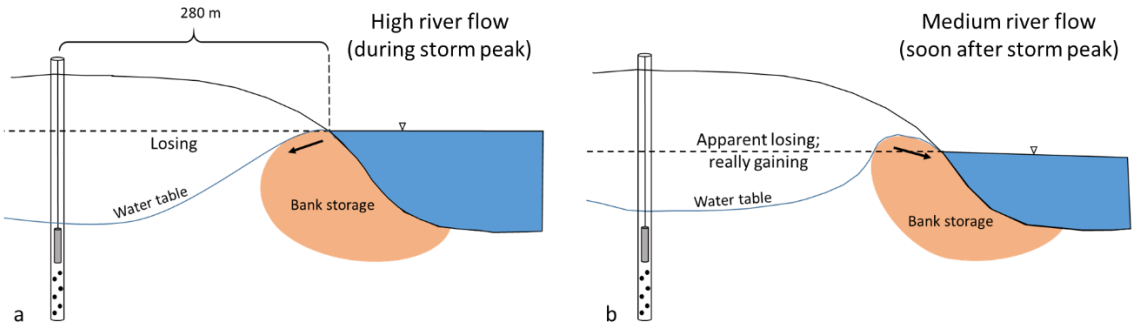

Figure 6-6: Our BRAA well that was 280 m away from the river was too far away to capture hydraulic gradient fluctuations that we believe are occurring between the bank storage and river. In (a) the well would have correctly assumed water losses from the river to the aquifer during high flows. In (b) the well would have incorrectly assumed river water losses to the aquifer during medium flows when our other methods measured groundwater discharge to the river.

6.2.4 Long-Term Trends

The stretch between SH21 and SH60 was consistently gaining through all differential gaging periods except the last one, period 8 (figure 6-1). During period 8, river discharge at SH60 dropped from 266 to 58 m^3/s as hydropeaking was occurring.

Groundwater discharge estimated by differential gaging dropped from 14 to -18 m^3/s (5% to -31% of flow). This change in direction of water flows may have been caused by a lack of biofilm clogging of the river bottom in the cold winter as described above and depicted in figure 6-5. It is also possible that near the end of our study period, three months after we completed our rating curves and stopped making frequent discharge measurements, our rating curves stopped being applicable to one or both of our SH21 and SH60 gage sites. This could be true if one of the gages was moved by debris passing during a high flow event.

Through dry periods 1 through 7, while groundwater discharge estimates remained positive, groundwater discharge positively varied with river discharge. During dry periods 2 and 3, which both lasted longer than a month, groundwater discharge can be seen to gradually decrease as river discharge decreases (figure 6-1). The same behavior can be seen over shorter time scales, from two days to two weeks, respectively, in periods 6 and 8. Percent of river water made up of groundwater generally increased in period 2, but decreased in period 3. The decrease in period 3 may be attributable to the aquifer draining out and the hydraulic gradient approaching zero adjacent to the river. Percent groundwater remained steady in period 6 at 5%, but decreased with river discharge in period 8 from 5% to -31% of flow.

6.2.5 Relationship between River Discharge and Q_{gw}

We found the relationship between river discharge and groundwater to be clearly positive between SH21 and SH60. River discharge at SH60 is plotted against differential-gaging-derived Q_{gw} for each differential gaging period in figure 6-7. Periods

1, 2, and 3 seem to fit the same curve. Periods 4 and 5 seem to fit a different curve, and periods 6, 7, and 8 appear to fit a third curve. There were always less than two large rain events between periods that fit the same curve. These periods that fit similar relationships between groundwater discharge and river discharge may have occurred during similar hydrologic conditions in the aquifer and river basin, including parameters like antecedent soil moisture that can affect groundwater discharge, but were not measured in this study. Periods with similar relationships may also have occurred when the river morphology was the most similar. Changes in the relationship between river discharge and groundwater discharge may indicate changes in river morphology, groundwater levels, or other hydrologic factors not measured during this study.

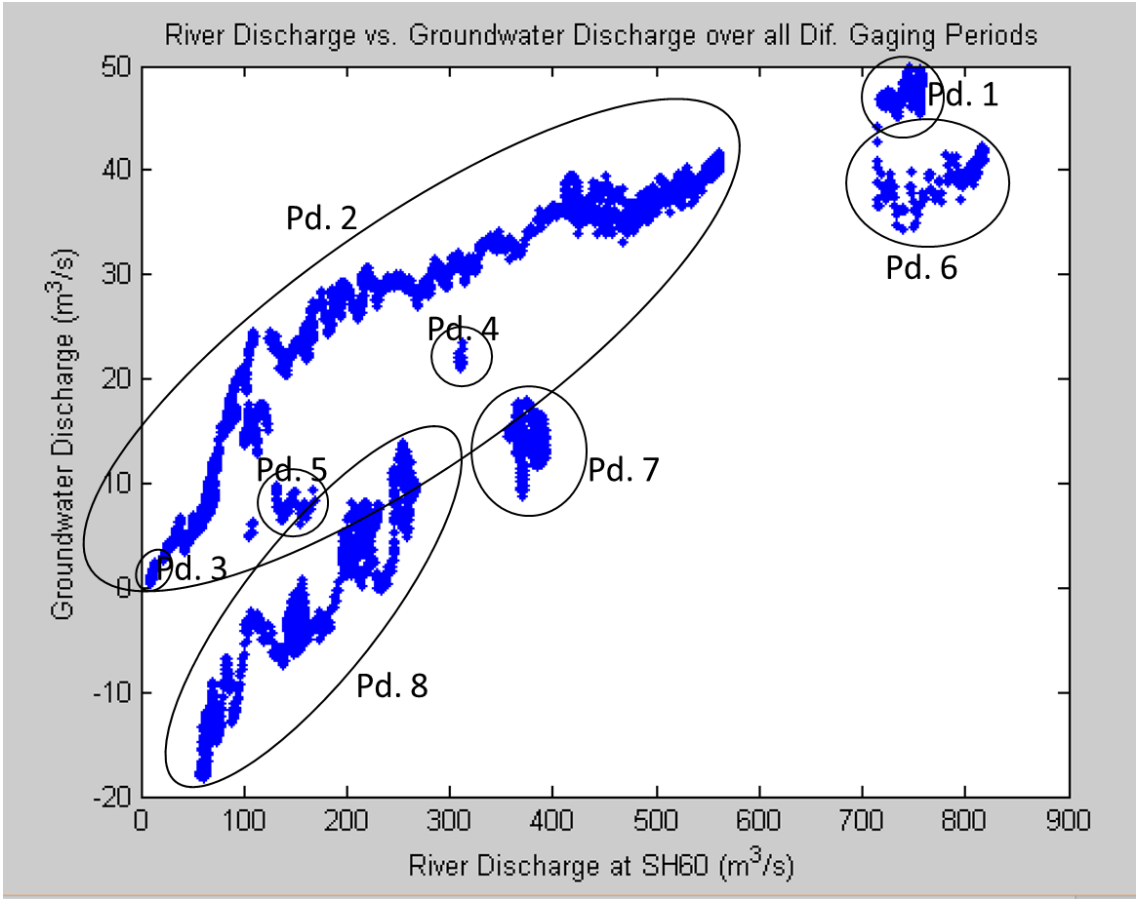

Figure 6-7: River discharge at SH60 versus groundwater discharge (from differential gaging) between SH21 and SH60.

6.3 Groundwater Discharge between SH60 and Navasota

6.3.1 Comparing All Methods of Estimating Groundwater Discharge

The only available EMMA-based groundwater discharge estimate for this stretch matched the results from hydrograph separation closely in terms of total groundwater discharge. The EMMA estimate on September 25, 2015, was -0.7 m^3/s (-6% of river discharge), while the hydrograph separation estimate was -1.8 m^3/s (-16% of river discharge), indicating slightly losing conditions. In contrast, the Dupuit-based estimate

on this day was larger and positive, at 26 m^3/s (200% of flow), indicating gaining conditions, but also more groundwater than was actually in the river.

During period 1 (October 6 to 22, 2015) of differential gaging, hydrograph separation, differential gaging, and specific conductance mass balance gave very similar estimates of 2 m^3/s, 2 m^3/s, and 8 m^3/s, respectively. In terms of percent of river discharge, however, the specific conductance estimate is very different from the hydrograph separation and differential gaging estimates: 60-65% of river flow from specific conductance, and 12-23% from the other two methods. The Dupuit equation gave larger estimates than the other methods, with values between 25 and 26 m^3/s through the entire period. These values are again close to 200% of river flow over the period.

The second dry period gave estimates within 12 m^3/s (and 6% of river flow) of each other from differential gaging and specific conductance mass balance, with values ranging from ~45 to 60 m^3/s. Differential gaging estimates increased from 22% to 30% of river flow, and specific conductance estimates stayed between 24% and 25%. Hydrograph separation gave estimates about 20 m^3/s greater than these other methods on November 27, 2015, the only day during this period with overlapping data from hydrograph separation. On this day, the hydrograph separation estimate was 68 m^3/s (33% of river flow), the differential gaging estimate was 46 m^3/s (30% of river flow), and the specific conductance estimate was 50 m^3/s (25% of river flow). Dupuit method Q_{gw} estimates for the period were between 16 and 18 m^3/s (7% to 8% of flow). They

were 30 to 40 m^3/s (15% to 22% of river flow) smaller than the specific conductance and differential gaging-based estimates over the period (figure 6-2).

During dry period 3 differential gaging suggested a losing stretch. Many specific conductance-based estimates were negative during this period (figure 6-2), but a specific conductance mass balance cannot measure losses from the river, so these values can only demonstrate that the river was not gaining during this time. Specific conductance-derived estimates increase rapidly at the end of this dry period, however, to 55 m^3/s (9% of river flow). The differential gaging estimates ranged from -154 to -94 m^3/s (-23% to -15% of river flow) in period 3, with the least negative value of -94 m^3/s occurring concurrently with the positive specific conductance estimate of 55 m^3/s (figure 6-2). Dupuit equation-based Q_{gw} estimates were less negative than the differential gaging results from period 3, with values ranging between -20 and -14 m^3/s (-3% to -2% of river flow) (figure 6-2).

During dry period 4, specific conductance mass balance provided considerably higher Q_{gw} estimates than differential gaging. The specific conductance estimates decreased slowly from 112 to 94 m^3/s (ranging only from 28% to 26% of river flow), while the differential gaging estimates decreased faster from 49 to -33 m^3/s (ranging from 12% to -9% of river flow) (figure 6-2). The difference between these methods ranged from 62 to 127 m^3/s (15% to 35% of river flow) during period 4. The Dupuit equation-derived Q_{gw} estimates in period 4 were more similar to the differential gaging than the specific conductance values, and had more stable Q_{gw} values than the other methods, only varying from 7 to 10 m^3/s (constantly ~2% of river flow) (figure 6-2).

These values remained positive for the entire period, while differential gaging suggested the river switched from gaining to losing in the middle of the period.

During period 5 the results from differential gaging and specific conductance are more similar than during periods 3 and 4. The difference between these methods in period 5 ranges only from 0 to 65 m^3/s (0 to ~27% of river flow), with the estimates overlapping at some points (figure 6-2). Specific conductance-based Q_{gw} estimates are positive for the entire period, ranging from 0 to 58 m^3/s (and 0 to 24% of river flow). Differential gaging suggests the stretch was losing for most of the first half of this period, giving a minimum Q_{gw} value of -33 m^3/s (-18% of river flow) (figure 6-2). During the second half of this period differential gaging suggests gaining conditions with Q_{gw} estimates reaching a maximum value of 38 m^3/s (33% of river flow). Dupuit equation estimates during this period are also similar to both the specific conductance and differential gaging estimates with values increasing slowly from 17 to 24 m^3/s (7% to 13% of river flow) (figure 6-2).

6.3.2 Dupuit Equation Estimates

The Dupuit equation estimates again clearly match the river fluctuations, similar to in the northern study stretch. They also provide the most different Q_{gw} estimates compared to our other methods (figure 6-2). They differ so much from our other estimates because of the same assumptions that were mentioned earlier: we assumed the same hydraulic gradient and aquifer K over this entire 34 km straight study stretch, and we assumed the same amount of groundwater discharge from both sides of the river. The assumption of a homogeneous aquifer with the same K and hydraulic gradient over

the entire stretch may be a worse assumption to make for this stretch than the northern stretch. It may be worse because this stretch is 20 straight kilometers longer than the northern stretch, allowing more space for more variability to occur. The second assumption, that Q_{gw} is the same from both sides of the river, is particularly bad over this stretch because the river abuts the side of the alluvium for nearly the entire length. It should not be assumed that the Eocene deposits on the peripheral of the alluvium have the same K, hydraulic gradient, or any other characteristics as the BRAA. It therefore also cannot be assumed that these deposits discharge the same amount of groundwater into the river as the BRAA.

6.3.3 Continuous High Frequency Specific Conductance Measurements

Groundwater discharge between SH60 and Navasota was calculated using a specific conductance mass balance during dry periods. The same time periods were used to conduct differential gaging between SH60 and Navasota. These time periods may have been flawed for specific conductance-based calculations, however, because Yegua Creek, one of the tributaries to the Brazos River between our SH60 and Navasota gages, is regulated by releases from a dam at Somerville Lake. While all other tributaries between these gages were likely active only until D days (equation 4-3) past the peak of each hydrograph, this significant tributary is not controlled by the same relationship. Therefore, many of the periods in which we expected to have no tributary inflow did in fact have inflow from Yegua Creek, as is clear from discharge data from the USGS gaging station 08110000 that is just downstream of the dam at Lake Somerville (figure 6-8). This may cause inaccuracies in the specific conductance-based calculations

because our equation (equation 4-5) assumed specific conductance changed from upstream to downstream only because of groundwater inputs. The equation did not account for tributary inflows. Yegua Creek discharges were not a problem for differential gaging-based calculations because the known discharges could be subtracted from the Navasota discharges.

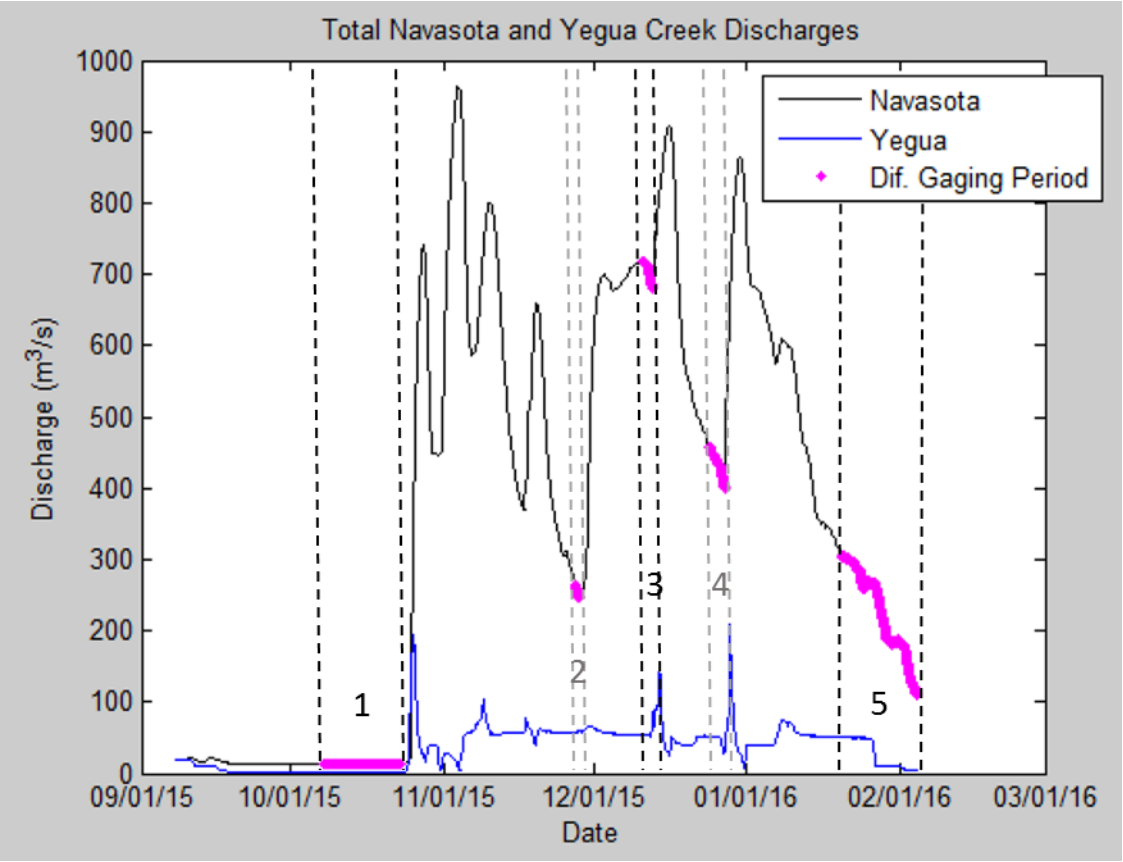

Figure 6-8: Discharge at Navasota with differential gaging periods highlighted in pink, and flow discharging from Yegua Creek in between our SH60 and Navasota gages.

When the periods of discharge from Yegua creek into the Brazos River are accounted for, the groundwater discharge measurements from times that Yegua Creek

had zero or nearly zero discharge (October 6-October 22, 2015, part of our first calculation period) are more similar to our groundwater discharge estimates using differential gaging (figure 6-2). When Yegua Creek discharge was about 50 m^3/s, or 17% of total river flow at the Navasota gage, during periods 2, 3, 4, and the beginning of 5, we saw greater differences between our specific conductance mass balance-based groundwater discharge estimates and our differential gaging-based groundwater discharge estimates (figure 6-2).

It can also be seen in figure 6-8 that during differential gaging periods 3 and 4 Yegua Creek discharge became highly unsteady. The estimate of travel time for water from the Yegua Creek gage to our Navasota gage was an average value that likely applies best at steady low flows. During periods 3 and 4, when Yegua Creek discharge was unusually high, this estimate of 1.4 days was probably not the true travel time. The water was likely moving faster at high flow and would have taken less than 1.4 days to reach our gage. This may have caused our differential gaging results to have large errors, and can explain why differential gaging and specific conductance-based estimates are very different during these periods (figure 6-2). Differential gaging and specific conductance estimates during period 5 are most similar starting on January 8, 2015, one day after discharge at Yegua Creek dropped from 50 m^3/s to 10 m^3/s (figure 6-8). The reduced influence from this tributary's inflow likely caused the two measures to converge on this date (figure 6-2).

The wastewater treatment plant between SH21 and SH60 may have affected our specific conductance-based Q_{gw} estimates. Specific conductance at SH60 changes

quickly and erratically during periods 3 and 5 as compared to the other study periods, which results in quick and erratic changes in estimated groundwater discharge. These results were likely caused by releases of treated wastewater during these periods from Thompsons Creek, 3.52 river-km upstream of our SH60 gage. We found Thompsons Creek water, measured with a YSI during our August 22, 2015, longitudinal specific conductance survey, to have a specific conductance of 1297 µS/cm. The presence of this wastewater treatment plant likely also explains some of the difference between the differential gaging and specific conductance mass balance estimates in periods 3 and 5.

6.3.4 Relationship between River Discharge and Q_{gw}

The relationship between river discharge and groundwater discharge derived from differential gaging and specific conductance in this stretch of the Brazos River appears to be negative, unlike for the stretch from SH21 to SH60. River discharge at SH60 is plotted against groundwater discharge calculated from differential gaging between SH60 and Navasota in figure 6-9. These results indicate that the river is losing in this stretch. The negative relationships do not appear as continuous as the positive relationships between river discharge and groundwater discharge observed between differential gaging periods from SH21 to SH60. They are, however, consistently negative.

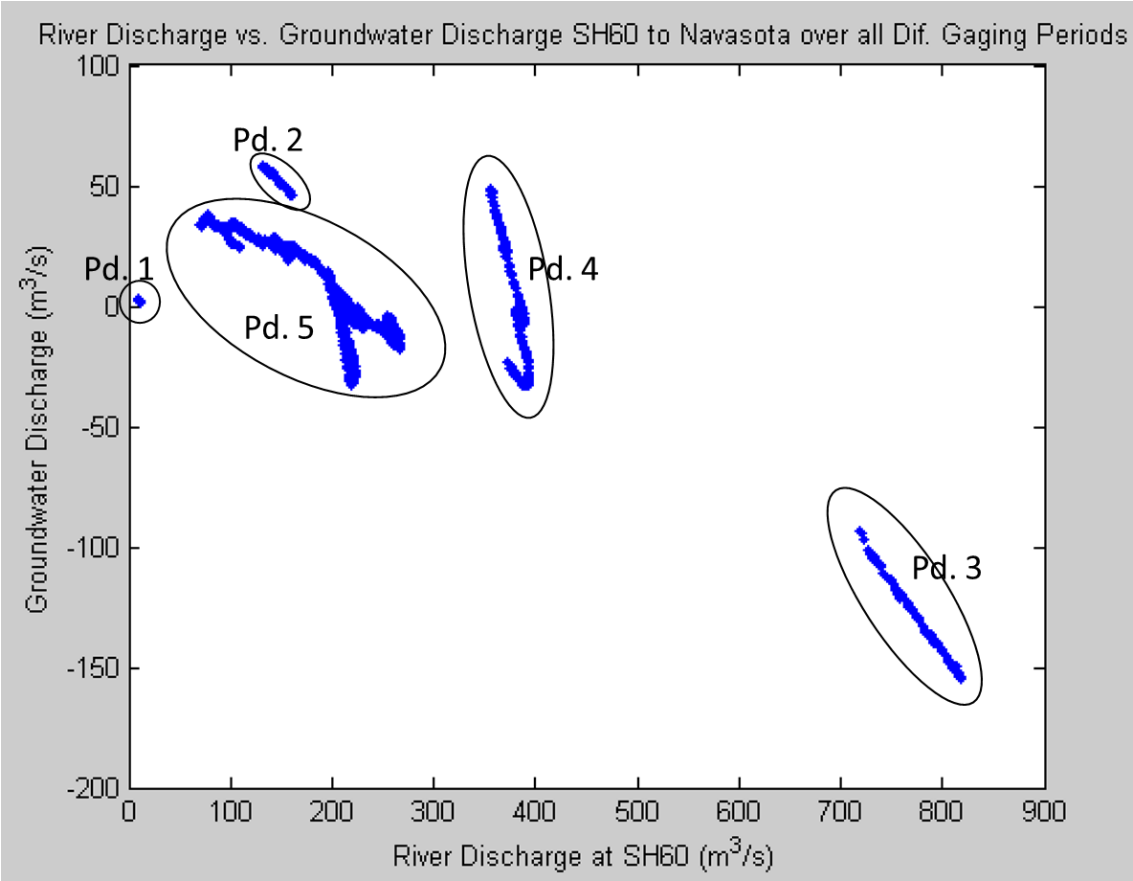

Figure 6-9: River discharge at SH60 versus groundwater discharge between SH60 and Navasota.

6.4 Contributions of Different Methods

Past studies have found hydrograph separation and differential gaging (physical methods) to measure total net groundwater discharge to rivers, while chemical methods measure different types of groundwater discharging to a river, such as bank storage and regional groundwater (Unland et al., 2013; Yu et al., 2013). The chemical methods' ability to measure different types of groundwater instead of all groundwater usually resulted in lower Q_{gw} estimates from those methods than from differential gaging and

hydrograph separation. In this study we did not observe hydrograph separation and differential gaging estimates that were consistently considerably higher than our specific conductance and EMMA estimates.

The closeness of our differential gaging, hydrograph separation, and EMMA results indicates that we identified all groundwater sources well for our EMMA analysis. If any groundwater sources were missing from EMMA, then EMMA Q_{gw} estimates should have been lower than the estimates from our two physical methods. The ability to split the total groundwater discharge into bank storage, BRAA, and Yegua endmembers, however, was a valuable contribution of the EMMA method. This greatly improved our understanding of the Brazos River-aquifer system by shedding light on the roles of the three identified types of groundwater in the system. EMMA's indication that bank storage discharge to the river decreases with time since a storm event, combined with the knowledge from our BRAA well that the aquifer level 280 m from the river is stable, helped us conclude that the hydraulic gradient adjacent to the river (in its banks) is very important for groundwater discharge volumes. EMMA also indicated that some Yegua formation water enters the Brazos River in this study stretch, which may have future implications for managing that aquifer and the Brazos River together.

From SH60 to Navasota specific conductance estimates were usually higher than differential gaging estimates, which is the opposite of what we would have expected. Usually chemical methods underestimate Q_{gw} compared to physical methods (Unland et al., 2013; Yu et al., 2013). This may indicate that we did not characterize the BRAA groundwater endmember's specific conductance well enough. It may also indicate that

specific conductance is not a great method for estimating Q_{gw} on the Brazos River. This is likely because the river receives highly saline water from Lake Whitney, resulting in little contrast between it and the surrounding groundwater. Contrast in ground and surface water values is essential for a water parameter to make a good tracer of groundwater discharge, but this contrast does not appear high enough in the Brazos River-BRAA system. The presence of wastewater treatment plants and tributaries with unknown specific conductances also made this method difficult to implement on the Brazos River.

Since four of our methods (all except Dupuit) gave very similar Q_{gw} estimates, any of the methods could be used to obtain reliable estimates of Q_{gw}. The method that would likely be best for everyday use by water managers, for example, is hydrograph separation. This was the easiest method that required the least effort, but it gave very similar results to the other more involved methods. It also gave more continuous results than any of the other methods. Hydrograph separation is the best method for obtaining a quick estimate of total groundwater discharge to the Brazos River, but using a combination of chemical and physical methods is the best way to garner a complete understanding of the system as a whole.

7. CONCLUSIONS

7.1 Implications for Water Managers

7.1.1 Maintenance of Water Quality

It is important for water managers and environmental agencies monitoring the water quality of rivers to understand that the most groundwater discharge occurs following storm events. Groundwater is usually high quality water, the discharge of which can help foster plant and animal life (Opsahl et al., 2007), as well as high quality water sufficient for recreation. To mitigate negative effects on water quality from waste water treatment plants, the findings of this study imply that the optimal time to release waste water is right after storm events. This would likely be the time that would be least harmful to the river and the plants and animals that live in it. High quality river water sufficient for recreation could also be maintained more easily all year long with this understanding of river dynamics.

7.1.1.1 Contaminant spills. Understanding the temporal connectivity between the Brazos River and the BRAA will be vital in the event of a chemical spill or other type of contamination. If the BRAA gets contaminated in a stretch where the river is gaining, that contamination would reach the river eventually. If it is spilled close to the river banks, where bank storage is flowing into the river, it would reach the river quickly. If it is spilled further from the banks, it would not reach the river until the bank storage has drained from the aquifer and the regional groundwater, now mixed with the contaminant, starts reaching the river. This is a decidedly relevant issue as there are

many oil and gas activities occurring on the BRAA between SH21 and SH60 visible in GoogleEarth aerial imagery.

If a serious contaminant spill does occur in the stretch between SH21 and SH60, it would eventually move to the river, and could quickly spread to more aquifers along the stretch from SH60 to Navasota where the river is losing water to the BRAA and neighboring formations. This would be especially likely at higher flows (i.e. greater than 212 m^3/s, though this number is dependent on antecedent river levels and aquifer conditions) when the southern stretch, according to our data, is losing. It would also be a larger problem in the winter time when the northern stretch from SH21 to SH60 is losing and appears to be more connected to the BRAA than during summer.

7.1.2 Dam Release Schedules

We learned from this study that water managers trying to maintain river flows and release water for downstream users can release less water following rain events. If it is practical for them (their reservoirs are not full to the point of overflowing), they can store water for a long time after large rain events. The river will naturally maintain higher flows through the release of bank storage for some time. Understanding this dynamic of the river system may help managers better understand the minimum threshold of river discharge at which they need to release water for downstream users.

This knowledge may influence the construction of future dams and reservoirs on the Brazos River. There may become a need to store larger amounts of water as droughts and water needs increase concurrently. If the Brazos River is maintaining its own flow through groundwater discharge for long periods after storm events, then

managers can store more water longer. Larger reservoirs may be necessary to store enough water to maintain sufficient river flows for wildlife during droughts, and meet the needs of more users for longer.

7.1.3 Paired Groundwater-Surface Water Management

This study and past studies have made it clear that the Brazos River and BRAA are connected. These two water bodies are not currently regulated together. They are instead treated as separate entities by Texas law (TWDB, 2012b). In times of severe drought when all water needs to be accounted for precisely, this may become a significant problem if groundwater and surface water managers do not work together. Since the Brazos River and BRAA are so clearly connected, the Brazos River Authority (BRA), the governmental body regulating the river, and local groundwater conservation districts (GWCDs), the governmental bodies regulating the BRAA, will need to coordinate when water is scarce. They will need to understand that high volumes of pumping from the aquifer may capture water that would otherwise have discharged into the river (Barlow and Leake, 2012), particularly if pumping occurs within 280 m of the river while river discharge is receding after storm events.

The BRA would better be able to decide the amount of water to release for downstream users if the GWCDs give them good estimates of how much pumping is occurring in the alluvium. Coordination with the groundwater managers would allow the BRA to take any potential losses in groundwater discharge to the river due to pumping into account when they are deciding how much water to release. Knowing that the aquifer and river are connected and that pumping in the BRAA can reduce Brazos

River discharge may protect the BRA in the future if they are accused of not releasing enough water to meet demands of downstream water rights holders. Lawmakers, however, may eventually find a need to limit pumping from the alluvium if so much water is being drawn out of the Brazos River that the water appropriated to downstream users never reaches them. Eventually, the state of Texas will need to decide who's water rights are more valuable—those pumping from the ground, or those pumping from the river.

7.2 Summary

In this study we investigated two stretches of the Brazos River: a northern stretch from SH21 to SH60, and a southern stretch from SH60 to Navasota. The northern stretch was found to mainly gain water from surrounding aquifers, and the southern stretch was found to often switch from losing to gaining. The difference in groundwater-surface water interactions between these two stretches is likely attributable to the location of the Brazos River in its floodplain over each stretch. In the primarily gaining stretch, the river is surrounded on both sides by the BRAA for nearly the entire length. In the gaining and losing stretch, the river flows against the side of its floodplain, losing water to peripheral formations at certain threshold discharges.

We found bank storage to make up a significant portion of flow in the river, particularly soon after rain events. Regional groundwater was found not to reach the river until much bank storage has drained out of the aquifer long after rain events. Bank storage recharge to the aquifer is suspected to cause an increase in hydraulic gradient between the aquifer and the river within 280 m of the river bank, causing the highest

groundwater discharges to occur soon after precipitation events and slowly decrease over time as the bank storage drains and the hydraulic gradient decreases. A detailed, high temporal resolution, multi-method approach to estimating groundwater discharge has not been performed before on a low-land coastal river like the Brazos River. The insights gained from this study of groundwater-surface water interactions in a low-land coastal setting can be applied to many similar rivers in the future, including many Texas rivers, as water supplies grow ever more scarce.

REFERENCES

Alden, A. S., and Munster, C. L., 1997, Assessment of river-floodplain aquifer interactions: Environmental & Engineering Geoscience, v. 3, no. 4, p. 537-548.

Ashworth, J.B., and Hopkins, J., 1995, Aquifers of Texas: Texas Water Development Board Report 345, 69 p.

Baeza, A., Delrio, L. M., Jimenez, A., Miro, C., and Paniagua, J. M., 1995, Factors determining the radioactivity levels of waters in the province of Caceres (Spain): Applied Radiation and Isotopes, v. 46, no. 10, p. 1053-1059.

Barlow, P.M., and Leake, S.A., 2012, Streamflow depletion by wells—Understanding and managing the effects of groundwater pumping on streamflow: U.S. Geological Survey Circular 1376, 84 p.

Barlow, P.M., Cunningham, W.L., Zhai, T., and Gray, M., 2015, U.S. Geological Survey groundwater toolbox, a graphical and mapping interface for analysis of hydrologic data (version 1.0)—User guide for estimation of base flow, runoff, and groundwater recharge from streamflow data: U.S. Geological Survey Techniques and Methods 3-B10, 27 p.

Battin, T. J., and Sengschmitt, D., 1999, Linking sediment biofilms, hydrodynamics, and river bed clogging: Evidence from a large river: Microbial Ecology, v. 37, no. 3, p. 185-196.

BRA, 2014, Technical report in support of the water management plan: Brazos River Authority, 220 p.

Brunke, M., and Gonser, T., 1997, The ecological significance of exchange processes between rivers and groundwater: Freshwater Biology, v. 37, no. 1, p. 1-33.

Chakka, K. B., and Munster, C. L., 1997, Atrazine and nitrate transport to the Brazos River floodplain aquifer: Transactions of the Asae, v. 40, no. 3, p. 615-621.

Chowdhury, A.H., Osting, T., Furnans, J., and Mathews, R., 2010, Groundwater-surface water interaction in the Brazos River basin: Evidence from lake connection history and chemical and isotopic compositions: Texas Water Development Board Report 375. 69 p.

Christophersen, N., Neal, C., Hooper, R. P., Vogt, R. D., and Andersen, S., 1990, Modelling streamwater chemistry as a mixture of soilwater end-members - A step towards second-generation acidification models: Journal of Hydrology, v. 116, no. 1, p. 307-320.

Cook, P. G., 2015, Quantifying river gain and loss at regional scales: Journal of Hydrology, v. 531, p. 749-758.

Cox, M. H., Su, G. W., and Constantz, J., 2007, Heat, chloride, and specific conductance as ground water tracers near streams: Ground Water, v. 45, no. 2, p. 187-195.

Cronin, J. and Wilson, C., 1967, Ground water in the flood-plain alluvium of the Brazos River, Whitney Dam to vicinity of Richmond, Texas: Texas Water Development Board Report 41, 70 p.

Dawson, D., VanLandeghem, M. M., Asquith, W. H., and Patino, R., 2015, Long-term trends in reservoir water quality and quantity in two major river basins of the southern Great Plains: Lake and reservoir management, v. 31, no. 3, p. 254-279.

de Oliveira Lucas, F., and Ribeiro, F. B., 2006, Radium content in ground water from a granitic batholith of the metamorphic basement, eastern São Paulo State, Brazil: Applied Radiation and Isotopes, v. 64, no. 6, p. 735-749.

Di Baldassarre, G., and Montanari, A., 2009, Uncertainty in river discharge observations: A quantitative analysis: Hydrology and Earth System Sciences, v. 13, no. 6, p. 913-921.

Dupuit, J., 1863, Etudes theoriques et pratiques sur le mouvement des eaux dans les canaux decouverts et a travers les terrains permeables: Paris, Dunod, 352 p.

Eckhardt, K., 2008, A comparison of baseflow indices, which were calculated with seven different baseflow separation methods: Journal of Hydrology, v. 352, no. 1-2, p. 168-173.

Filippini, M., Stumpp, C., Nijenhuis, I., Richnow, H. H., and Gargini, A., 2015, Evaluation of aquifer recharge and vulnerability in an alluvial lowland using environmental tracers: Journal of Hydrology, v. 529, p. 1657-1668.

Gamlin, J. D., Clark, J. F., Woodside, G., and Herndon, R., 2001, Large-scale tracing of ground water with sulfur hexafluoride: Journal of Environmental Engineering-Asce, v. 127, no. 2, p. 171-174.

Gracz, M. B., Moffett, M. F., Siegel, D. I., and Glaser, P. H., 2015, Analyzing peatland discharge to streams in an Alaskan watershed: An integration of end-member mixing analysis and a water balance approach: Journal of Hydrology, v. 530, p. 667-676.

Halford, K. J., and Mayer, G. C., 2000, Problems associated with estimating ground

water discharge and recharge from stream-discharge records: Ground Water, v. 38, no. 3, p. 331-342.

HDR Engineering, Inc., 2001, Brazos River alluvium groundwater model and conjunctive use analysis: HDR Engineering, Inc., File Copy 2002-0152, 27 p.

Hooper, R. P., Christophersen, N., and Peters, N. E., 1990, Modeling streamwater chemistry as a mixture of soilwater end-members - an application to the Panola Mountain catchment, Georgia, USA: Journal of Hydrology, v. 116, no. 1-4, p. 321-343.

Huggenberger, P., Hoehn, E., Beschta, R., and Woessner, W., 1998, Abiotic aspects of channels and floodplains in riparian ecology: Freshwater Biology, v. 40, no. 3, p. 407-425.

Kammerer, J.C., 1990, Largest rivers in the United States: U.S. Geological Survey Open File Report 87-242, 2 p.

Kendall, C., McDonnell, J. J., and Gu, W. Z., 2001, A look inside 'black box' hydrograph separation models: a study at the Hydrohill catchment: Hydrological Processes, v. 15, no. 10, p. 1877-1902.

Kronholm, S. C., and Capel, P. D., 2015, A comparison of high-resolution specific conductance-based end-member mixing analysis and a graphical method for baseflow separation of four streams in hydrologically challenging agricultural watersheds: Hydrological Processes, v. 29, no. 11, p. 2521-2533.

Langhoff, J. H., Rasmussen, K. R., and Christensen, S., 2006, Quantification and regionalization of groundwater-surface water interaction along an alluvial

stream: Journal of Hydrology, v. 320, no. 3-4, p. 342-358.

Larkin, R. G., and Sharp, J. M., 1992, On the relationship between river-basin geomorphology, aquifer hydraulics, and groundwater-flow direction in alluvial aquifers: Geological Society of America Bulletin, v. 104, no. 12, p. 1608-1620.

Li, P. Y., Wu, J. H., and Qian, H., 2016, Preliminary assessment of hydraulic connectivity between river water and shallow groundwater and estimation of their transfer rate during dry season in the Shidi River, China: Environmental Earth Sciences, v. 75, no. 2.

Linsley, R.K., Kohler, M.A., and Paulhus, J.L., 1975, Hydrology for Engineers: New York, New York, McGraw-Hill, 508 p.

Maupin, T. P., Agouridis, C. T., Barton, C. D., Warner, R. C., and Yu, X., 2013, Specific conductivity sensor performance: I. Laboratory evaluation: International Journal of Mining Reclamation and Environment, v. 27, no. 5, p. 329-344.

McCallum, A. M., Andersen, M. S., and Acworth, R. I., 2014, A new method for estimating recharge to unconfined aquifers using differential river gauging: Groundwater, v. 52, no. 2, p. 291-297.

McCallum, J. L., Cook, P. G., Berhane, D., Rumpf, C., and McMahon, G. A., 2012, Quantifying groundwater flows to streams using differential flow gaugings and water chemistry: Journal of Hydrology, v. 416, p. 118-132.

Nathan, R. J., and McMahon, T. A., 1990, Evaluation of automated techniques for base-flow and recession analyses: Water Resources Research, v. 26, no. 7, p. 1465-1473.

Nazaroff, W. W., 1992, Radon transport from soil to air: Reviews of Geophysics, v. 30, no. 2, p. 137-160.

Negulescu, M., and Rojanski, V., 1969, Recent research to determine reaeration coefficient: Water Research, v. 3, no. 3, p. 189-202.

Nielsen-Gammon, J.W., 2011, The changing climate of Texas, *in* Schmandt, J., North, G.R., and Clarkson, J., ed., The impact of global warming on Texas: Austin, Texas, University of Texas Press, 318 p.

NOAA, n.d., Location of US climate divisions: http://www.esrl.noaa.gov/psd/data/usclimdivs/ data/ map.html#Texas (accessed April 2016).

O'Connor, D.J., and Dobbins, W.E.: Mechanisms of reaeration in natural streams, Trans. Am. Soc. Civil Eng., 123, 641-684, 1958.

O'Rourke, D., 2006, Conjunctive use of the Brazos River Alluvium aquifer *in* Mace, R., Davidson, S., Angle, E., and Mullicam, W. ed., Aquifers of the Gulf Coast of Texas: Texas Water Development Board Report 365, p. 61-80.

Opsahl, S. P., Chapal, S. E., Hicks, D. W., and Wheeler, C. K., 2007, Evaluation of ground-water and surface-water exchanges using streamflow difference analyses: JAWRA Journal of the American Water Resources Association, v. 43, no. 5, p. 1132-1141.

Pai, H., Villamizar, S. R., and Harmon, T. C., 2015, High resolution synoptic salinity mapping to identify groundwater-surface water discharges in lowland rivers: Environmental Science & Technology, v. 49, no. 8, p. 4842-4850.

Payn, R. A., Gooseff, M. N., McGlynn, B. L., Bencala, K. E., and Wondzell, S. M., 2009, Channel water balance and exchange with subsurface flow along a mountain headwater stream in Montana, United States: Water Resources Research, v. 45, doi: 10.1029/2008WR007644.

Proffitt, T., 2015, Geologic and hydrogeologic characteristics of a shallow heterogeneous aquifer, Brazos River, Texas [MS Project]: Texas A&M University, 63 p.

Rahman, K., Besacier-Monbertrand, A. L., Castella, E., Lods-Crozet, B., Ilg, C., and Beguin, O., 2015, Quantification of the daily dynamics of streamflow components in a small alpine watershed in Switzerland using end member mixing analysis: Environmental Earth Sciences, v. 74, no. 6, p. 4927-4937.

Rencher, A., and Christensen, W.F., 2012, Methods of multivariate analysis: Hoboken, New Jersey, John Wiley and Sons, Inc., 800 p.

Shabana, E.-S., 2013, Natural radioactivity in the groundwater of Wadi Nu'man, Mecca Province, Saudi Arabia: Radiochimica Acta, v. 101, no. 7, p. 461-470.

Shah, S.D., Houston, N.A., and Braun, C.L., 2007, Hydrogeologic characterization of the Brazos River alluvium aquifer, Bosque County to Fort Bend County, Texas: U.S. Geological Survey, Scientific Investigations Map 2989, 5 sheets.

Shuai, P., Sanders, J., and Hastings, H., 2014, Report of the hydrogeologic characterization of the Brazos River Alluvial Aquifer study site, College Station, TX [Class project]: Texas A&M University, 95 p.

Swarzenski, P. W., 2007, U/Th series radionuclides as coastal groundwater tracers: Chemical Reviews, v. 107, no. 2, p. 663-674.

TNRIS, 2016, Data search and download: https://tnris.org/data-download/#!/statewide (accessed April 2016).

TPWD, 1974, An analysis of Texas waterways: A report on the physical characteristics of rivers, streams, and bayous in Texas: Texas Parks and Wildlife.

Tufenkji, N., Ryan, J. N., and Elimelech, M., 2002, The promise of bank filtration: Environmental Science & Technology, v. 36, no. 21, p. 422A-428A.

Turco, M., East, J., and Milburn, M., 2007, Base flow (1966–2005) and streamflow gain and loss (2006) of the Brazos River, McLennan County to Fort Bend County, Texas: U.S. Geological Survey, Scientific Investigations Report 2007-5286, 35 p.

TWDB, 2012a, Climate of Texas, *in* Water for Texas 2012 state water plan: Texas Water Development Board, p. 144-155.

TWDB, 2012b, Water for Texas 2012 state water plan: Texas Water Development Board, 314 p.

Unland, N. P., Cartwright, I., Andersen, M. S., Rau, G. C., Reed, J., Gilfedder, B. S., Atkinson, A. P., and Hofmann, H., 2013, Investigating the spatio-temporal variability in groundwater and surface water interactions: A multi-technique approach: Hydrology and Earth System Sciences, v. 17, no. 9, p. 3437-3453.

van Plantinga, A. A., Grossman, E.L., and Roark, E.B., Chemical tracer evaluation of water mixing and evaporation in a damned Texas river during drought: In review.

Wong, S., 2012, Developing a geospatial model for analysis of a dynamic, heterogeneous aquifer: The Brazos River Alluvium Aquifer, central Texas [MS Thesis]: Baylor University, 88 p.

Wurbs, R., and Lee, C., 2009, Salinity budget and WRAP salinity simulation studies of the Brazos River/reservoir system: Texas Water Resources Institute, Technical Report No. 352, 327 p.

Wurbs, R., Karama, A., Saleh, I., and Ganze, C., 1993, Natural salt pollution and water supply reliability in the Brazos River Basin: Texas Water Resources Institute, Technical Report No. 160, 177 p.

Yu, M. C. L., Cartwright, I., Braden, J. L., and de Bree, S. T., 2013, Examining the spatial and temporal variation of groundwater inflows to a valley-to-floodplain river using Rn-222, geochemistry and river discharge: the Ovens River, southeast Australia: Hydrology and Earth System Sciences, v. 17, no. 12, p. 4907-4924.

APPENDIX

A.1 Method to Compare USGS Gage to Collected Data

To compare our SH60 gage data for the first three months and last four months of the project (May 28 to September 10, 2015, and October 2, 2015, to February 5, 2016, respectively) to the USGS's gage data at SH21, I had to find the height of the USGS's gage in meters above sea level (masl). With this information, I would be able to convert all of the USGS gage measurements from feet to masl units, thus making them comparable to our measurements taken at SH60, also in masl. To find the absolute elevation of their gage, I compared their gage measurements and our gage measurements taken at the same time over a month long period, from September 4th, 2015, to October 2nd, 2015. The gage measurements lined up on the hour, every hour during this period, giving us 532 points to compare. I used Microsoft Excel's Solver function to find a consistent difference between ours and the USGS's gage measurements. Solver found the difference that minimized the sum of square errors between our modelled USGS gage heights and the actual USGS gage heights to be 58.6084 m. This gives the elevation of the USGS gage above sea level. To convert USGS gage heights from feet to masl, I multiplied the heights in feet by 0.3048 m/ft, then added the computed difference between their gage heights and ours, 58.6084 m, to each USGS gage height.

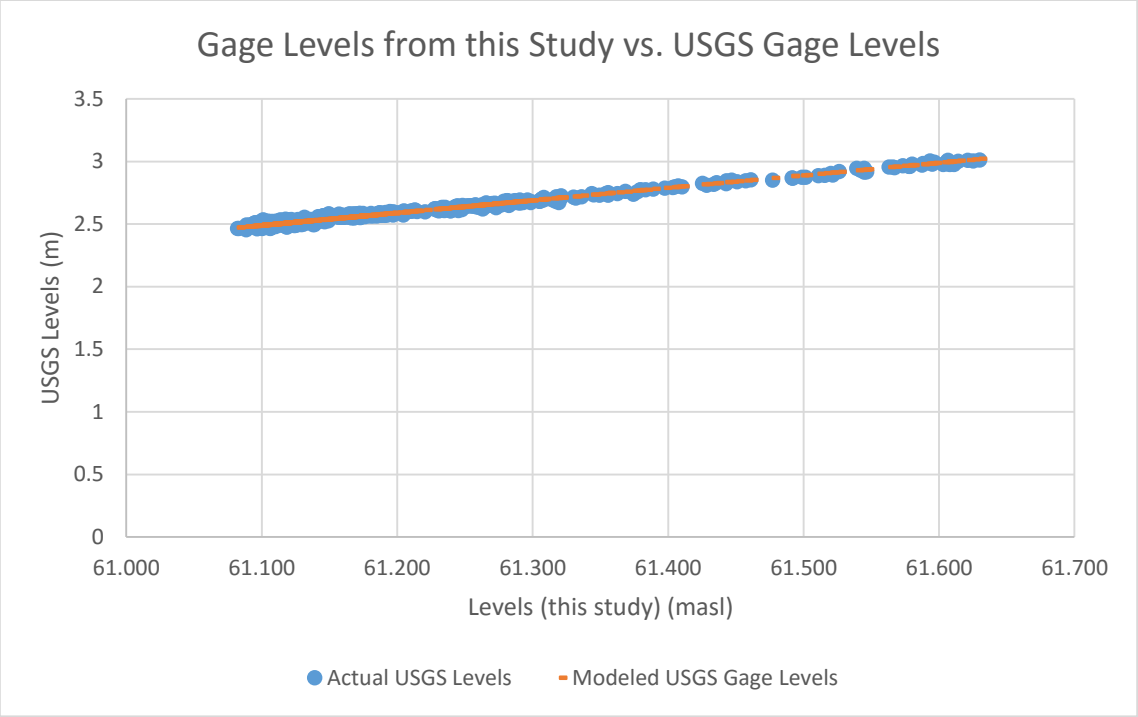

Figure A-1: Our gage heights compared to the USGS's actual and modelled gage heights. The data are hourly measurements taken by our gage and the USGS gage from September 10th to October 2nd, 2015. The modelled gage levels used the difference between our gage heights and the USGS gage heights calculated by Microsoft Excel's Solver function, and added it to the USGS gage heights.

A.2 Method to Calibrate YSI

The YSI was calibrated for pH, Specific Conductance, and ORP every morning before a day of measurements. The pH meter was calibrated using pH 4, pH 7, and pH 10 standard solutions. The specific conductance was calibrated with one point at 1413 µS/cm. The calibration of ORP also used only one point, at 220 mV.

A.3 Method to Calibrate LTC Logger

The LTC Junior Leveloggers were calibrated using a two point calibration the morning before deployment. The calibration used 1413 µS/cm and 5000 µS/cm calibration solutions.

A.4 ADCP Calibration and Setup

To calibrate the ADCP, the instrument was attached to the front of the canoe in the position it would be in while taking measurements. The RiverSurveyorLive software's calibration program was then turned on, and the paddlers spun the boat around in two full circles over the span of two minutes. When the magnetic influence was found to be acceptable, the calibration was accepted and we went on to perform our discharge measurements. If they were not acceptable, we would make sure to move the boat far away enough from any large metal bridges that may have influenced the magnetism in the calibration area, and calibration was redone until it was acceptable.

Before taking discharge measurements, the magnetic declination for College Station of 3.3 was entered into the RiverSurveyorLive software interface. The depth of the ADCP sensors under the water was also entered, usually ranging from 7 to 12 cm.

A.5 Finding Ion Concentrations using Ion Chromatography

After running our samples through the Ion Chromatograph, areas under a curve that corresponded to the concentration of each anion and cation in each sample were output in the Chromeleon software program. The timing of peaks were checked to make sure they were assigned to the appropriate ions. Standard ion solutions were processed with each sample run so that area under the curve could be correlated to known

concentrations using a calibration curve. The calibration solutions for the first cation run included a standard solution with concentrations of cations as listed in table 8-1, as well as the solution diluted 5 times, 10 times, 50 times and 100 times. The resulting concentrations from these dilutions are also shown in table 8-1. Subsequent IC runs used further dilutions of standard solutions in an attempt to minimize confidence intervals and limits of detection.

Table A-1: Standard solution concentrations used to calibrate the first cation run.

Cations	Standard Solution Concentration (ppm)	5x Dilution (ppm)	10x Dilution (ppm)	50x Dilution (ppm)	100x Dilution (ppm)
Lithium	50	10	5	1	0.5
Sodium	200	40	20	4	2
Ammonium	250	50	25	5	2.5
Potassium	500	100	50	10	5
Magnesium	250	50	25	5	2.5
Calcium	500	100	50	10	5

Table A-2: Standard solution concentrations used to calibrate the second cation run.

Cations	Standard Solution Concentration (ppm)	5x Dilution (ppm)	10x Dilution (ppm)	50x Dilution (ppm)	100x Dilution (ppm)	500x Dilution (ppm)
Lithium	50	10	5	1	0.5	0.1
Sodium	200	40	20	4	2	0.4
Ammonium	250	50	25	5	2.5	0.5
Potassium	500	100	50	10	5	1
Magnesium	250	50	25	5	2.5	0.5
Calcium	500	100	50	10	5	1

Table A-2 continued.

Cations	1000x Dilution (ppm)	2000x Dilution (ppm)
Lithium	0.05	0.025
Sodium	0.2	0.1
Ammonium	0.25	0.125
Potassium	0.5	0.25
Magnesium	0.25	0.125
Calcium	5	1

Table A-3: The standard solution concentrations used to calibrate both anion runs.

Anions	Standard Solution Conc. (ppm)	5x Dilution (ppm)	10x Dilution (ppm)	50x Dilution (ppm)	100x Dilution (ppm)	500x Dilution (ppm)	1000x Dilution (ppm)
Fluoride	20	4	2	0.4	0.2	0.04	0.02
Chloride	100	20	10	2	1	0.2	0.1
Nitrite	100	20	10	2	1	0.2	0.1
Bromide	100	20	10	2	1	0.2	0.1
Nitrate	100	20	10	2	1	0.2	0.1
Phosphate	200	40	20	4	2	0.4	0.2
Sulfate	100	20	10	2	1	0.2	0.1

A calibration curve was constructed for each ion using these standard known concentrations on the X-axis and their corresponding areas under the curve on the Y-axis. Calibration point concentrations that were far larger than concentrations found in our samples were excluded from calibration curves.